2018

EXPERIMENTAL INVESTIGATION OF IMPINGED DROPLET DYNAMICS

Nitisha Ahuja
Michigan Technological University, nahuja@mtu.edu

EXPERIMENTAL INVESTIGATION OF IMPINGED DROPLET DYNAMICS

By

Nitisha Ahuja

A REPORT

Submitted in partial fulfillment of the requirements for the degree of

MASTER OF SCIENCE

In Mechanical Engineering

MICHIGAN TECHNOLOGICAL UNIVERSITY

2018

This report has been approved in partial fulfillment of the requirements for the Degree of MASTER OF SCIENCE in Mechanical Engineering.

Department of Mechanical Engineering - Engineering Mechanics

Report Advisor: *Dr. Seong Young Lee*.

Committee Member: *Dr. Sajjad Bigham*.

Committee Member: *Dr. Ahmed Abdul Moiz.*

Department Chair: *Dr. William W. Predebon*

TABLE OF CONTENTS

LIST OF FIGURES

LIST OF TABLES

ACKNOWLEDGEMENTS

I would like to express my sincere gratitude to my research advisor Dr. Seong-Young Lee, for all the support and guidance while pursuing my graduate education. Particularly he provided me the opportunity to pursue my research of my interest. I appreciate a lot, your participation in daily based discussions with patience and your valuable advices on my research work. As well, I owe my strong scientific confidence built up from my interactions with Dr. Lee on my ideas. I was also able to establish many contacts with experts in the field due to the opportunities created by Dr. Lee, giving me more chances to present my work outside hence helping me grow in the academic society. All the above made my master's study a fruitful, memorable and joyful journey.

Secondly, I would also like to acknowledge my committee members, Dr. Bigham and Dr. Moiz for taking time to serve on my committee and be involved in my graduate education. I am thankful to Dr. Moiz also for the guidance he has provided from the beginning of my graduate studies. In addition, I thank Dr. Bigham for providing the support for my research work as well as the brief opportunity for collaborative research work, which has enhanced my understanding beyond the scope of my project.

I would like to acknowledge my colleagues, Dr. Le Zhao, Xiucheng Zhu, Zhihao Zhao and Jiachen Zhai. I am thankful for all the support you have provided and believe that my learning during these two years have been boosted by working with all of you.

In addition, I would like to thank my family and friends, who have been supportive and understanding. You have always guided me to stay focused on my studies and helped in achieving my goals.

ABSTRACT

The fuel spray wall interaction phenomenon plays an essential role in determining the emissions and performance of an internal combustion engine. The investigation of single droplet wall interaction is crucial to understanding of a spray wall impingement process. This report is a compilation of the experimental work done to understand the droplet impingement characteristics, through optical diagnostics and temperature measurement. Different fuels and different surface under ambient and elevated temperature conditions are used for these tests, with two objectives: Development of a common deposition-splashing criteria; and Understanding droplet post impingement dynamics variation with factors like: Weber number (ratio of inertia and surface tension forces), and with temperature. The droplet post impinging characteristics include spread factor, height ratio, contact line velocity and dynamic contact angle. The effect of Weber no on droplet impingement characteristics is investigated using water and diesel. The effect of temperature is divided into two subsections: Isothermal (cold wall-cold droplet and hot wall-hot droplet) and non-isothermal conditions (hot wall-cold droplet and hot droplet and cold wall), to understand the influence of both variation in thermophysical properties and heat transfer between droplet and surface. Using the experimental results, a comprehensive review of splashing criteria is done, along with a proposed new correlation for same and concept of splashing probability is introduced. The observation presented for variation in post-impingement characteristics with the mentioned factors are useful for future development of numerical codes.

1 INTRODUCTION

1.1 MOTIVATION

Spray wall interaction is a common phenomenon observed in a wide range of industrial applications such as internal combustion engines, fire suppression, thermal power plants, microprocessor cooling and ink-jet printing [1]. In internal combustion engines the fuel spray-wall interaction can significantly alter the engine performance and emissions. For example, in port fuel injection equipped engines, the fuel puddle formed in the intake manifold can cause a lag in the air fuel ratio control, and eventually increase the amount of fuel injected to achieve the desired air fuel ratio. Similarly, in direct injection engines, emissions increase as fuel impinges on the piston and forms a film [2,3,4]. During the thermal cooling processes, the spray-wall interaction should result in minimum evaporation to obtain maximum heat transfer and overall higher cooling efficiency [5]. Hence, spray-wall impingement phenomenon is researched extensively to achieve more desirable results. However, spray-wall interaction involves complex physics and the underlying mechanism of this phenomena can be better understood by investigating a single drop wall interaction at the application specific operating conditions.

When a droplet interacts with a surface, it can produce various outcomes ranging from deposition, spreading, rebound, splash or disintegration, depending on numerous factors. These factors involve liquid properties, surface properties as well as ambient temperature and pressure [6]. Generally, in engine applications it is desirable that liquid drop-wall interaction results in rebound, as it will tend to reduce wetting and result in complete evaporation of fuel. Where as in spray wall painting, deposition outcome is more desirable than rebound or splash and in cooling applications, maximum spread is desirable when the droplet impinges on the wall. Thus, exploring the variation in post impingement characteristics of a liquid droplet with the above-mentioned factors is essential for predicting these outcomes in spray wall interaction. The numerical models developed by these studies can then be implemented in the CFD codes for accurate modelling of liquid drop-wall as well as spray wall interaction.

Building these numerical models involves extensive experimentation at different operating conditions. These experiments help in determination of the parameters that influence the droplet post impingement characteristics. These parameters as mentioned can range from the geometry and dynamics of droplets (velocity and diameter), angle of incidence, droplet-liquid properties (surface tension, viscosity and density), heat transfer between droplet and wall, surface properties (roughness and wettability), and ambient conditions (ambient pressure and temperature) [7]. These parameters, having a different weightage in influencing the post impingement droplet characteristics, can be comprised into a relation of dimensionless numbers, to represent a criterion of transition from one outcome to another. The work in this report focuses on spread to splash transition and explores the spreading dynamics of droplet with varying factors like weber number (We no), thermophysical properties and heat transfer occurring between droplet and wall.

1.2 OBJECTIVES

Several experimental studies have been reported in the literature which were directed at understanding the background physics of droplet impingement dynamics. These studies cover various criteria's that predict transition among the droplet impingement outcomes. Many of them have tried to find the empirical relation between the dimensionless numbers, such as Weber number, Reynolds number, Capillary number and Ohnesorge number.[1] These dimensionless numbers represent the fluid properties and give a quantitative comparison of different forces effecting the impingement dynamics.

The deposition-splash transition criteria, is one of the most sought after, because of its major industrial applications. Numerous recent studies have pointed towards the instability in the lamella as the cause of splash initiation and secondary droplet generation. These instabilities can be initiated by air entrainment or roughness of the surface, leading to two different kind of splashes: Corona and prompt respectively. As per Riboux and Gordillo [8] the corona splashing occurs because of the breakup of a small liquid film that lifts off the surface just after the impact due to the lift force generated by the surrounding air. In their model, both the fluid and substrate properties govern the splashing as well as the air viscosity. Thus, the understanding of splashing mechanism requires understanding of wetting behavior for a given pair of liquid and surface at different operating conditions.

In addition, the post-impingement parameters which characterize the liquid-solid interaction are important to understand the droplet impinging dynamics. Essentially, surface wettability governs the wall-film formation and dynamics. After the droplet impinges on a flat plate, wall surface wettability is a significant factor in deciding the growth of spreading diameter with time [9]. The surface wettability has an influence on the maximum wetting wall-film area and determines whether the impinged droplets in a spray undergoes coalescence to form a continuous film on the wall or not. Thus, the impinging dynamic process for the database of the relevant studies expansion is necessary to be evaluated.

The goals of this report can be narrowed down in the following points.

1. Bring understanding of the droplet impingement dynamics processes under wide range of operating conditions through experimental work.

2. Incorporate optical diagnostics and heat flux measurement techniques to visualize and quantify the effect of thermophysical properties and heat transfer on the macroscopic droplet structure and characteristics.

3. Develop MATLAB programs to measure the droplet characteristics, including droplet spreading factor, height ratio, contact line velocity, and dynamic contact angle, and heat flux.

5. Develop a deposition-splashing threshold transition for different fuels by impinging a single droplet on the wall over a wide range of conditions, including different liquid fuels, and smooth, roughened, isothermal and heated surfaces.

6. To help the numerical model (i.e., dynamic contact angle model [10] development via detailed Direct Numerical Simulation (DNS) models), the current study studied the dynamic process of droplet-wall interaction.

1.3 ORGANIZATION OF REPORT

Chapter 2 of this report discusses in detail the theory of droplet wall impingement dynamics. It also presents the previous numerical models developed to predict splashing and rebound criteria. This chapter also gives a review of the effect of Weber number, temperature dependent properties and heat transfer on the post impingement droplet characteristics, such as contact line velocity, spread factor and contact angle.

Chapter 3 presents the experimental setup and techniques in detail for capturing the droplet impingement dynamics and temperature variation of the surface. It also discusses the data analysis techniques for calculating the droplet impingement parameters and the heat flux between the droplet and the wall.

Chapter 4 details the results of the project in two parts. The first part focuses on the results obtained for the developing a splashing criterion of different fuels on different surfaces. Splashing criterion is drawn for an ambient temperature droplet interacting with smooth, rough and heated dry wall. Further results are shown for additional experiments done to draw a probability map finding the tendency of a droplet to splash with different impact velocity. In the second part, droplet impingement dynamics is discussed. Detailed experimental results are presented for the variation in post impingement characteristics with impacting droplet weber number, surface temperature, surface roughness and droplet temperature. A key attention is paid towards understanding the hand in hand variation of thermophysical properties and droplet dynamics.

Chapter 5 summarizes the findings of the report with important conclusions. It also recommends few steps to continue this work in future to obtain a more comprehensive understanding of the topic.

Appendix A includes all the MATLAB code developed to fulfill this study.

2 THEORY AND LITERATURE REVIEW

2.1 DROPLET IMPACT OUTCOME TRANSITION CRITERIA FOR DEVELOPMENT OF NUMERICAL MODEL

Many researchers have worked towards accurate modelling of spray wall interaction, which requires identification of different outcomes of a single droplet impact and development of corresponding transition criterion. As these outcomes determine the post-impact mass, momentum and energy distributions of the droplets. [11]. When a droplet impacts a surface, it spreads and form a lamella bounded by a thicker rim. The droplet tends to spread to maximum spreading diameter, and then undergo equilibrium with or without the process of recoiling and spreading again. The process of recoiling after reaching maximum spreading diameter depends on the competition among surface tension, capillary, inertia and viscous forces.

The initial spreading just after the impact can show splashing phenomena at higher impact velocities. However, as mentioned for droplet impinging dynamics, the critical impact velocities at which splash occurs depends significantly on the liquid, surface, and ambient gas properties. Therefore, many studies have been conducted to find a common threshold for different liquids in terms of non-dimensional numbers. The very first study was conducted by Stow et al. [12], in which the experimental studies focused on understanding the droplet-wall interaction phenomena and its dependence on liquid's Reynolds number (Re), Weber number (We) and surface roughness. They studied water droplets impinging on a roughened aluminum surface. They postulated a splashing threshold $K = We^{0.5}Re^{0.25}$, in which value of K was highly dependent on the surface roughness [13], although further studies by Yarin et al. [14] and Mundo at al. [15] showed the opposite trends. Yarin et al. [14] studied the single train of droplets falling on a solid substrate with a thin film at a known impinging frequency (f). They proposed a splash mechanism and found a splashing threshold as a function of impact parameters of droplet: Capillary number (Ca) and viscosity length (λ), as shown in Equation (1) (U_0, being the impact velocity, and ρ, σ, and ν are the density, surface tension and kinematic viscosity, respectively), where the dimensionless impact velocity (u) is introduced . They found that splashing threshold does not depend on droplet diameter and is slightly affected by mean surface roughness, but mainly caused by the velocity discontinuity propagating over the liquid layer on the wall. They also concluded that the splashing threshold at u = 17 to 18 corresponds to developed crown instability, strong enough to produce a group of secondary droplets.

$$Ca\lambda^{\frac{3}{4}} = Constant = u = \frac{U_0}{\left(\frac{\sigma}{\rho}\right)^{\frac{1}{4}}\left(\frac{\boldsymbol{\nu}}{\rho}\right)^{\frac{1}{8}} f^{\frac{3}{8}}} > 17\sim18$$

Nevertheless, this criterion does not hold true for many cases, as the derived splashing threshold provides an explanation only for corona splash but not for prompt splash

mechanism. Corona splash arises from the instabilities in the rim of the crown [14] and prompt splash arises at the contact line in the beginning of spreading phase [16]. In addition, this correlation posed under an assumption of no interaction of droplet with the solid dry surface rather a thin liquid film; therefore, it may not be applied for droplet impingement directly on a dry surface.

Another major study in terms of deposition-splashing process of droplet impinging on a flat surface was done by Mundo et al. [15]. They formulated an empirical model for deposition and splashing regimes, using the train of monodispersed droplets by varying liquid properties, surface tension, droplet diameter, and impingement angle. A deposition-splashing criterion as a function of Ohnesorge number (Oh) and Re of the impinging droplet was derived as $K = OhRe^{1.25} = 57.7$. Note that Oh and Re are calculated from the normal velocity component of the impinging droplet. This splashing threshold was based upon the energy conservation of impinging droplet, in which the pre-impact kinetic energy and surface energy of the droplet was conserved into the surface energy of the drop spread and viscous dissipation. Further, the spread factor and dynamic contact angle were considered as constant properties for any two-given liquid and solid in the deposition-splashing process. However, in the current study, both the spread factor and contact angle varies with the impinging droplet We during the droplet impinging on the plate.

The experimental studies mentioned above laid the foundations of droplet/spray-wall interaction study. A number of numerical models for the dynamics and vaporization of the liquid wall film in IC engines were then developed to help further understand the wall-film formation and characteristics, as well as predict the engine performance [17]. Naber et al. [18] firstly developed a relevant model used in multidimensional engine simulations, where they proposed three different outcomes of a droplet impingement on the wall, depending on the incident droplet *We*. The three outcomes were stick (drops adhere to the wall), reflect (drops rebound) and jet (drops slide along the wall); however, this model does not consider all the possible outcomes of droplet-wall interaction such as splash. Splashing is an important factor since it affects the atomization and vaporization in the vicinity of the wall, and the wall-film formation [19]. Additionally, the surface conditions (wet/dry surface and surface roughness) can widely contribute in varying the results of a droplet/spray-wall interaction. Bai et al. [20] predicted the outcomes of spray impinging on both wet and dry walls through gasoline spray droplet impingement simulations. Their model covered all of impingement regimes and they found that these processes are strong functions of the incident droplet *We*. The calculated wall spray characteristics also showed favorable agreement with the experimental results. Stanton et al. [2] developed a fuel film model in KIVA-II code and showed the same impingement regimes for a droplet impinging on a thin liquid film. Their criterion showed that when a low impact energy droplet ($We < 5$) impinges on a thin liquid film, it tends to stick. As the impact energy increases, $5 < We < 10$, the air layer between drop and surface causes low energy loss, and droplet tends to rebound. Further increase in impact energy ($10 < We < \mathbf{18^2 D_0 (\frac{\rho}{\sigma})^{1/2} \nu^{1/4} f^{3/4}}$, where $\boldsymbol{D_0}$ is droplet diameter, ρ, σ, ν and *f* are the drop density, surface tension, kinematic viscosity, and frequency) droplet tends to spread and droplet with higher impact energy ($We >$

$\mathbf{18^2 D_0 (\frac{\rho}{\sigma})^{1/2} \nu^{1/4} f^{3/4}}$) splashes and produces secondary droplets. The impingement regime developed by Stanton et al. [2] is widely used in many multidimensional engine models.

O'Rourke and Amsden [17,21] proposed a most complete film particle tracking method and developed the wall-film model for the transport of vapor mass, momentum, and energy in the turbulent boundary layers above the film in KIVA-3V code. The wall-film model, especially for splashing regime and secondary droplet distributions, was derived and extrapolated based on the previous experimental work from Mundo et al. [15] and Yarin et al. [14]. The splash criteria in O'Rourke and Amsden model is shown in Equation (2), the droplet splashes after impinging on the wall when $E^2 > 3330$, where E is a splash Mach number based on the impact velocity and the capillary wave speed. In Equation (2), a boundary layer thickness δ_{bl} was introduced and replace of initial film thickness (h_0) when h_0 goes to 0.

$$E^2 = \frac{\rho_l U_0^2 D}{\sigma} \quad \frac{1}{\min\left(\frac{h_0}{D_0}, 1\right) + \frac{\delta_{bl}}{D_0}} > 57.7^2$$

where ρ_l is the liquid droplet density, σ is surface tension, U_0 is the impact velocity, D_0 is incident droplet diameter, h_0 is initial wall-film thickness, δ_{bl} is the boundary layer thickness as shown in $\delta_{bl} = \frac{D_0}{\sqrt{Re}}$, *Re* is the incident droplet Reynolds number.

After O'Rourke and Amsden's work, Han et al. [19,22] extended and improved the impingement regimes splash criterion for both dry and wet surface including the surface roughness effect. The authors provided a new splash threshold in consideration of the experimental and numerical studies from [14,15,21] in Equation (3) as follows:

$$H_{cr} = \left(1 + 0.1Re^{0.5} \min\left(\frac{h_0}{D_0}, 0.5\right)\right)(1500 + \frac{650}{\beta^{0.42}})$$

where *Re* is the incident droplet Reynolds number, h_0 is initial wall-film thickness**,** β is dimensionless roughness parameter with respect to the incident droplet diameter.

When $WeRe^{0.5} > H_{cr}$, droplet impinging on wall tends to splash. Other regimes in Han et al. [19] follow the similar transition criteria for a wetted wall by Stanton et al.[2]. However, the splash threshold was mentioned in Han et al. [19] to be valid on the relatively smooth surfaces at which the initial film thickness should be much larger compared with the surface roughness.

Most recently, Ma et al. [23] numerically studied spray/wall impingement based on droplet impact phenomenon. In the paper, they summarized the previous experimental work from many researchers [24-27] based on incident *Re* and *Oh*. They found a splash criterion line of *OhRe* = 17 for those experimental data. Despite this, there still showed

un-sharp criterion for droplet splash at high *Re* region (more than 4000) and a clear splash criterion shown in low and medium *Re* range.

However, some recent studies have indicated the influence of ambient gas parameters on splashing criteria. Xu et al.[28] found that with the decrease in ambient pressure (ambient gas density) the corona splash phenomenon can be completely suppressed. They derive the splashing threshold by comparing the stress induced by restraining pressure of the gas on the spreading liquid which destabilizes and lifts the advancing lamella and the stress due to surface tension which opposes the disintegration of droplet. The stress due to ambient gas accounts in the gas density, speed of sound and velocity of the expanding lamella, whereas the opposing stress in liquid incorporates surface tension pressure at the front of the advancing lamella. Similar study was conducted by Riboux and Gordillo [8], in which they pointed out that splashing occurs when lamella lifts off from the surface due to the vertical lift force imparted by the gas. Therefore, it is necessary to understand the near wall gas effect on droplet impinging dynamics. The near wall gas can also be affected by the plate temperature, as due to radiation the density of air can be influenced.

More description on the splash criterion by Ma et al. [23], Yarin et al.[14] and discussion about a probability band for splashing is presented in Results section.

2.2 DROPLET IMPACT DYNAMICS

Further, knowledge of the maximum spread a droplet can achieve or whether the droplet will recoil after impingement can also improve the numerical codes. The surface wettability has an influence on the maximum wetting wall-film area and determines whether the impinged droplets in a spray undergoes coalescence to form a continuous film on the wall or not. Therefore, it is important to qualitatively and quantitively study the factors that affect surface wettability. One of the factors that characterizes the surface wettability is the liquid solid contact angle formed at the solid-liquid-surrounding gas three-phase contact line [29]. The contact angle formed between the liquid-gas and liquid-solid interface dramatically depends on the flow at three-phase contact line and the corresponding stresses acting on it. The final shape of the deposited droplet is determined by equilibrium contact angle and the maximum spreading of the droplet is significantly influenced by dynamic contact angle [30]. The contact angle formed at a moving contact line is called the dynamic contact angle which is usually required as a boundary condition for modeling in capillary hydrodynamics, including certain stages of the drop impact problem [31]. Dynamic contact angle is appreciably related to the contact line velocity. However, the static equilibrium contact angle as per the Young's equation [32] is only a function of surface tension at liquid-gas-solid interfaces. To account for dynamic contact angle variations during droplet impingement, advancing, receding and equilibrium are differentiated by the motion at the three-phase contact line. On the strength of the experiments, there are various dynamic contact angle models implemented in computational fluid dynamics (CFD) codes to help predict the underlying physical mechanisms of droplet-wall interaction [33].

There have been numerous studies, both theoretical and experimental, conducted to understand the dynamic contact angle variation during the impingement process. Sikalo et al. [31] conducted an experimental study to measure the dynamic contact angle and maximum spread factor for varying surface wettability and correlated them with the capillary number. In addition, the flow at three-phase contact line and the contact angle at the moving contact line influence the spreading rate [34]. The dynamics of spreading is characterized into four regions by the impinging droplet *We* and *Oh*, as reported by Schiaffino et al.[35]. *We* measures the driving force for droplet spreading and *Oh* scales the force to resist the spreading. The four regions are described as: inviscid-impact driven (at low *Oh*, high *We*); inviscid-capillarity driven (at low *Oh*, low *We*); highly viscous-capillarity driven (at high *Oh*, low *We*); highly viscous-impact driven (at high *Oh*, high *We*). The spreading regime for the experiments conducted in this study are explained in Results section.

Researchers have tried to widen the operating conditions for measuring the impinged droplet dynamics, some of which are droplet Weber number and surface temperature. Surface temperature as one of the important operating conditions introduces additional complexity to the analysis of droplet-surface impingement phenomena due to the droplet evaporation and heat transfer between solid-liquid and solid-surrounding gas. Jadidbonab et al.[36] measured the spreading factor and dynamic contact angle of a diesel droplet impinging a heated surface with different Weber number. They determined the temporal variation of apparent contact angle and spreading factor as a function of Weber number and surface temperature. They concluded that, with increase in surface temperature, maximum spreading diameter increases, and a stronger recoiling tendency is observed. Further similar studies from Ahn et al. [37] showed that dynamic contact angle varied significantly with increase in surface temperature, due to the phase change and thermophysical property change. Further, when the temperature of the surface is increased, different heat transfer regimes are formed. In general, four different heat transfer regimes are identified when a droplet is deposited on a hot surface [38-40].

I) When the surface temperature is lower than the droplet saturation temperature, the droplet falls into the natural convection regime. In this regime, the droplet evaporation is primarily driven by the vapor diffusion and the heat transfer occurs by conduction and free convection.

II) When the wall temperature is larger than the droplet saturation temperature but below the critical heat flux temperature, the droplet enters the nucleate boiling regime. In this regime, the droplet evaporation is primarily driven by the heat transfer from the hot surface to the droplet. Vapor bubbles form near the hot surface in this regime and the buoyancy moves these vapor bubbles towards to the liquid-surrounding gas interface. Vaporization removes the heat, and the droplet reaches the maximum evaporation rate at critical heat flux temperature [41].

III) When the wall temperature is above the critical heat flux temperature but below the Leidenfrost temperature, the droplet evaporation enters the transition boiling regime. In

this regime, an insulating vapor layer forms at the solid-liquid interface with the increase of the vaporization rate. The heat flux reduces to a local minimum value when the Leidenfrost temperature is achieved [42].

IV) When the wall temperature is larger than the Leidenfrost temperature, the film boiling regime occurs. In this regime, a thin vapor film forms and prevents the physical contact between droplet and the wall. The heat transfer is dominated by conduction initially, but radiation starts to take a significant role at higher temperatures. Afterwards, the heat flux to the droplet slightly decreases.

The various phenomena as observed at the cold impingement must be re-considered within each boiling regime. The phenomena of non-isothermal droplet impact are more complex, due to added influential factors related to heat transfer process, evaporation and temperature dependence of the liquid physical properties. When $T_W < T_{BP}$, the heat transfer does not affect the phenomenon at the beginning of the droplet impact process [43]. However, later during spreading, the temperature rise inside the droplet alters the evaporation process and the physical properties of the droplet (i.e. surface tension and viscosity); this may result in modification of the spreading rate. In [44], the equilibrium and dynamic advancing and receding contact angles of water droplet impacting on copper and stainless-steel surfaces at wall temperatures ranging from 120 to 200°C, were reported. They observed notable change in dynamic receding contact angle with respect to surface temperature and noted this effect as an indicative parameter of change in boiling regime. However, for the non-isothermal conditions, researches were only focusing on varying the wall temperature. None of the studies have examined the droplet temperature influence which can significantly change the impact dynamics since it directly affects the heat transfer process and the liquid thermal properties during impacting.

3 EXPERIMENTAL PROCEDURE

In this study, different liquids with wide variation of density, surface tension, viscosity and vapor pressure were interacted with dry smooth, dry rough and elevated dry smooth surface. The goal of these experiments was to build a common splashing criterion, based on the non-dimensional numbers and provide wide variation of post-impingement characteristics at different operating conditions. This section is divided into three sections: 1) Experimental setup; 2) Test Matrix for achieving different goals of study; and 3) Data analysis.

3.1 EXPERIMENTAL SETUP

The experimental investigation of a liquid droplet interaction with a dry, rough and elevated temperature wall was conducted using a test setup shown in Figure 1. The experimental setup consists of a high precision syringe pump, a metal plate, an optical setup, a real time control box for elevating and recording the temperature of both the metal plate and diesel droplet. The high precision syringe pump delivers the fuel at 0.2ml/min. The impact velocity of droplet is varied by varying the height of the tip of nozzle, from where the drop is released when the inertial and gravitational forces overcomes the capillary forces. The droplet diameter is governed by the thermophysical properties of liquid and the nozzle diameter. Although the initial droplet diameter varies with temperature, due to variation in thermophysical properties, Weber number remains in the same range at same impact velocity. The optical setup consists of an analog LED light source which is converted to planar light rays using an aperture and a lens of focal length # mm. The collimated planar light provides shadowgraph imaging capabilities using the Fastcam SA 1.1 high-speed camera. The high-speed camera was equipped with a 200 mm Nikon focusing lens with the shutter set f11 and frame speed at 20000 frames per second.

To test single droplet impinging on the surface with various elevated temperatures, the heat flux probes was deployed on the heated impinging plate. This heat flux probes are shown in Figure 2. The heat flux probe is a 3-wire heat flux probe that consists of a 0.060 inch probe and two welded junctions. The surface junction is a platinum junction between an independent positive lead and a common negative lead. The embedded junction shares the common negative lead and is paired with another independent positive lead. The 3-wire probe provides the ability to measure surface, embedded, and differential temperatures. One probe essentially is two “J” type thermocouples (TCs), one is installed at the surface of the plate and the other is at 2 mm directly underneath the surface thermocouple. The small size of the junction provides the fast time response that can satisfy the data acquisition requirement within injection duration of 2 ms. The voltage signal from the heat flux probes is sent to a National Instrument PXI DAQ system (two PXI 6251 cards and two SCB-68a blocks with CJC built in). Figure 2 shows the schematic of the 3-wire heat flux probe and the testing location of the heat flux probe is

always set at the center of the impinging plate. The temperature of droplet was controlled by a separate “K” type thermocouple sensor and PID controller.

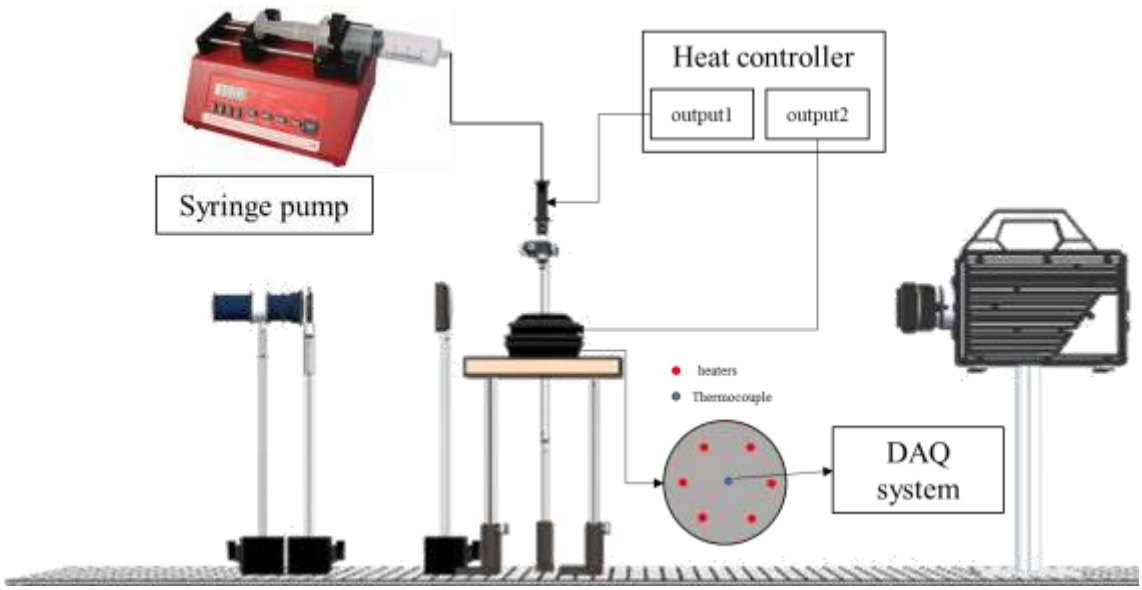

Figure 1. The Experimental setup for image and temperature recording of a droplet -wall interaction.

To avoid any uncertainties, all the tests were repeated three times and the average and standard deviation values were reported for the analysis. Heat flux tests were done independently to not influence the droplet dynamics and done in such a manner that thermocouple lies in the center of droplet. This was done to negate any variations occurring in the physical dynamics of droplet, as the wall with thermocouple junction would have different structure. During the isothermal case the heat flux was measured and ensured to be zero to maintain isothermal conditions between the surface and the droplet at different temperatures.

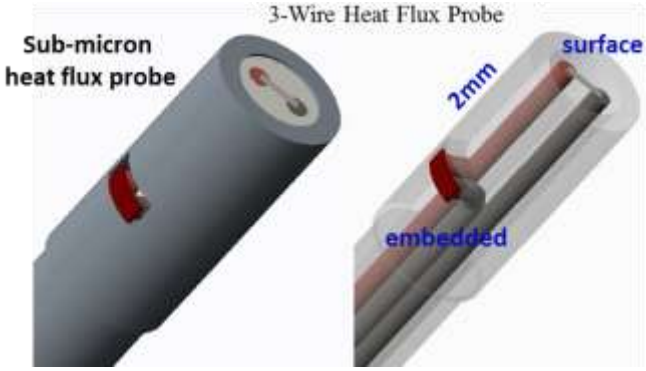

Figure 2. 3-wire heat flux probe used in the heat flux and temperature measurement

3.2 TEST MATRIX

In this section test matrix are shown for finding the splashing criteria and measuring the post impingement characteristics at different operating conditions.

3.2.1 TEST MATRIX FOR SPLASHING CRITERIA

The Splashing criteria was initially recorded for each fuel by changing the Weber no of the fuel for dry surface, hot surface and rough surface. The critical splashing velocity was measured for each fuel. The test matrix for the same is shown below in Table 1.

Table 1. Test matrix fro splashing criteria development

Parameter	Values
Ambient temperature (°C)	25
Ambient pressure (atm)	1
Fuel	diesel, water, n-dodecane, n-heptane
Surface temperature (°C)	25; 130 (heated surface)
Average surface roughness Ra (μm)	1.6 (smooth); 16 (roughened)

Although, with the given tests and the derived critical impact velocity for splashing a common threshold was developed, but on further experimentation it was found that splash did not occur always at the same impact velocity. Therefore, to get the probability band of splash phenomena was derived for isothermal case of diesel and Ethanol. To maintain the isothermal conditions both droplet and surface was heated. The test matrix for finding the splashing probability is shown in the Table 2. Elevated temperature conditions splashing criteria was only tested for diesel, whereas for water, n heptane and ethanol splashing criteria was recorded at ambient conditions. For the second tests on splash criteria n dodecane was replaced with ethanol to cover wider viscosity and surface tension range, as diesel and n-dodecane has very similar properties.

Table 2. Test matrix for splashing probability band development

Parameter	Values
Ambient temperature (°C)	25
Ambient pressure (atm)	1
Fuel	diesel, water, ethanol, n heptane
Surface temperature (°C)	25, 75,100,125
Droplet temperature (°C)	25, 75,100,125
No of repeats	15 of each

3.2.2 TEST MATRIX FOR MEASURING DROPLET DYNAMICS

To understand the droplet dynamics, the factors influencing it are separated into two sections. First the effect of Weber no is analyzed, with varying surface roughness. The test matrix is for the same is shown in Table 3.

Table 3. Test matrix for variation inpost impingement characteristics due to Weber no

Fuel	Temperature of Wall/Drop	Weber no	No of repeats
Diesel	25/25 (°C)	26,53,105	5 of each
Water	25/25 (°C)	26,53,105	5 of each

As mentioned in the literature review, the studies done so far focus only on the variation of surface temperature. Therefore, to fill the gap and to understand the effect of heat transfer and thermophysical properties on dynamics of droplet-wall interaction better, different conditions for diesel droplet impingement were framed to explore the impact of thermophysical properties of the droplet. These conditions were grouped into two; 1) Isothermal: cold wall-cold droplet and heated wall-heated droplet and 2) Non-Isothermal: cold wall-heated droplet and heated wall-cold droplet. Droplet and wall temperature was varied from 25°C to 150°C. The impact velocity of the impinging droplet was 1.43 m/s. The test matrix is shown in Table 4 with Figure 3 explaining different isothermal and non-isothermal conditions.

Table 4. Test matrix for variation inpost impingement characteristics due to temperature and heat flux.

Fuel	Temperature of Wall/Drop	Impact Velocity	No of repeats
Diesel	25, 75, 100, 125, 150 (°C)	1.4 m/s	3 of each
Diesel	25/100, 25/125, 25/150 (°C)	1.4 m/s	3 of each
Diesel	100/25, 125/25, 150/25(°C)	1.4 m/s	3 of each

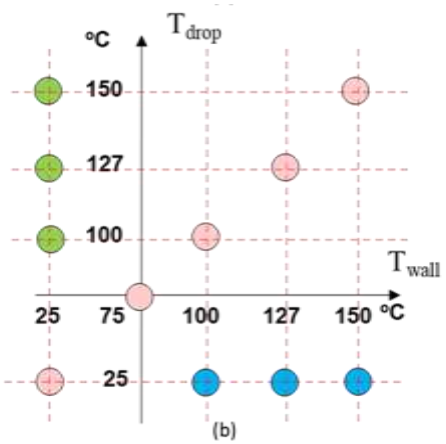

Figure 3. Explaination of isothermal and non isothermal conditions

Figure 3 displays the isothermal and non-isothermal test conditions for diesel droplet wall interaction. The temperatures were chosen according to the thermophysical variations plot of the diesel, as shown in Figure 3, which majorly occurs till 150 °C. These temperatures are also under the saturation temperature range of diesel so as the major variation in post impingement droplet dynamics can only be attributed to thermophysical property changes and not phase change.

To specifically understand the temperatures chosen for this study, the variation of thermophysical properties are shown in Figure 4. Based on the Eötvös rule [45], Eötvös Ramsay-Shield relation of surface tension and temperature is shown as:

$$\left(\frac{M}{d}\right)^{\frac{2}{3}} * \gamma = k * (t_c - t - 6) \text{Eq. 1}$$

where, M = molecular weight; d = density; γ = surface tension; k = Eötvös-Ramsay Coefficient; t_c = critical temperature; t = system temperature. This equation relates the surface tension and temperature linearly. As shown in Figure 4 [46], surface tension of diesel shows linear trend of decrease with the increase of the fuel temperature. However, the viscosity of diesel shows obvious nonlinear variation with temperature. At low temperature (below 50°C), the viscosity of diesel declines very fast with temperature increase. At elevated temperature (above 100°C), the variation speed in viscosity with temperature is very small. The transition in the viscosity variation speed happens in temperature between 50 and 100°C.

It should be noted with impact velocity 1.43, the We no lies in the range of 170~189, for different conditions.

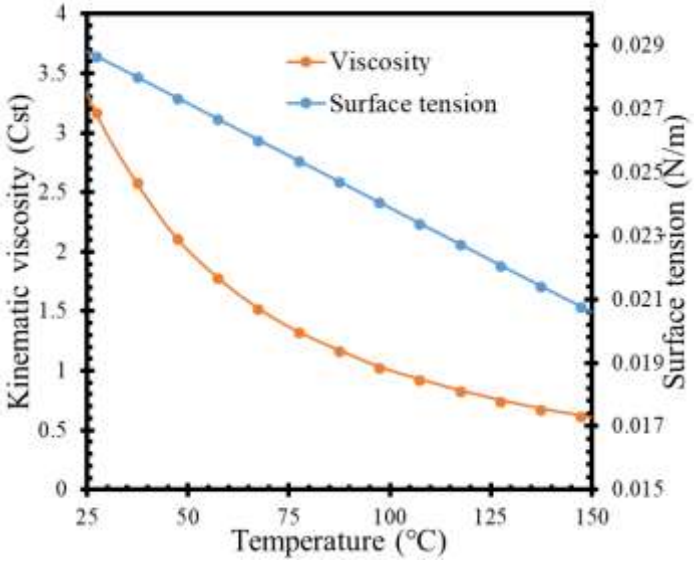

Figure 4. Diesel physical property variation with temperature

3.3 Data Analysis

Two kinds of raw data are extracted from the experimental setup. The high-speed images are batch processed whereas temperature data is extracted from the NI system.

3.3.1 Image Processing

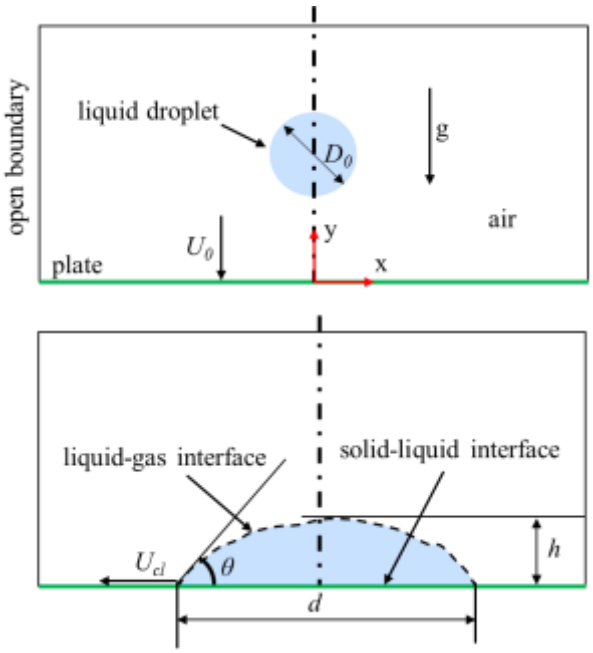

Figure 5. Schematic of droplet impingement on the flat surface

Figure 5 (top) shows the schematic of a single droplet placed at a certain location over the impinged plate with an initial velocity and Figure 5 (bottom) provides the schematic after the droplet impinging on the surface. The various global parameters such as the initial droplet diameter (D_0), the impact velocity (U_0), spreading diameter (d), spreading factor (Δ), contact line velocity (U_{cl}), height ratio (h/ D_0) and dynamic contact angle (θ), are described to characterize the process of droplet impacting on the surface.

Spreading diameter (d) is the distance between the left and right visible three-phase contact points. The three-phase contact points are defined as the points where all three phases meet, i.e. solid, liquid, and gas. Spreading factor (Δ) is the ratio of spreading diameter (d) to initial droplet diameter (D_0). Impinged height is defined as the maximum height in the perpendicular direction with respect to the impinged surface and impinged height ratio (h/ D_0) is the ratio of impinged height to initial droplet diameter (D_0). The contact line velocity (U_{cl}) is the rate of change of spreading diameter (d) with respect to the time. The angle formed between the liquid gas interface and solid-liquid interface at the three-phase contact point is defined as contact angle. The dynamic contact angle (θ) can be defined as the contact angle observed at this moving contact line during the droplet impingement process. In general, three stages are observed during a droplet impinging on the surface based on contact line velocity: advancing, receding and equilibrium. In the present work, if the $U_{cl} > 0$, the dynamic contact angle is advancing contact angle; if $U_{cl} < 0$, the dynamic contact angle is receding contact angle; and if $U_{cl} = 0$, the droplet becomes stable which corresponds to the equilibrium contact angle. The averaged contact angle at each phase is calculated by taking the mean of the instantaneous contact angles of respective phases.

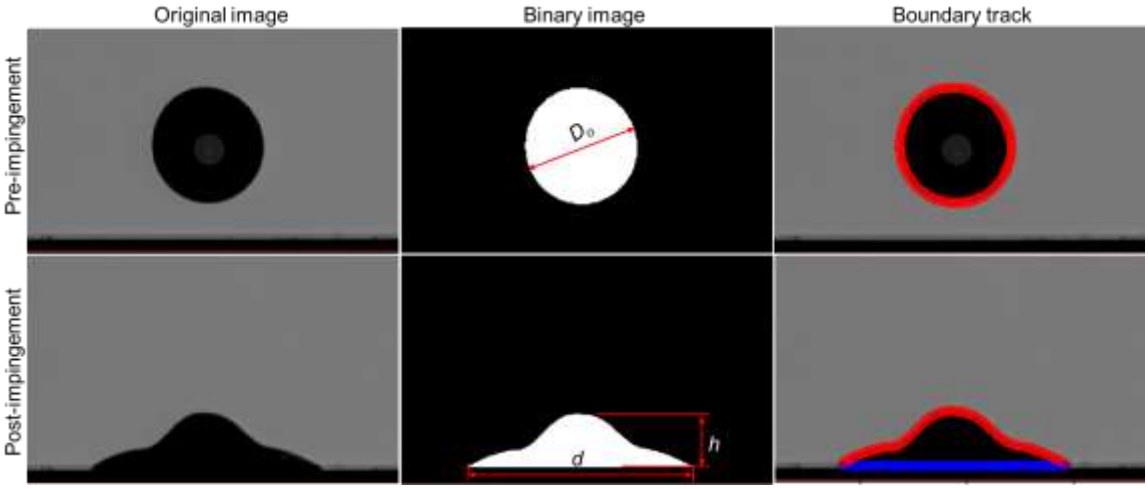

Figure 6. Image processing procedure for initial diameter, spread factor and height ratio

To analyze the droplet impinging on a flat surface, an in-house MATLAB code was developed to process the images. The procedure of image processing is shown in Figure 6. In Figure 6 (top), first, the background was subtracted to remove the unnecessary object other than the droplet based on the original image. Then, the image was converted into a binary image based on a threshold which is a constant value chosen by applying

Otsu's method [47] to aid in accurately predicting the droplet boundary. The possible deformation of an impacting droplet due to drag force was measured by determining the difference between horizontal and vertical diameters. We found this difference to be less than ±1 % for all measurements, showing that the drag force does not have a substantial influence on droplet size. Therefore, the image of the droplet is approximated as a circle, based on the area of this circle, the initial diameter of the droplet is extracted. A sensitive analysis for the threshold value was done on a sample case by increasing and decreasing default threshold by 20 % and the initial droplet diameter shows only ±2 % for different threshold values. In some cases when the droplet was not completely circular the radius was calculated by averaging the distance of each pixel point on circumference with the centroid.

The processing of post-impingement images is shown in Figure 6 (bottom). The boundary points are separated into two interfaces: solid-liquid interface (blue) and liquid-gas interface (red). The spreading diameter (d) is calculated as the distance between leftmost and rightmost visible three-phase contact points. The spread factor (Δ), ratio of spreading diameter and initial droplet diameter is then calculated at each time step. Similarly, the height of the impinged droplet is measured as a distance from the topmost point of the droplet to the flat surface and the impinged height ratio (h/ D_0) is found. The contact line velocity (U_{cl}) follows the same way to be obtained.

The dynamic contact angle measurement was performed using two methods.

1. Linear Fitting of points adjacent to three phase contact point
   The dynamic contact angle (θ) is processed as an angle between the tangent to drop profile at the moving contact line and horizontal solid-liquid interface. The boundary points corresponding to the liquid-gas interface are considered, as shown in Figure 7. Only the pixels, very near to the three-phase contact point on the liquid vapor interface, are considered to curve-fit a line. This curve fitted line is used as a tangent to the droplet from the three-phase contact point as shown in Figure 7 (right). The contact angle is finally obtained from the slope of the curve fitted line. The dynamic contact angle is extracted from each image by averaging the visible left and right contact angles as shown in Figure 7. Besides, the reference scale in the experiment was determined by measuring the number of pixels corresponding to a known length and the known length was oriented normal to the camera's line-of-sight.

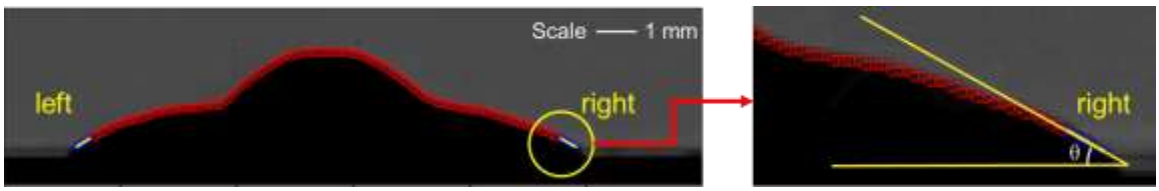

Figure 7. Contact angle measurement technique using linear fitting

2. Polynomial Fitting of points adjacent to three phase contact point.

A variation in contact angle measurement was done from the previous study as the impingement of an elevated temperature diesel droplet impingement resulted in very thin film. This methodology is well explained in Figure 8. Initially the background subtracted image is divided from the center location into two parts: Left Image and Right Image. This is done to eliminate any variations due to slight angle in the plate profile. Then the mirror portion of the image is subtracted from the image. Then the Boundary of each image is calculated and 20 adjacent points to the Triple phase contact point are curve fitted. The order of this polynomial curve fitting was varied from 1 to 4, to get a curve with best fitting for the given points by comparing R^2 value. Then the three-phase contact point is determined by extrapolating the best fit curve and a tangent line is drawn at this point on the curve. The angle of this tangent from the liquid solid interface(horizontal) is considered as the contact angle.

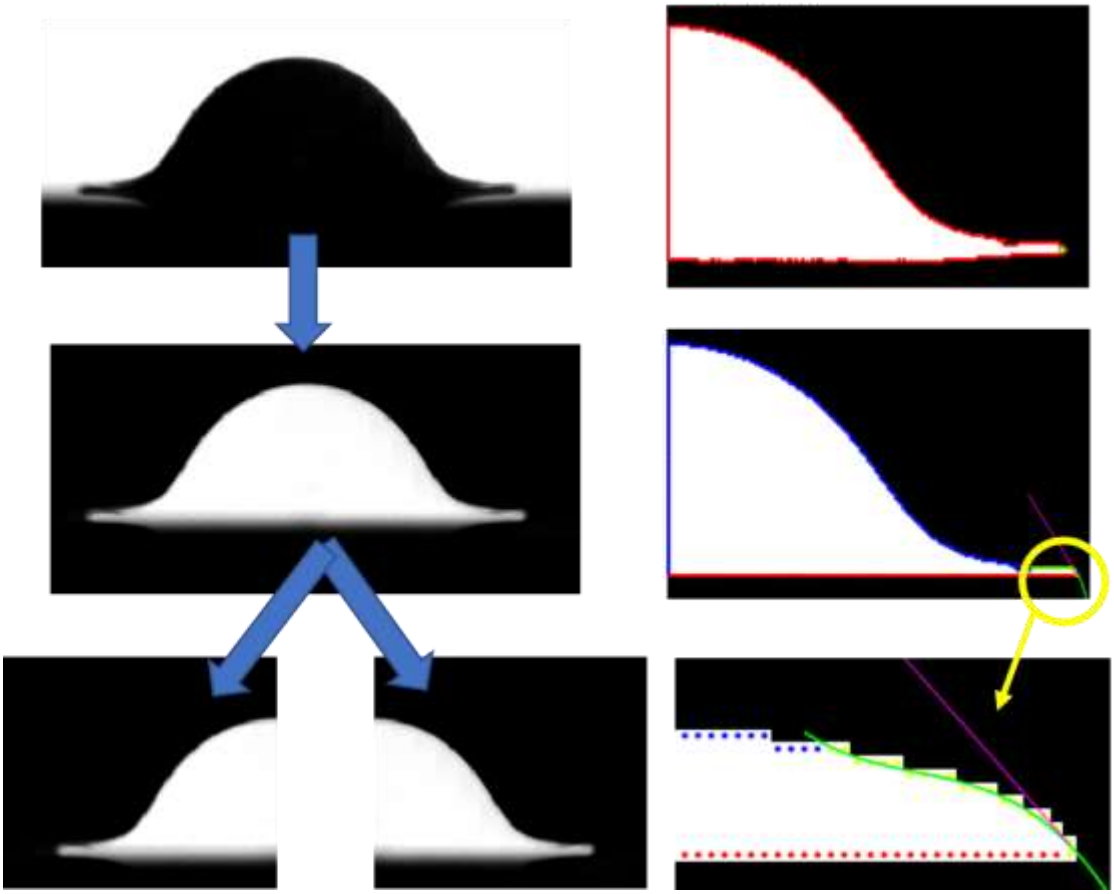

Figure 8. Contact angle measurement technique using optimized polynomial fitting

The first method was used when the ambient temperature droplet interacted with ambient temperature surface, and only Weber no and droplet liquid was varied. The second method was used when elevated temperature droplet and surface interacted. The reason for this is at elevated temperatures the spreading factor became higher (approximately ranging to 4.5), and thus the film height became much smaller. This reduced film height

accounted for few pixels in the image, thus causing inaccuracy in calculation of contact angle using the linear fitting method.

3.3.2 HEAT FLUX CALCULATION

Heat flux calculation was done using the Fourier's law of conduction. Time varying temperature data of both the surface and embedded thermocouple junctions as shown in Figure 2 was acquired during the droplet impingement. This data was utilized to calculate transient heat flux between the surface and the droplet, assuming a one-dimensional heat conduction from the surface to embedded thermocouple junction. This assumption is based on the negligible diameter of the probe connecting the two thermocouples.

$$q'' = -k_{ss}\frac{dT}{dy}$$

where q'' is the heat flux (W/m^2), k_{ss} is the thermal conductivity of the stainless steel 44.5 W/m-K. dT is the change in temperature between the embedded thermocouple and surface thermocouple and dy is the linear distance between the two thermocouples which is 2 mm. Although the effective heat transfer between droplet and wall can only be accurately calculated when the integrated heat flux values over droplet wall contact area is taken, but heat transfer at a single point in the center of droplet impingement also is enough to indicate a trend with the variations in temperature for both the droplet and wall.

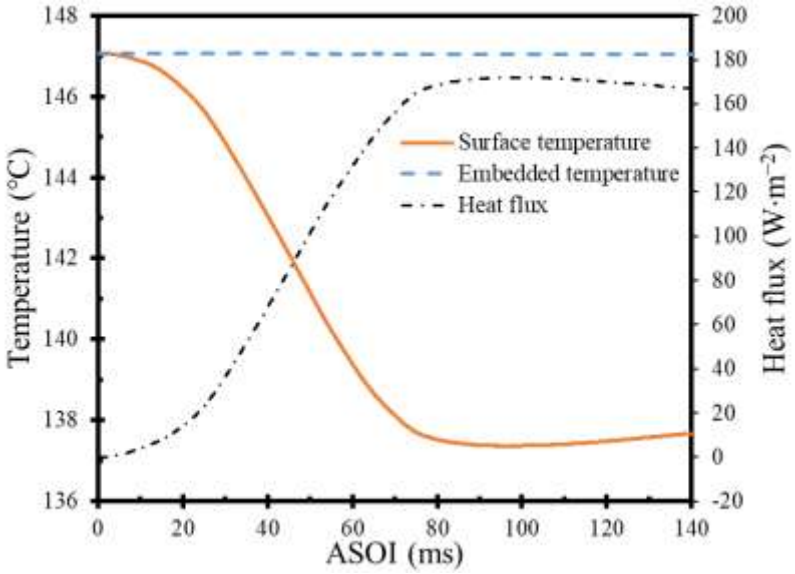

Figure 9. Sample data of the temperature and heat flux measurement at the non-isothermal condition: heated wall (150°C) and cold droplet (25°C).

Due to the noise shown in the original signal during the fuel injection, median filter is applied to the original temperature profile. The smooth signal based on the above filter is

obtained to generate the final data. Figure 9 shows a sample data of the temperature and heat flux at the non-isothermal condition: heated wall (150°C) and cold droplet (25°C). Time after impingement is presented for the evolution of heat flux. In this study, it is also noted that time is measured after start of impingement (ASOI).

4 RESULTS AND DISCUSSION

This section is similarly divided into two parts. The first part covers the results obtained for splashing criterion and the second part presents the post impingement droplet characteristics.

4.1 SPLASHING CRITERIA AS PER THE EXPERIMENTAL INVESTIGATION

Figure 10 shows a sequence of droplet shape evolution at various time instants for diesel and water with the dynamic impingement process of a liquid droplet onto a smooth heat treated stainless steel surface. Non-splashing condition is given in Figure 10 (top) and splashing condition is found in Figure 10 (bottom). The initial droplet-impact velocity of 1.01 m/s was chosen as the baseline non-splashing condition, the corresponding impact *We* for diesel is 104 and impact *We* for water is 53. The initial droplet-impact velocity of 2.4 m/s was chosen to show splashing process, the corresponding impact *We* for diesel is 569 and impact *We* for water is 289. Since the initial droplet-surface height is a large value compared with the droplet size, the initial location of droplets is not shown in Figure 10, instead, in the report, the center of droplets to the plate are set to the same distance of 4 mm for all conditions to show the pre-impingement phenomena. In addition, due to the different exposure time applied for different fuels, there is an obvious difference of the visualization of liquid droplet with background images. Besides, the time stamps are selected with respect to the time when droplet just impacts on the plate (i.e., t = 0 ms when droplet interacting with the plate). The time stamps along with each image illustrate slightly variances in water and diesel fuels as a result of the particular events occurring at the different time, especially after droplet impinging on the surface.

A series of *non-splashing* events for droplet impinging on a smooth plate with the baseline test condition is observed in Figure 10 (top). From left to right, there are (a) pre-impingement, (b) impingement, (c) post-impingement, (d) maximum spreading, and (e) receding. In Figure 10 (top) (a), the initial water droplet size (D_0 = 3.6 mm) is larger than diesel droplet (D_0 = 2.87 mm); In Figure 10 (top) (b), as stated in Image processing section, the droplet size shows no substantial change before and after impinging on the surface due to the insignificant influence of the drag force on it; After impingement, it can be clearly seen in Figure 10 (top) (c) that droplets start spreading radially with the current view, the diesel droplet spreads more rapidly compared with water droplet at 1.8 ms due to the larger surface tension of water; In Figure 10 (top) (d), the water droplet reaches its maximum spreading diameter of 9.72 mm around 6.0 ms and diesel droplet achieves its maximum spreading distance of 8.89 mm around 11.0 ms; In short period after spreading as shown in Figure 10 (top) (e), the water droplet begins receding under the effect of hydrostatic force and capillary force, however, it is difficult to observe the receding in diesel droplet due to higher viscosity of diesel fuel. Afterwards, the droplets tend to be stable which corresponds to the equilibrium stage (not shown here). The

quantitative comparison of spreading for non-splashing case will be discussed in the following sections.

Similarly, Figure 10 (bottom) shows a series of *splashing* events for droplet impinging on a smooth plate with the baseline test condition. From left to right, there are (a) pre-impingement, (b) impingement, (c) splashing, and (d) further splashing, and (e) equilibrium. In Figure 10 (bottom) (a) and (b), the initial diesel and water droplet size are the same as mentioned in the non-splashing case; After interacting with the plate, in Figure 10 (bottom) (c) droplets spread radially and splash at 1.0 ms with the current view, the stronger splashing is observed in diesel droplet in comparison to water, based on Yarin et al. [14] and O'Rourke and Amsden [17,21] the splash threshold corresponds to the formation of a kinematic discontinuity. The velocity discontinuity, located at the boundary between fluid moving outward from the splash location and slower moving fluid on the surface, leads to fluid to be ejected away from the surface. The secondary splash droplets are then generated; In Figure 10 (bottom) (d), the diesel and water droplets further splash into several secondary droplets, because of smaller surface tension in diesel case, more satellite droplets are formed in diesel case. On the other hand, oscillation is observed in water case due to the lower viscosity of water; Around 40 ms after droplets impinging on the plate, as shown in Figure 10 (bottom) (e), both diesel and water droplets tend to achieve the equilibrium stage while the spreading distance in diesel is longer than that in water case.

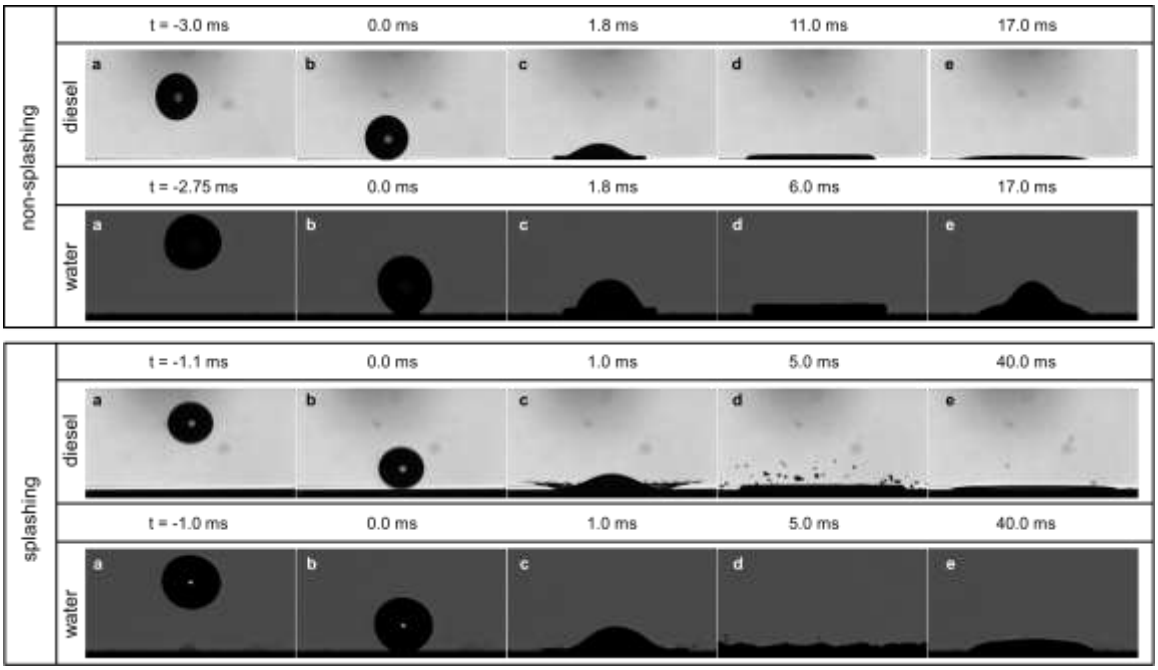

Figure 10. A sequential visualization of droplet-wall impingement experiment for diesel and water: non-splashing (top); splashing (bottom)

As discussed in literature review section, the splashing threshold of $\boldsymbol{Ca\lambda^{\frac{3}{4}} = u > 17 \sim 18}$ is found by Yarin et al. [14], who studied a single train droplets falling on a solid substrate

with a thin film at a known impinging frequency (f). Figure 11(left) provides the correlation between Capillary number (Ca) and non-dimensional diffusion length (λ), the black solid line represents the splashing criteria line obtained from Yarin et al. [14]. The data points shown in Figure 11 (left) represent our experimental results at various conditions (including variation of liquid viscosity, surface tension, smooth and roughened surfaces, heated plate), where the red points denote the splashing events while the blue points signify the non-splashing events. Overall, our experimental results follow the same trend in predicting the non-splashing phenomena with the literature for water, diesel, and n-dodecane, but not for n-heptane. The data points from non-splashing cases with n-heptane fuel are observed to shift towards the splashing region. On the other hand, the data points representing splashing characteristics from other fuels cross the Yarin et al.'s splashing criteria line (solid black line). As stated in previous, the Yarin et al.'s criterion may not work for many cases since the derived splashing threshold provides an explanation only for corona splash but not for prompt splash mechanism. Moreover, this correlation posed under an assumption of no interaction of droplet with the solid dry surface instead of a thin liquid film; therefore, it may not be applied for droplet impingement directly on a dry surface. Therefore, the best fit for the current experimental data is found to be between a dash line showing $\boldsymbol{Ca\lambda^{\frac{3}{4}} = 12}$ and a round dot line exhibiting $\boldsymbol{Ca\lambda^{\frac{3}{4}} = 10}$ in Figure 11 (left). It should be noted that the frequency (f) in the current work is assumed to be U0/D0 [48], λ can be further derived as $\boldsymbol{\lambda = \frac{Re^{1.5}}{We}}$. As well, $\boldsymbol{Ca = \frac{We}{Re}}$, $\boldsymbol{Oh = \frac{We^{0.5}}{Re}}$. Therefore, the correlation-based Ca and $\boldsymbol{\lambda}$ is also noticed as the relation in terms of Oh and Re.

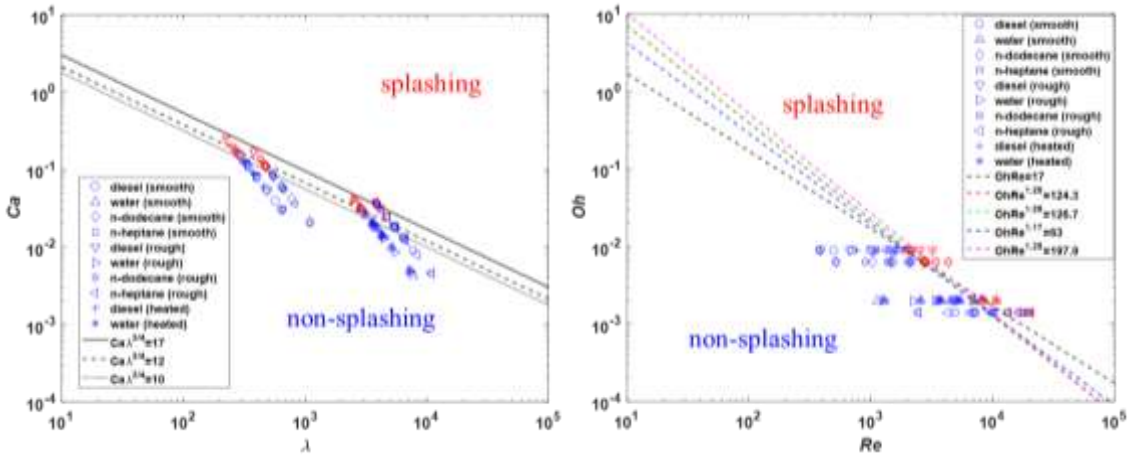

Figure 11. Splashing criteria for various fuels: Ca vs. λ (left); Oh vs. Re (right).

Similarly, we have discussed another splashing criteria based on Ohnesorge number (*Oh*) and Reynolds number (*Re*) in Introduction section, which was presented by Ma et al. [23] by summarizing a larger number of researchers' experimental data at various test conditions shown in Figure 11 (right). The black dash line stands for the splashing correlation of $OhRe = 17$ from Ma et al. [23], the rest of four dash lines exhibit the correlations of $OhRe^{1.25} = 124.3$, $OhRe^{1.25} = 126.7$, $OhRe^{1.17} = 63$, and $OhRe^{1.29} = 197.9$ from Geppert et al. [49], Cossali et al. [50],Vander Wal et al. [51], and Bernard et al.

[52], respectively. Most of blue points from our experiment are below these critical lines while most of red data points are above it. However, one of the exceptions occurs again in n-heptane case, rather than following the splashing criteria line of *OhRe* = 17, n-heptane data points resides at *OhRe* of 26. It is also observed that splashing on the roughened plate happens slightly below the *OhRe* = 17 because the probability of prompt splash increases as the amplitude of roughness increases [16].

Although a substantial number of experimental studies done on the droplet-wall interaction, due to the complexity of physics of droplet-wall interaction and the limitations of the experimental data, the splashing criteria is necessary to be studied and improved. The best correlation in terms of the current experimental data and test conditions is found as follows:

	$OhRe^{0.826} = 3 \sim 6$	(14)

As discussed in chapter of literature review, according to Schiaffino et al. [33], the spreading process after droplet impact is classified into four regimes characterized by impact *We* as a driving force and *Oh* as a resisting force as shown in Figure 12. In region I, at low *Oh* and high *We*, the spreading is driven by dynamic impact pressure and resisted primarily by inertia, and viscous effect is relatively weak. The data points marked in blue in Figure 12 represent our experimental results at various conditions (including variation of liquid viscosity, surface tension, smooth and roughened surfaces, heated surface), it is observed that all experimental data points fall in region I as the range of *We* is 26 to 925 and the range of *Oh* is 0.0014 to 0.009. Therefore, it can be concluded that the droplet-wall interaction results at the conditions described in this work are inviscid-impact driven. In this region, from the high-speed images (as shown in Figure 10), in the final stage of spreading, the contact line advance slows after the main part of the spreading is over. Additionally, other three regimes are inviscid-capillarity driven (at low *Oh*, low *We*); highly viscous-capillarity driven (at high *Oh*, low *We*); highly viscous-impact driven (at high *Oh*, high *We*), respectively.

Since all of our experimental data sets fall into region I, we then examine spreading characteristics of the additional three liquid fuels (glycerol, perfluorohexane, and 1-decanol) by theoretically calculating *We* and *Oh* numbers with the estimated droplet size based on Tate's law [57]. The three liquids are selected due to their significant difference with the experimental tested liquid fuels on liquid properties, such as density, viscosity, etc. For instance, the density of glycerol is about 1.5 times larger than that of diesel and the viscosity of glycerol is more than 400 times larger than that of diesel. However, as the red symbols in Figure 12, the data points from these three fuels still enter into the region I due to the small variance on *We* and wide range of *Oh* crossed in this region. Furthermore, the data point obtained from the diesel spray-wall impingement test and simulation (i.e. D_0 = 5.97 µm, U_0 = 77 m/s), indicating the droplet near the impinged surface, is marked in black in Figure 12. This droplet also falls into the region I with respect to its size and velocity. Therefore, by the above analysis, most of spreading at the

operating conditions in both single droplet and spray-wall interaction tests occurs fast due to dynamic pressure of impact and resisted primarily by inertia.

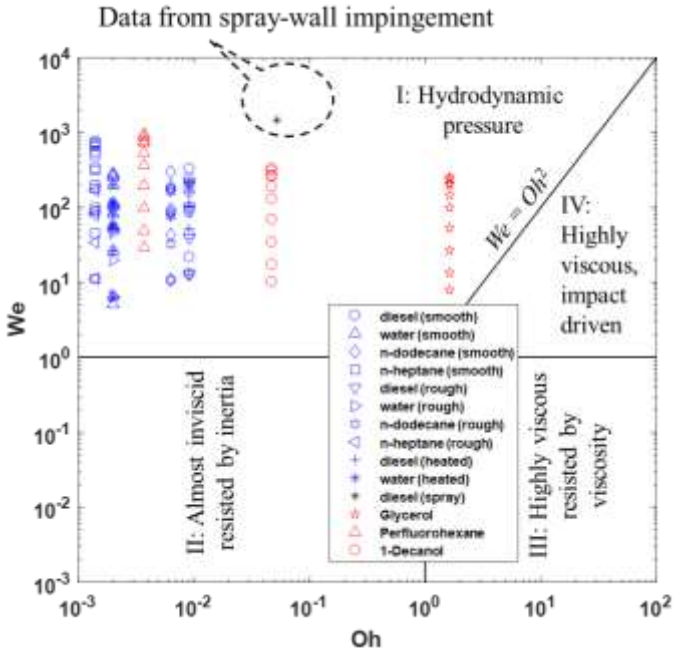

Figure 12. Regime map of spreading.

However, on further investigation of Splashing criteria at different temperature rather than a single threshold a band of probability of splash is found for all the fuels: Water, diesel, n heptane and Ethanol. Splashing probability variation with temperature is recorded isothermally for diesel. These tests are conducted on a non heat treated plate as the thermocouples are fixed inside the plate for temperature measurment.

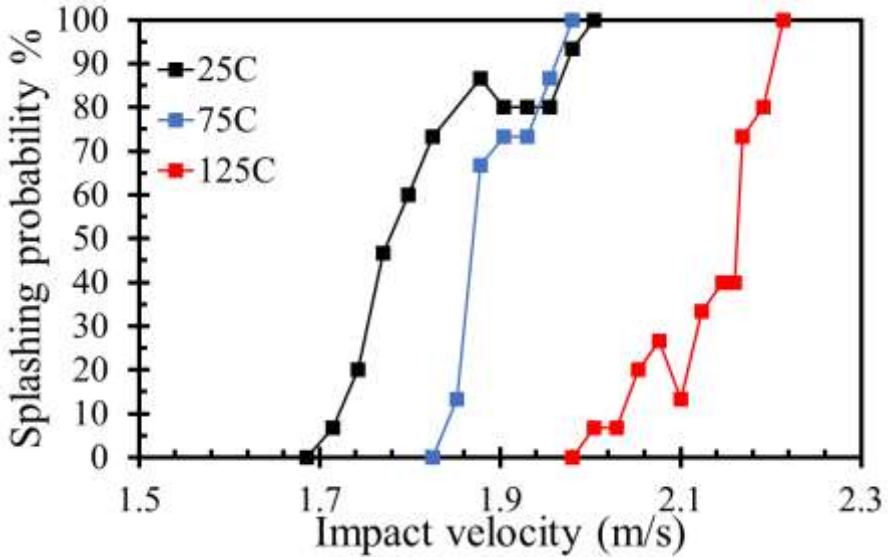

Figure 13. Variation in splashing probability of diesel with variation in wall/droplet temperature

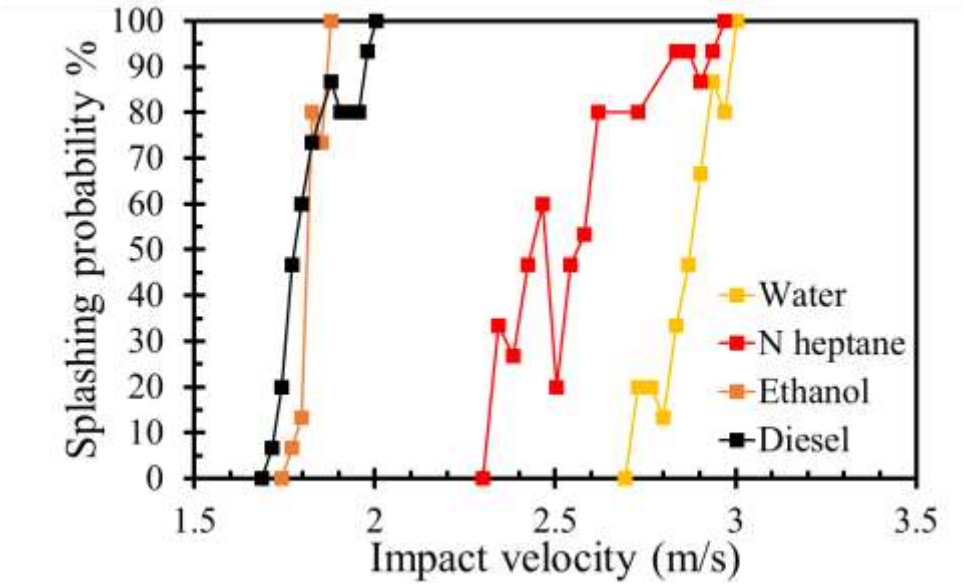

Figure 14. Variation in splashing probability of different fuel at ambient temperature wall/droplet interaction

Splashing probability is calculated as percentage of no of cases those splashed out of 15 repeats for each case. Figure 13 shows the effect of varying the temperature of diesel droplet on the splashing conditions. It is observed that the impact velocity at which splash begins increases with increase in temperature. The Figure 14 shows the variation in splashing probability for the different fuels at 25ºC impinging on a non-heat-treated plate maintained at 25ºC. It is noted the bandwidth for n heptane is widest and water does not show splashing till very high impact velocity. Water showed varied impact velocity for the beginning of splash when interacting with heat treated and non-heat-treated plate. Water shows splashing 2.36 m/s at heat treated plate, whereas on a non-heat-treated plate splashing begins at 2.7 m/s for water. Table 5 shows the 50 % splashing probability impact velocity and the bandwidth for each fuel.

Table 5. Summary of the splashing probability

Fuel	Droplet/Wall Temperature (°C)	Bandwidth (m/s)	50 % splashing probability impact velocity (m/s)
Diesel	25/25	0.99	1.75
Diesel	75/75	0.7	1.8
Diesel	125/125	0.94	2.15
Ethanol	25/25	0.54	1.8
N heptane	25/25	1.8	2.42
Water	25/25	1.25	2.86

4.2 DROPLET DYNAMICS

4.2.1 EFFECT OF WE NO

Initially, the effect of impact *We* (or initial droplet-plate height) on the temporal evolution of spreading and dynamic contact angle for diesel and water will be presented. The results of the effect of impact *We* on spreading factor, height ratio, contact line velocity, and contact angle for a single droplet impinging on an unheated smooth surface are presented in this section. Due to a larger number of test conditions, diesel and water are chosen as the reference fuels, three non-splashing conditions for each fuel are selected to be shown in the paper. In terms of the height between initial location of droplet and the impinged plate, these three conditions are 26 mm, 52 mm, and 104 mm, the corresponding impact *We* is 52, 104, 207 for diesel; 26, 53, 105 for water, respectively. Nevertheless, the relevant results from the remaining different impact *We* conditions are summarized in Table 6 and Table 7. Additionally, the experimental results at each condition are averaged from 5 repeats and after start of impingement (ASOI) time is presented for the post-impingement evolution.

4.2.1.1 DIESEL

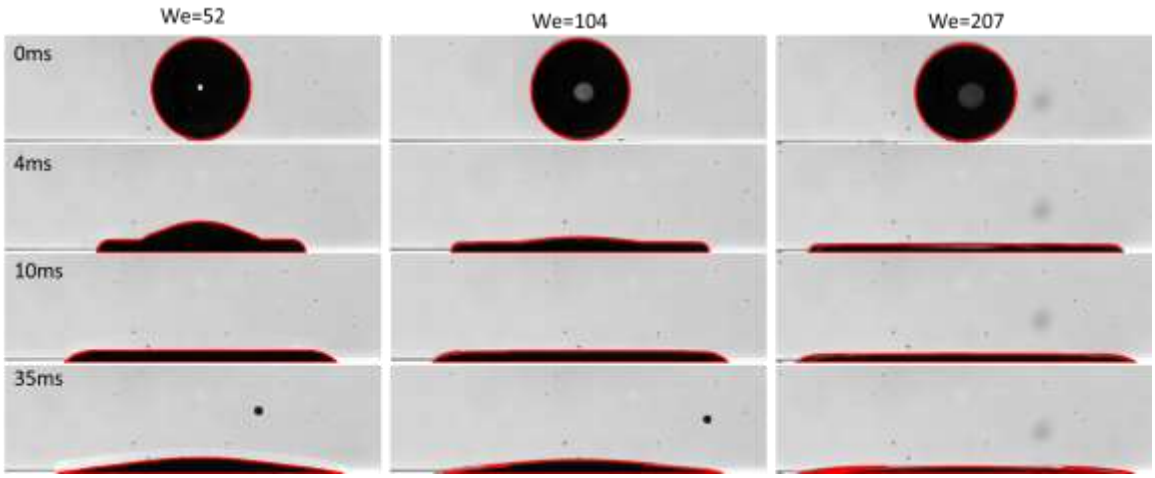

Figure 15. Ambient condition diesel droplet interaction with ambient temperature smooth plate at different Weber no.

Figure 15 shows the variation in temporal evolution of a diesel droplet with Weber number increase. The post impingement characteristics are obtained from these images. Figure 16 shows the spreading factor (top) and height ratio (bottom) for diesel fuel at various impact *We* conditions. During the initial stage of the impingement, the droplet reaches the plate and starts expanding outward with respect to the impinging point under the impact pressure. In general, the spreading factor increases as the impact *We* increases while the height ratio decreases with the impact *We*, which is caused by the relatively higher impact velocity and momentum at the higher impact *We* case driving the droplet to

move outward. In sequence, the droplet achieves its maximum spreading distance and the maximum spreading factors obtained are 3.4, 3.1, and 2.8 around 8 ms, 11 ms, and 24 ms as the impact *We* reduces. The flattened droplet then starts to recede under the capillary force and the spreading factor slightly decreases due to this recoiling. There is no oscillation observed due to the high viscosity of diesel, finally, spreading factor and height ratio remain unchanged when the droplet becomes stable.

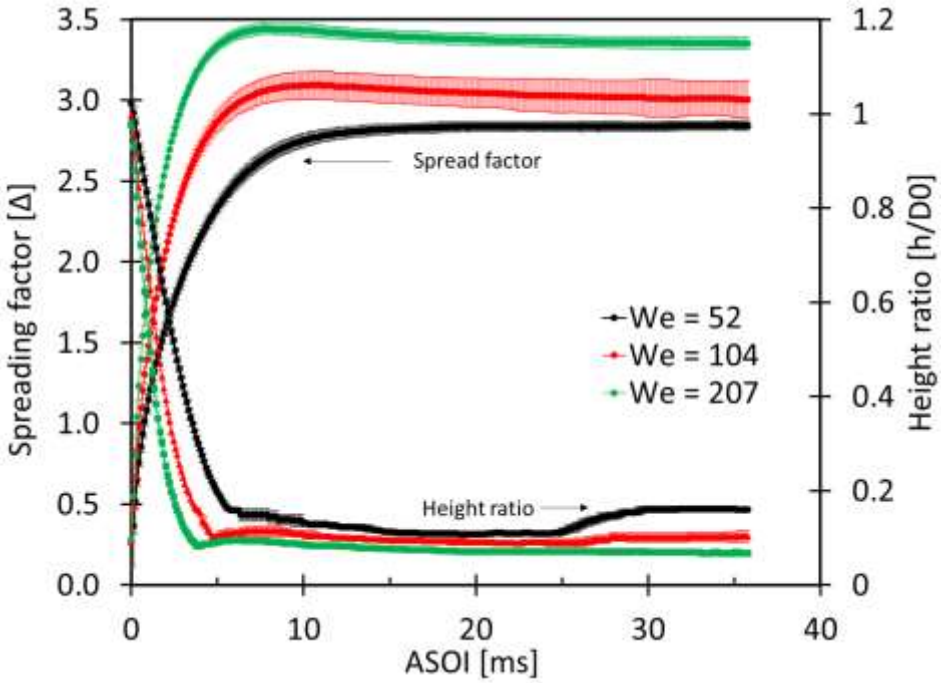

Figure 16. Spreading factor and height ratio for diesel at various impact We.

The results of the dynamic contact angle for diesel droplet impinging on a smooth surface with different impact *We* is presented in Figure 17, with varying spread factor. This representation is done to understand the variation of contact angle with both time and spread factor during distinct phases of the post impingement. It can be observed that the impact *We* has an insignificant effect on the contact angle as it can be seen it becomes constant after reaching maximum spread factor. In addition, the contact angle for last frame of all the three *We* is same, thus emphasizing negligible effect of Weber no on the same.

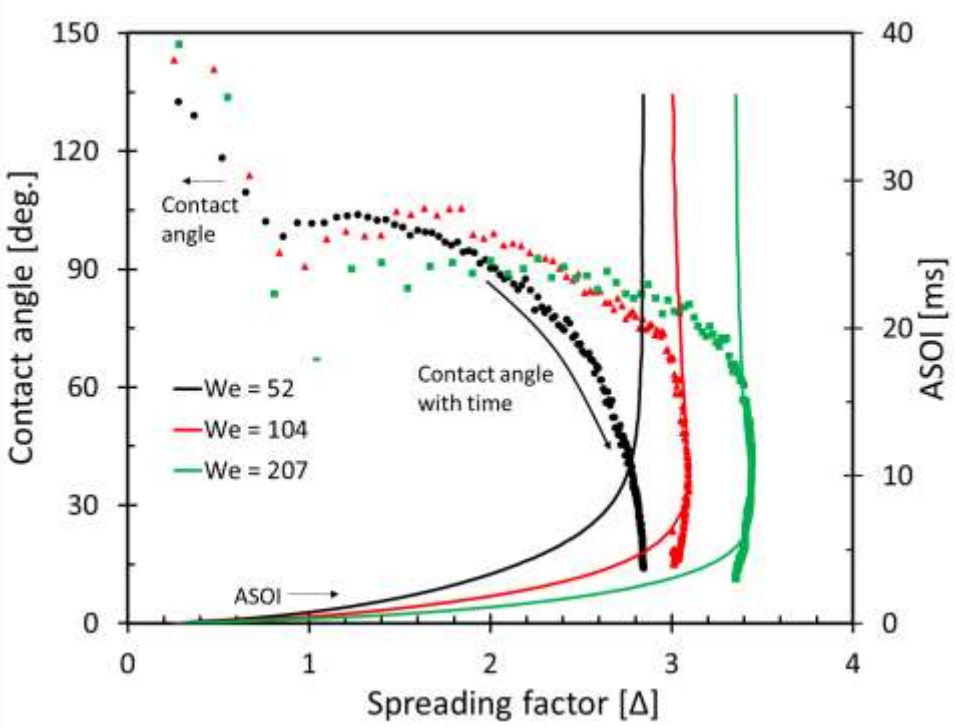

Figure 17. Contact angle vs Spread factor for diesel with time, at different Weber no. The second y-axis is time after start of impingement

The variation in contact line velocity and contact angle is shown in Figure 18. In Figure 18, initially, a spike on the contact line velocity graph at each condition is detected when the droplet impinges on the plate. Then, an almost exponential reduction of its magnitude with time is shown before the contact line velocity drops close to 0 m/s. This stage is known as the advancing phase. Next, at the impact *We* of 52 and 104 cases, it is difficult to observe the negative contact line velocity, however, at the impact *We* of 207, the contact line velocity starts to fluctuate around 0 m/s during the stage of time interval between 6.5 ms and 7.5 ms, the corresponding contact angle in Figure 18 decreases from the advancing contact angle to the receding contact angle in this stage. At later stage of the impact *We* of 207 case, after 10 ms, the contact line velocity exhibits negative values with the substantially smaller magnitude compared with the advancing phase, at which the droplet recedes. After 30 ms, the contact line velocity tends to 0 m/s and the equilibrium stage occurs. Despite all this, the receding and equilibrium stages are unapparent to be distinguished in the diesel case. Simultaneously, the dynamic contact angle is approximately 150° when the liquid droplet just interacts with the plate. Subsequently, the contact angle reduces rapidly to around 100°, and decreases during the rest of the advancing phase. The receding phase initiates when the dynamic contact angle drops to 30° around 10 ms and slowly decreases till 30 ms. After 30 ms, the contact angle becomes stable, which indicates the start of equilibrium stage.

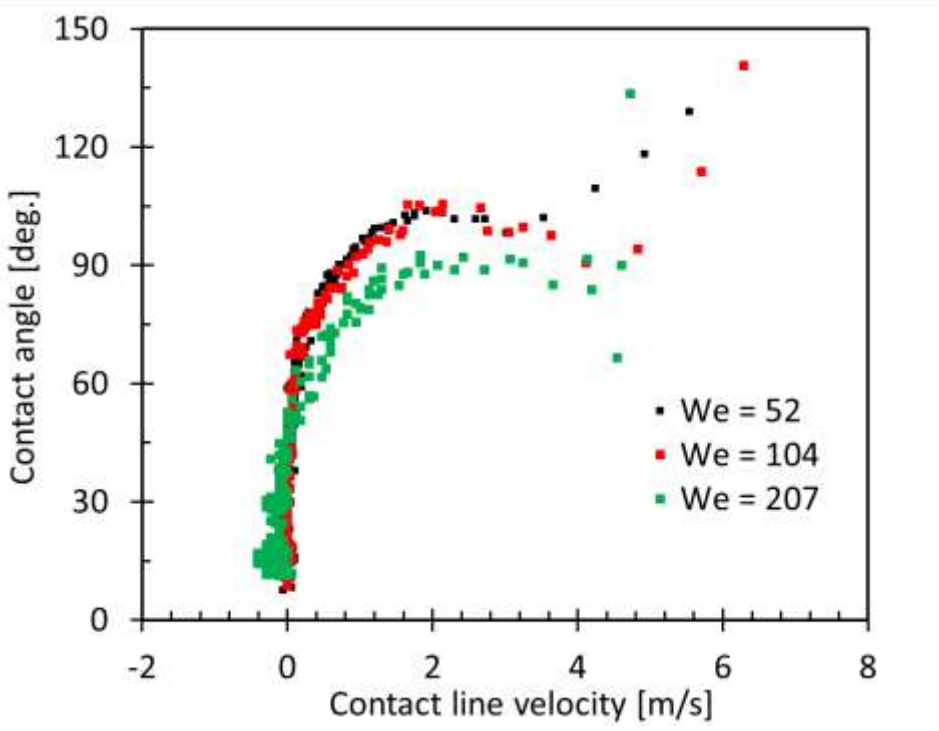

Figure 18. Contact line velocity vs Contact angle for diesel at various impact We.

4.2.1.2 WATER

Figure 19 shows the temporal evolution of water with increase in Weber no, which starts with impingement, spreading, receding and equilibrium. Figure 20 shows the spreading factor (top) and height ratio (bottom) for water at the various impact *We* conditions. The similar observation with diesel is shown here that the droplet impacts on the plate and spreads outward under the impact pressure in the beginning of the impingement. The spreading factor increases as the impact *We* increases while the height ratio decreases with the impact *We*, due to the relatively higher impact velocity and momentum at the higher impact *We*. The droplet reaches its maximum spreading distance and the maximum spreading factors obtained of 3.25, 2.4, and 2.0 around 5.5 ms, 6.0 ms, and 6.2 ms as the impact *We* reduces. Unlike diesel, the flattened droplet then starts to show an obvious recoiling under the capillary force and reshaping perpendicularly (see Figure 10 (top)). Additionally, because of higher surface tension and lower viscosity of water, an obvious decrease of spreading factor and increase of height ratio are observed in Figure 20. Around 22 to 25 ms with different impact *We*, the spreading factor tends to be stable while the height ratio shows small fluctuations because of slight oscillation occurred in water case. The height ratio at the impact *We* of 105 turns out to be stable after 30 ms.

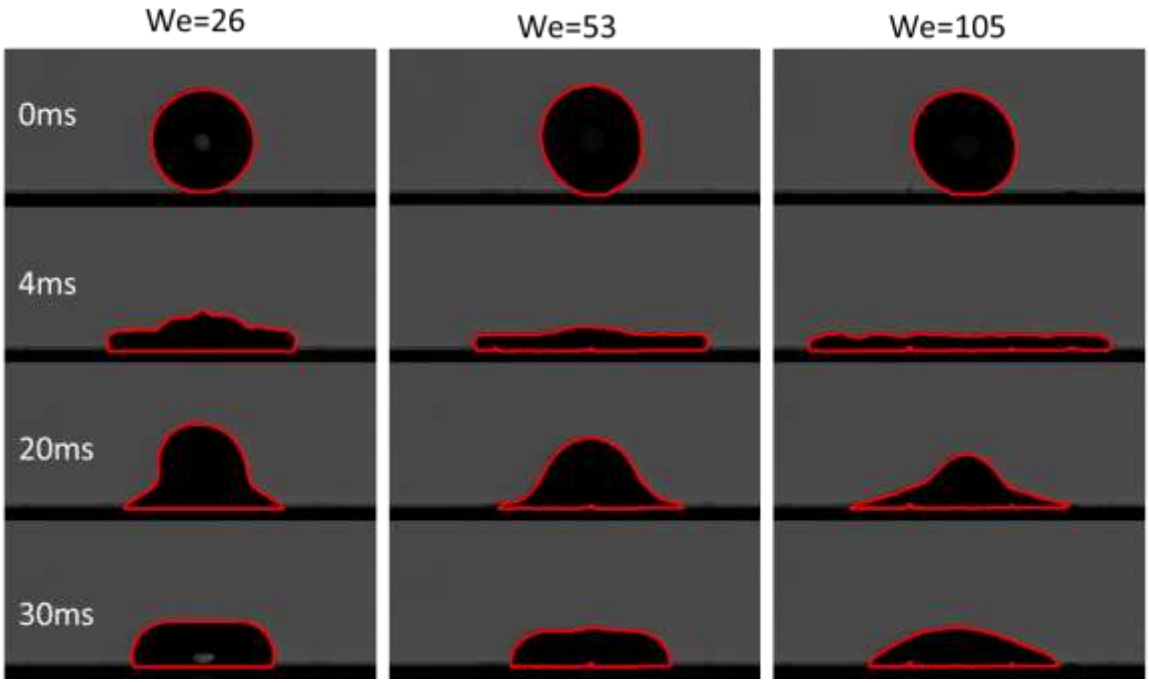

Figure 19. Ambient condition water droplet interaction with ambient temperature smooth plate at different Weber no.

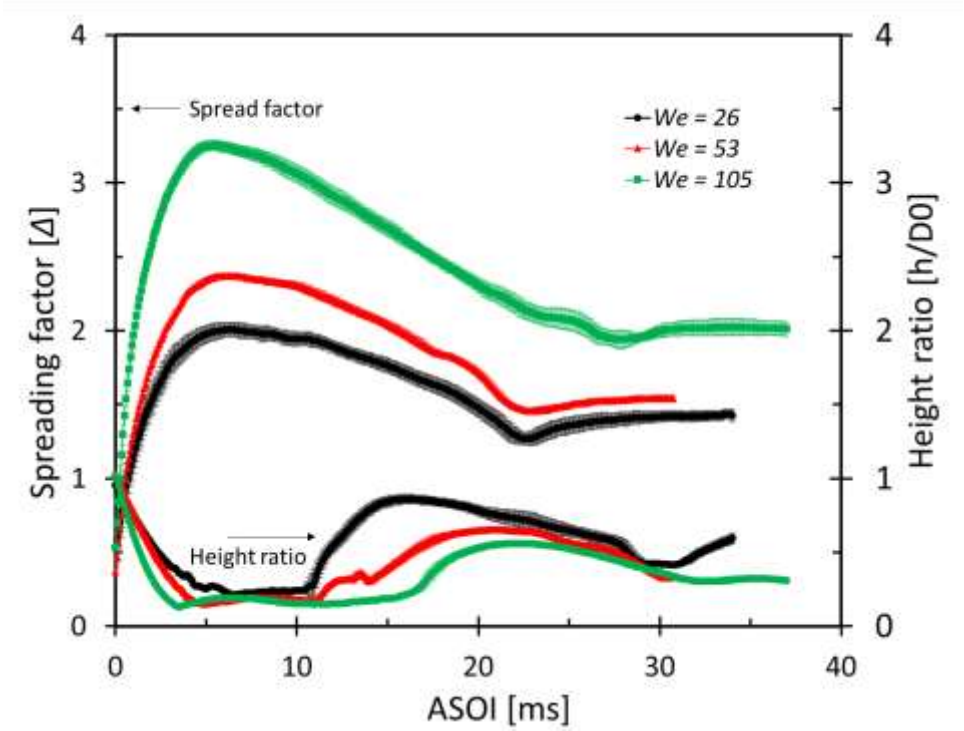

Figure 20. Spreading factor (top) and height ratio (bottom) for water at various impact We.

Figure 21 shows the results of the dynamic contact angle with spread factor variation for water droplet impinging on a smooth surface with different impact *We*. The dynamic contact angle for water is very different for diesel than water. The dynamic contact angle is approximately 150° when the liquid droplet just interacts with the plate. Subsequently, the contact angle reduces rapidly and then increases during the rest of the advancing phase. The receding phase initiates around 5 ms and the contact angle in this stage decreases till approximately 20 ms, then raises again due to the oscillation of water droplet, as the spread factor tends to rise again. After 30 ms, the equilibrium stage starts to begin. It can be observed from the figure, that the dynamic contact angle for water decrease with increase in *We* in all the phases, advancing, receding and equilibrium.

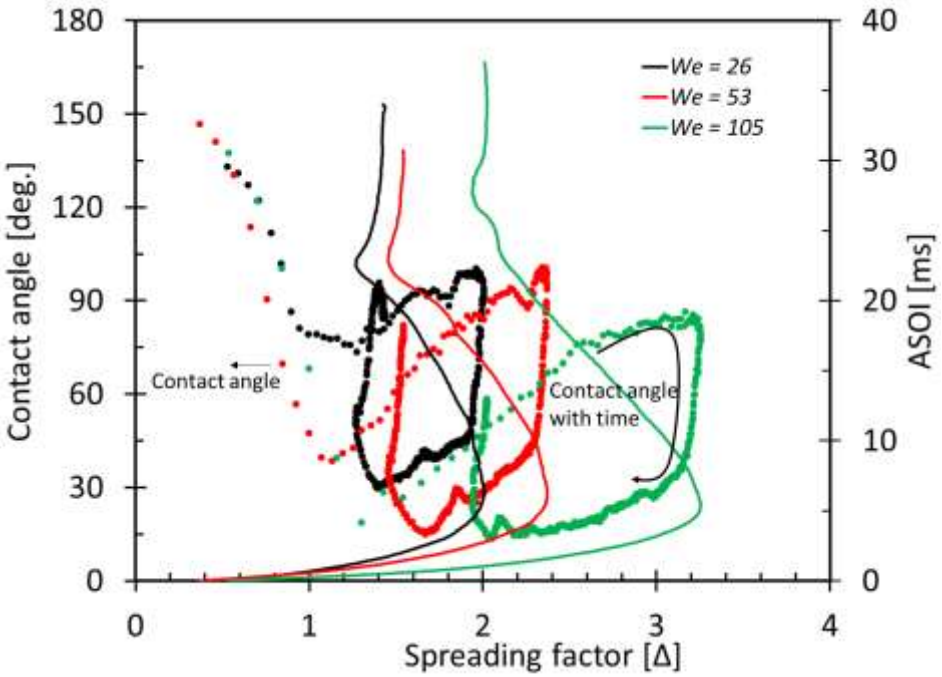

Figure 21. Contact angle vs Spread factor for water with time, at different Weber no. The second y-axis is time after start of impingement

The impact *We* has an insignificant effect on the contact line velocity as can be seen in the Figure 22. A similar phenomena of contact line velocity with diesel is seen in water in Figure 22. When the droplet impinges on the plate, a spike on the initial contact line velocity graph at each condition is observed. Followed by a dramatic reduction of its magnitude with time before the contact line velocity drops close to 0 m/s. After advancing phase, the contact line velocity starts to fluctuate around 0 m/s at 5.0 ms, the receding phase occurs. The equilibrium phase is presented afterwards. In Figure 22 the receding is prominent due to negative contact line velocity, which is different from diesel.

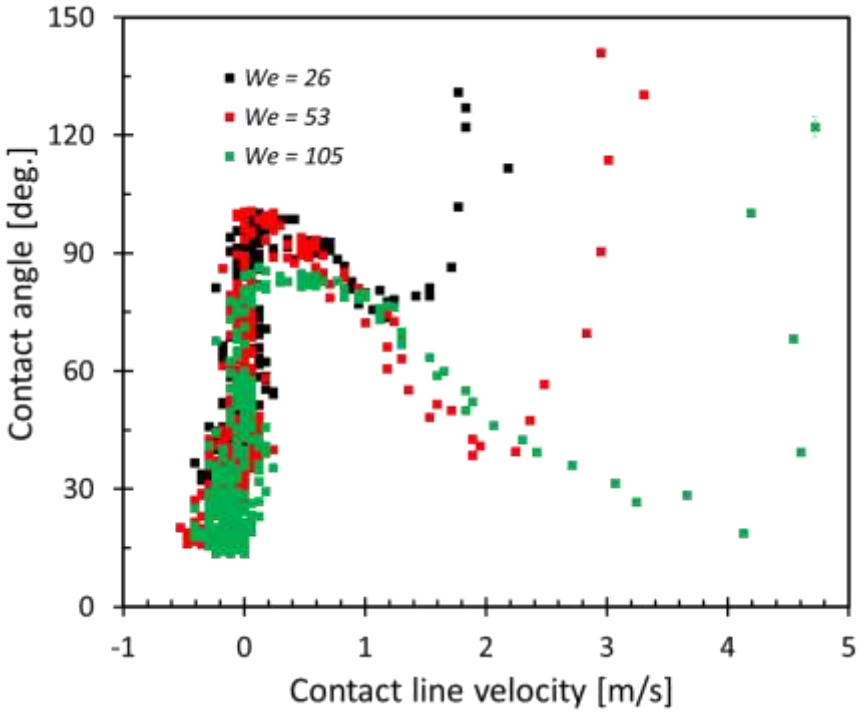

Figure 22. Contact line velocity vs Contact angle for water at various impact We.

Tables 6 and 7 summarized the results of the maximum spreading factor, advancing, receding, and equilibrium contact angles for both diesel and water at non-splashing conditions with various impact We. The maximum spreading factor both in diesel and water cases increases with the impact We due to the higher impact velocity and momentum at the higher impact We which drives the droplet moves outward. The averaged advancing contact angle from diesel case ranges from 55° to 76° which shows insignificant difference as displayed in Figure 16, the averaged advancing contact angle based on different conditions is around 68°. Furthermore, in diesel case, the receding and equilibrium contact angles at various impact We change at a small scale. The averaged receding contact angle is 20° that is around 3° larger than the averaged equilibrium contact angle of 17°. At water case, the range of averaged advancing contact angle is from 53° to 93° and the averaged advancing contact angle in terms of all various conditions is about 75°. Unlike diesel case, the receding contact angle is quite smaller compared with the equilibrium contact angle at each condition. As well, the receding and equilibrium contact angles at each condition show clear differences, they decrease with the impact We. The averaged receding contact angle is 30° and the averaged equilibrium contact angle is around 55°.

The differences in the behavior of droplet dynamics of water and diesel arises because of the differences in property of diesel and water. The higher viscosity of diesel and lower surface tension, the viscous dissipation energy during diesel impingement is higher causing bigger liquid-surface contact.

Table 6. Post-impingement properties for diesel at various impact We.

Case	Height (mm)	Impact We	Max. Δ	θ_{adv} (°)	θ_{rec} (°)	θ_{eq} (°)
1	26	52	2.9	55	15	15
2	52	104	3.1	76	22	19
3	57	113	3.2	70	23	20
4	104	207	3.5	74	20	12
5	114	226	4.5	67	20	16

Table 7. Post-impingement properties for water at various impact We.

Case	Height (mm)	Impact We	Max. Δ	θ_{adv} (°)	θ_{rec} (°)	θ_{eq} (°)
1	26	26	2.0	93	45	88
2	52	53	2.4	83	36	61
3	57	57	3.1	79	33	53
4	104	105	3.3	73	25	52
5	114	115	3.3	69	25	42
6	195	196	3.7	53	18	36

4.2.2 EFFECT OF TEMPERATURE

As mentioned in the Experiments chapter, to effectively capture the effect of temperature of droplet and plate, different conditions are derived: Isothermal and Non-isothermal. Isothermal conditions help to focus on only the variation in droplet dynamics dur to variation in thermophysical properties. Whereas non-isothermal conditions help us understand the effect of heat transfer from droplet to plate. Accurate modelling of spray wall interaction requires distinction of different outcomes of a single droplet impact and development of corresponding transition criterion. These outcomes determine the post-impact mass, momentum and energy distributions of the droplets. When a droplet impacts a solid, stationary surface, it spreads and form a lamella bounded by a thicker rim. The droplet tends to spread toward maximum spreading diameter, and then undergo equilibrium with or without the process of receding and spreading again. The event of receding after reaching maximum spreading diameter depends on the competition among surface tension, capillary, inertia and viscous forces. The images captured for each test condition, are shown in sequence in Figures 19,20 and 21, efficiently describing these events. Figure 23

illustrates the droplet shape evolution at isothermal conditions at various time instants. The non-isothermal conditions are displayed in Figure 24 and Figure 25. In Figure 23 the droplet temperature is held constant at 25℃ and plate temperature is varied from 100, 125 and 150℃. Whereas in Figure 25 the plate temperature is constant at 25℃ and diesel droplet temperature is varied from 100, 125 and 150℃. The impact velocity is maintained same for all the conditions at 1.43 m/s, by maintaining the same height of the droplet release. The corresponding droplet properties, including diameter (D_0), surface tension (σ), kinetic viscosity (ν), liquid density (ρ), Reynolds number (Re), Weber number (We), and Ohnesorge number (Oh), are listed for each droplet temperature (T_d) in Table 8. To capture the droplet dynamics events accurately the area which covers the droplet on the wall is kept in focus. The time stamps for each image is selected to emphasize the milestone events which differentiate these conditions from each other.

Table 8. Droplet properties at different test temperature.

Td	Do	Σ	ν	ρ	Re	We	Oh
$°C$	mm	N/m	cSt	kg/m3			
25	2.81	0.0288	3.36	848	1197	170	0.011
75	2.73	0.0253	1.37	811.6	2852	179	0.0047
100	2.64	0.0235	1.01	793.4	3741	183	0.0036
125	2.5	0.022	0.77	775.2	4647	180	0.0029
150	2.44	0.02	0.61	757	5725	189	0.0024

A series of non-splashing events for droplet impinging on a smooth plate with the baseline test condition, i.e. 25℃ droplet and 25℃ plate, is observed in Figure 23. From top to bottom, there are (a) impingement, (b) post-impingement, (c) maximum spreading, and (e) equilibrium. Since no receding is observed in this case, equilibrium event is shown directly after advancing. The droplet diameter for the baseline case is 2.81 mm. The diesel droplet size reduces as the temperature of droplet is increased, due to changes in density and surface tension with temperature. The diesel droplet size for all the cases are listed in Table 8. The impinged droplet clearly starts to spread much more rapidly with increase in temperature as can be seen at 2ms. This can be attributed to lower viscosity and lower surface tension. Since there is no heat loss at the isothermal conditions, these variations can be attributed to thermophysical property changes.

The maximum spread factor is reached at around 10 ms for all the isothermal conditions. After 10 ms the contact angle of the impinged droplet keeps on decreasing, whereas the liquid solid contact area remains same. No receding is observed in any of the isothermal

case, except 75°C. A slight difference in the spreading diameter is observed between 10 ms and 40 ms for 75°C.

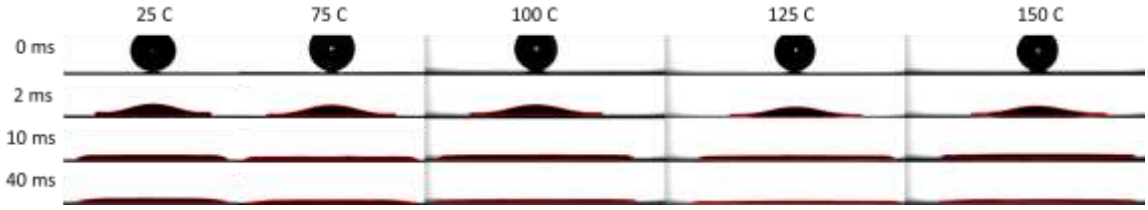

Figure 23. Isothermal conditions with same temperature wall and droplet as represented.

Figures 22 and 23 show the non-isothermal test condition sample images. Figure 24 shows the non-isothermal case with heated wall-cold droplet. The time stamps chosen here are more than those shown in isothermal case, due to increase in the events happening after the impingement. When a cold droplet impacts on a heated plate, the droplet initially spreads to maximum spreading diameter and then starts to recoil and reaches a certain spread factor. The process of transition from spreading to recoiling continues and the strength of recoiling depends on the temperature of the plate. The maximum height ratio is a good indicator of the strength of recoiling. For the heated wall and cold droplet conditions the droplet attains equilibrium only for 100°C, whereas the damped oscillations continue for 125°C and 150°C plates even after recorded time of 140 ms. The events in Figure 24 are shown corresponds to 1) impingement; 2) spreading; 3) maximum spreading; 4) receding; 5) spreading again; 6) attaining almost equilibrium.

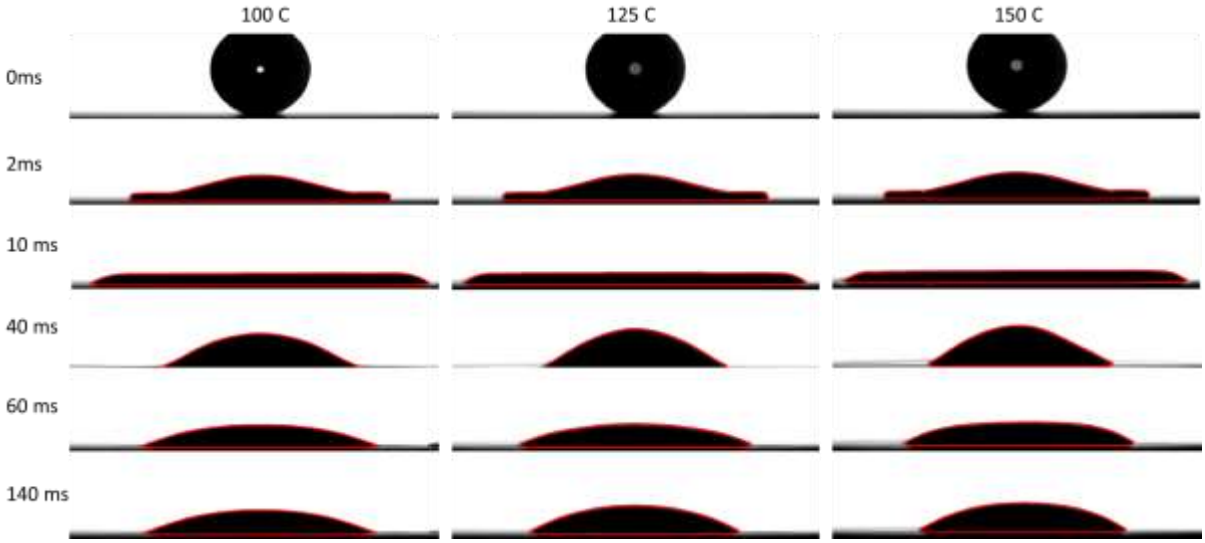

Figure 24. Non-isothermal conditions with heated wall-cold droplet. From the left to right the images: 1) 100C wall and 25 C droplet; 2) 125C wall and 25C droplet; 3) 150C wall and 25C droplet.

Figure 25 displays the impingement dynamics of a heated droplet impinging on a cold plate. This condition is the similar conditions occurred in the cold-start condition of internal combustion engines. For these conditions only spreading and equilibrium phases are observed, and no receding is seen in any case. Even for these conditions the maximum Spread factor occurs around 10 ms. Figure 25 shows the following events: 1) impingement; 2) spreading; 3) maximum SF and 4) equilibrium.

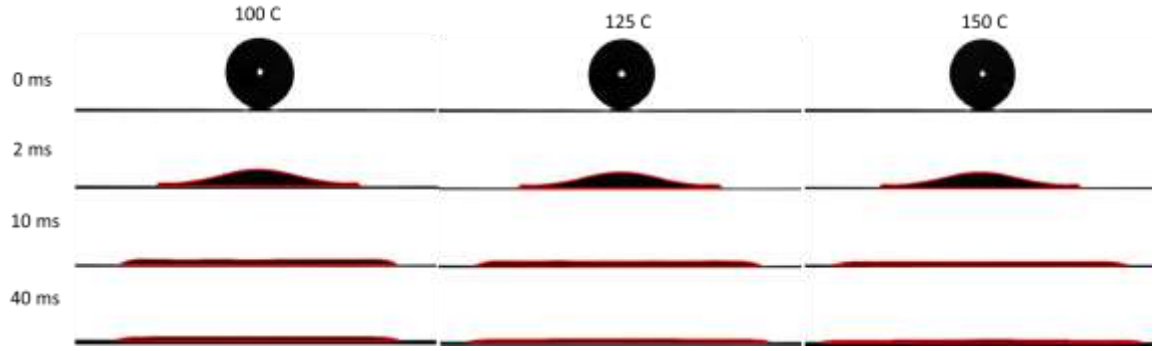

Figure 25. Non-isothermal conditions with heated droplet-cold wall. From the left to right the images: 1) 100C droplet and 25C wall; 2) 125C droplet and 25C wall; 3) 150C droplet and 25C wall.

4.2.2.1 ISOTHERMAL CONDITIONS

The effect of thermophysical properties on the droplet impingement dynamics characteristics is presented in this section. As explained before, these characteristics includes spreading factor, height ratio, Contact line velocity, and dynamic contact angle of an impinging droplet. The test conditions are selected to cover the variations in thermophysical properties of diesel with increase in temperature. As the properties seen in Figure 4, the surface tension and viscosity of the droplet at 25℃ are high, and they both decrease with the increase in temperature. Although there is a linear decrease for surface tension, viscosity decreases exponentially. All the impinged droplet characteristics presented are averaged from 3 repeats. The data shown here is after start of impingement (ASOI), when the spreading diameter becomes larger than the impact droplet diameter. This is done to remove uncertainties introduced by the rapid evolution in the droplet shape during the initial stages.

Figure 26 shows the spread factor and height ratio for diesel fuel at various isothermal conditions. During the earlier stage of impingement, the droplet spreads rapidly by transforming the kinetic energy into the translational energy. All the isothermal conditions reach maximum spreading diameter at around same time, but significant differences are observed between the magnitude of spread factor achieved at each condition. The maximum spread factor ranges between 3.5 to 4.75. Although the impact velocity for all the isothermal conditions are same, but the decrease in viscosity is much higher when increasing the temperature of the droplet, than the decrease in density. This is confirmed by a constant increase in Reynolds number with increase in temperature. In addition, the difference in maximum spread factor starts to reduce at higher temperature, as maximum spread factors for 125℃ and 150℃ are 4.6 and 4.7, respectively. This is

due to asymptotic nature of decrease in viscosity with temperature, as variation in viscosity for the two temperature is very less. In addition, for 100 and 125℃ cases the spread factor keeps on increasing negligibly after 10 ms. The height ratio expectedly follows opposite trend. The low temperature conditions have higher height ratios than the higher temperature. The height ratios for 100, 125 and 150℃ are similar, whereas the height ratio at 75℃ is showing a higher value, and 25℃ case has the highest height ratio. A relatively small up and down trend is seen in the height ratio, for all cases around 5-10 ms. This is because when the liquid droplet impinges the surface and spreads out completely initially, most of the liquid is pushed into the rim, making the rim thicker and hence the lamella region develops a void near the center. When the droplet stabilizes, after reaching maximum spread factor, this extra liquid from the rim moves back into the lamella center uniformly and thus decreases the overall height of the impinged droplet.

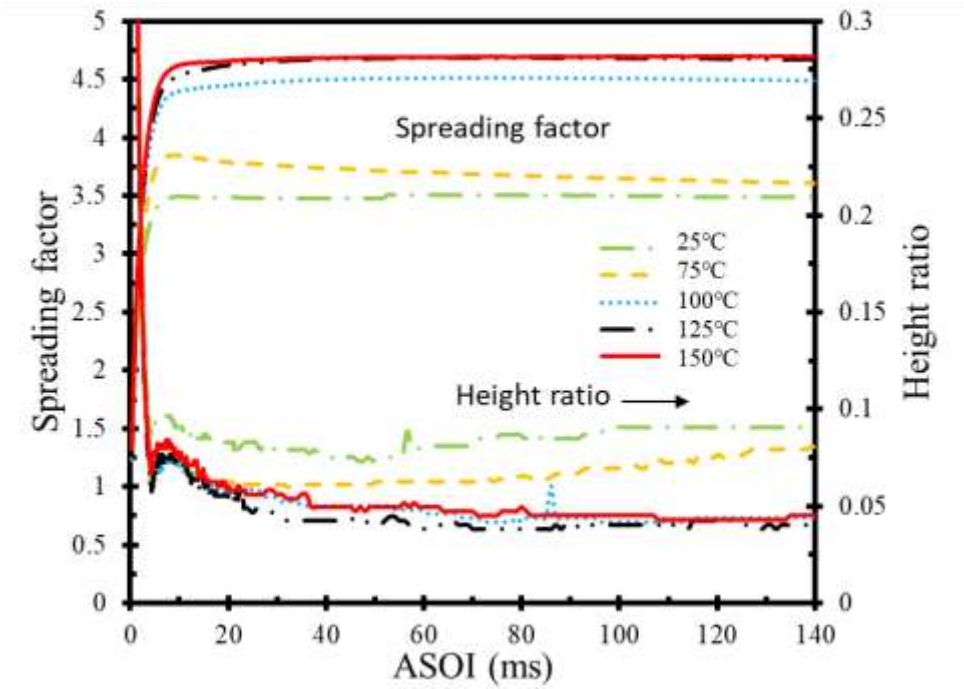

Figure 26. Spread factor and height ratio of impinging droplet at isothermal conditions of temperature in range of 25-150℃.

After the maximum spreading, the droplet hardly recedes in any case, except for 75℃. Receding for 75℃ is justified by not just observing the increasing trend of height ratio, but also a reduction in spread factor. This is an anomalous behavior and can be pointed towards the difference in the rate of decrease of surface tension and viscosity. The asymptotic decrease in viscosity of diesel leads to very low viscous forces, but sufficiently high surface tension forces. Thus, the lower viscous forces and higher surface tension forces makes it possible for receding to take place. On further increase or decrease in temperature the viscous forces and surface tension forces are close enough again to eliminate any receding. Overall this test indicates that decrease in thermophysical properties of diesel makes it more prone to spread to a larger area.

To understand the relation between spread factor and contact angle, they are plotted together against time in Figure 27, in which the contact angle data is in time sequential from left to right following the clockwise direction. The graph shows the variation of spread factor with time and displays corresponding contact angle at each spread factor. The contact angle initially increases during the rapid advancing phase of droplet till around 5ms. When the advancing becomes slightly slower the contact angle reaches a maximum and start decreasing even when the droplet is expanding. Once the droplet hits maximum spread factor and tries to achieve equilibrium phase, the contact angle rapidly decreases and becomes stable near 20 degrees. A slightly different trend is observed for 75°C which has the lowest contact angle value at the equilibrium condition. In addition, 75°C also showed a different decreasing slope for contact angle when the spread factor becomes constant. This contact angle be attributed to the receding nature of 75°C diesel droplet.

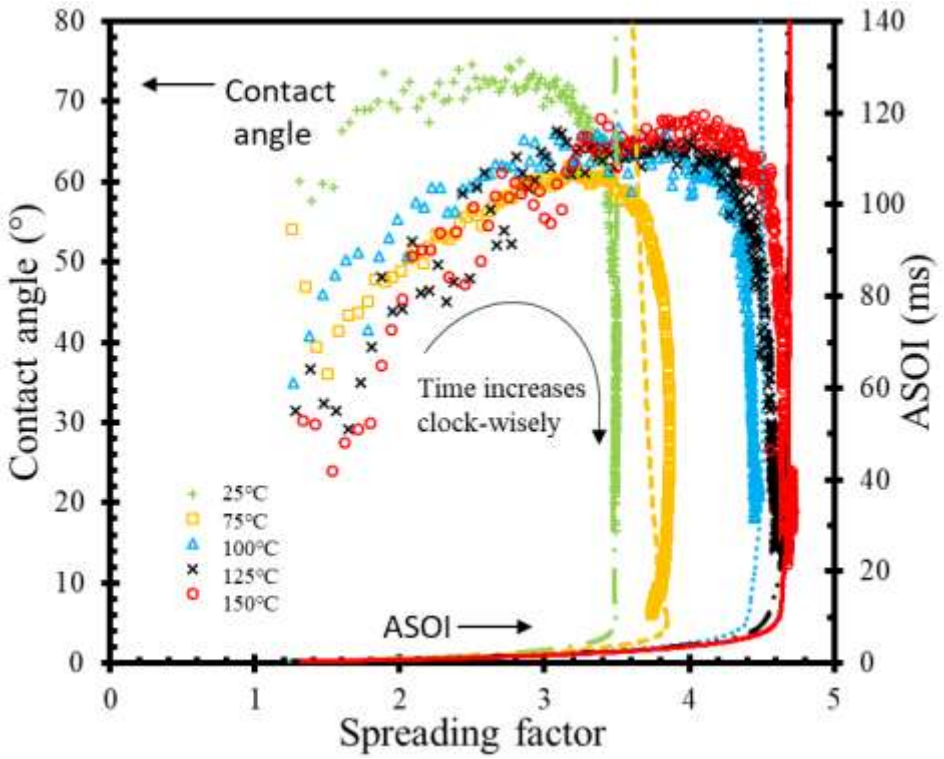

Figure 27. Contact angle vs spreading factor at isothermal conditions of temperature in range of 25-150°C, the second y-axis is time after start of impingement

The contact line velocity plot shown in Figure 28 does not shown any variation in contact line velocity with increase in temperature, therefore, similar relationship plot is plotted between contact angle and contact line velocity in Figure 28. The main observation that can be drawn from this figure is the contact angle initially increase when the contact line velocity rapidly decreases from 3 m/s to 0.5 m/s (0-3 ms ASOI), and then decrease after 10 ms. When the droplet impinges, the liquid from lamella center is pushed to the rim during rapid spreading, contact angle using an increase in the contact angle. When the

droplet almost reaches maximum spread factor, the contact line velocity slows down enough. This causes the liquid from the rim to flow back into the center of the lamella, hence reducing the contact angle. Secondly in these isothermal cases, the negative contact line velocity is negligible and only prominent for 75℃. Thus, the variation in thermophysical properties, though does not affect the contact angle directly, but determines whether the droplet will recoil or not. neglecting the initial high contact line velocity part, the contact angle of 25℃ remains relatively stable when the contact line velocity is larger than certain value (~0.5m/s), which is called contact angle saturation. However, with the elevated temperature, the saturation effect doesn't exist anymore, which is also found in the non-isothermal conditions.

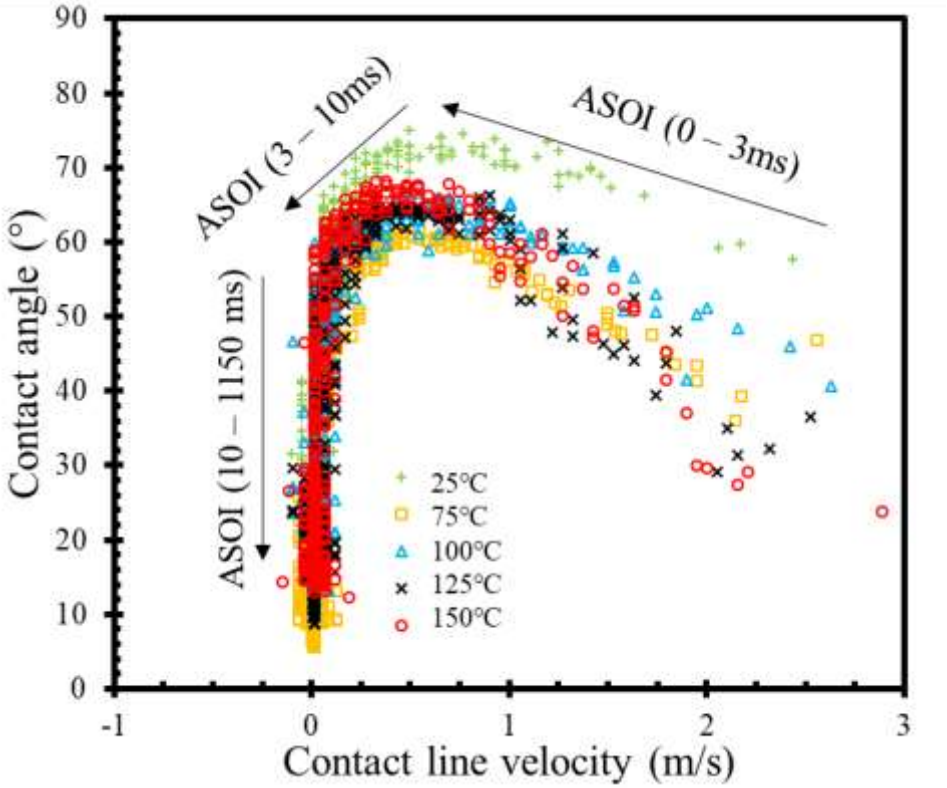

Figure 28. Contact angle vs contact line velocity factor at isothermal conditions of temperature in range of 25-150℃.

Table 9 summarizes all the findings for isothermal conditions. the advancing contact angle is calculated as the average of dynamic contact angle achieved during the spreading phase. The equilibrium contact angle was estimated at ASOI = 140 ms, as the equilibrium is achieved by then. It is noted here the advancing phase of the impinged droplet is only considered until 10 ms. The maximum spread factor shows a positive correlation with the temperature increase. However, there is no clear trend of the equilibrium contact angle. the lowest advancing and equilibrium contact angles are found when temperature is at 75℃.

Table 9. Spread factor max, Height Ratio min and advancing, receding and equilibrium Contact Angles for all cases in isothermal conditions.

Droplet and Wall Temperature (^oC)	Spread factor (max)	Height ratio (min)	Advancing Contact Angle (deg.)	Equilibrium Contact Angle (deg.)
25	3.5	0.087	64.9	11.6
75	3.85	0.064	52.4	7.9
100	4.4	0.056	58.3	9.7
125	4.54	0.058	56	12.14
150	4.62	0.067	59	10.04

4.2.2.2 NON-ISOTHERMAL CONDITIONS

4.2.2.2.1 COLD WALL-HEATED DROPLET

Analysis of the post impingement dynamics was solely focused on the thermophysical properties variations at the isothermal conditions. However, the droplet-wall interaction process is more complicated in non-isothermal conditions due to the present of transient heat transfer process. This section is going to present the quantities results of the non-isothermal conditions with varied wall temperatures. When the droplet temperature was kept at 25℃, the plate temperature was heated to 100, 125 and 150℃ for non-isothermal conditions. The change of the spread factor and height ratio of the droplet with time under various plate temperature are shown in Figure 29. It is observed from the plot, when the ambient temperature drop interacts with elevated temperature metal plate, it tends to rapidly spread and then recoil significantly. Then the transition between advancing and receding occurs several times before finally reached the equilibrium phase, which is called oscillation. One consequent advancing and one receding together is defined as an oscillation cycle. The amplitude of these oscillation keeps decreasing as time goes on.

The initial maximum spread factor is approximately same, 3.6, for all three plate temperature and occurs around the same time of 10 ms. However, the receding has different rate depending on temperature, i.e higher temperature plate shows faster and higher receding. This is observed via both spread factor and height ratio plots; i.e interaction with 150^{o}C leads to highest height ratio of 4.8 and lowest spread factor of 1.8, once receding ends, whereas interaction with 100^o C leads to maximum height ratio of 4.1 and minimum spread factor of 2.1 after receding ends. The amplitude of these oscillation cycle also increases with increase in plate temperature, and equilibrium is delayed.

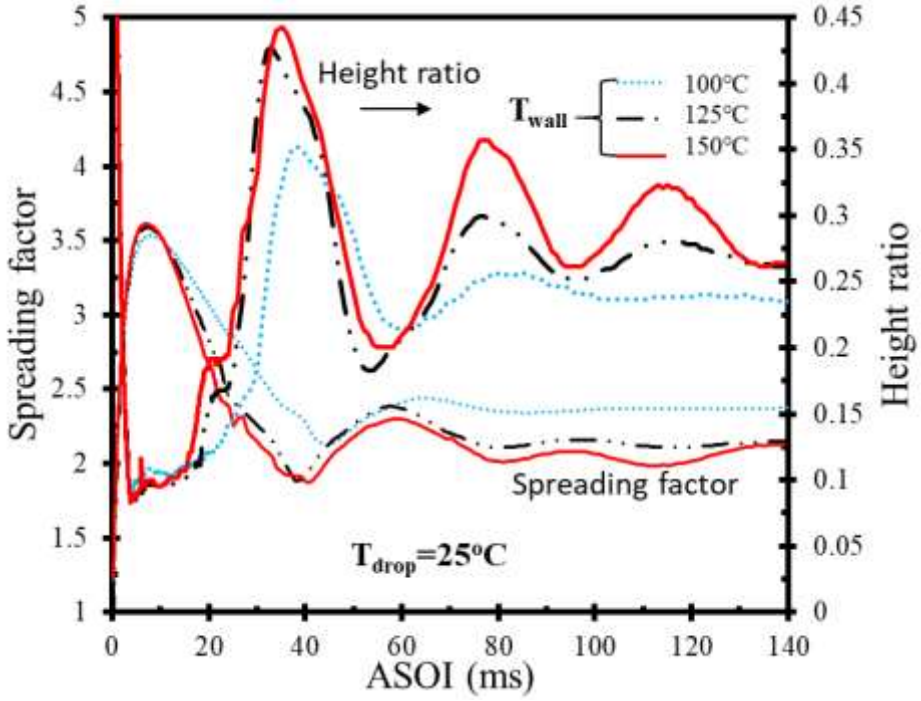

Figure 29. SF and HR of impinging droplet at non-isothermal conditions (heated wall and cold droplet) of temperature in range of 25-150°C.

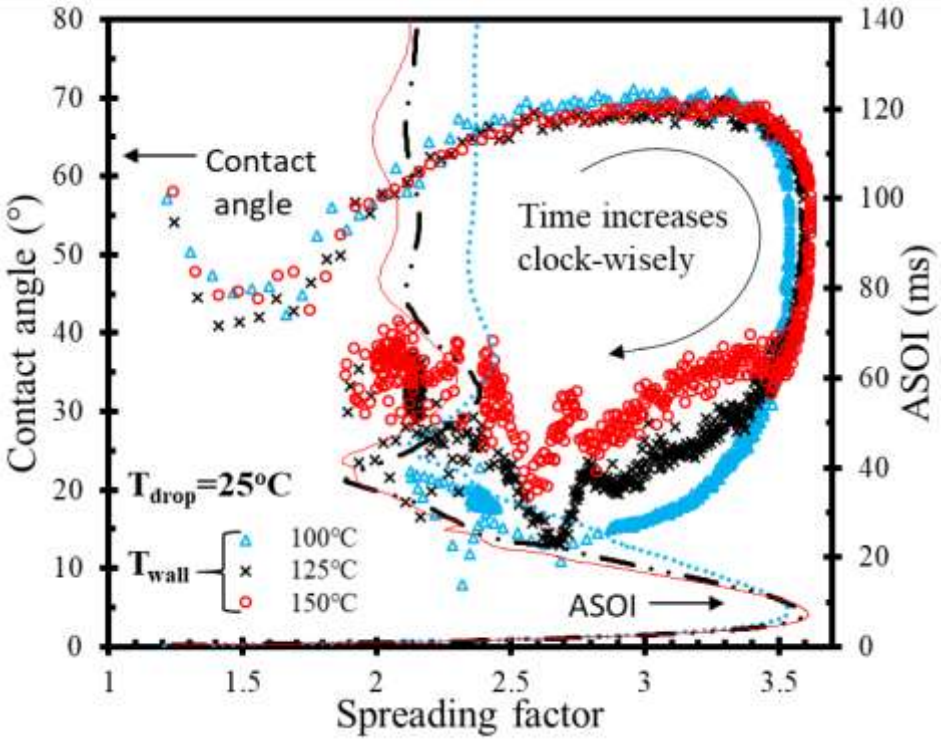

Figure 30. Contact angle vs spreading factor at non-isothermal conditions (heated wall and cold droplet) of temperature in range of 25-150°C

The relationship between contact angle and spread factor and the change of spread factor with time is shown in Figure 30. As shown in Figure 30, with the passage of time, the spread factor reaches its highest point at around 10ms. This illustrates the first spreading process after droplet impinging on the plate. During this process, as the spread factor increases, the contact angle declines first (shown at the top left of the figure), then rise to its peak and decreases rapidly, due to the motion of fluid from center to rim of lamella. During the oscillation phase, after the receding begins, the dynamic contact angle increases with plate temperature.

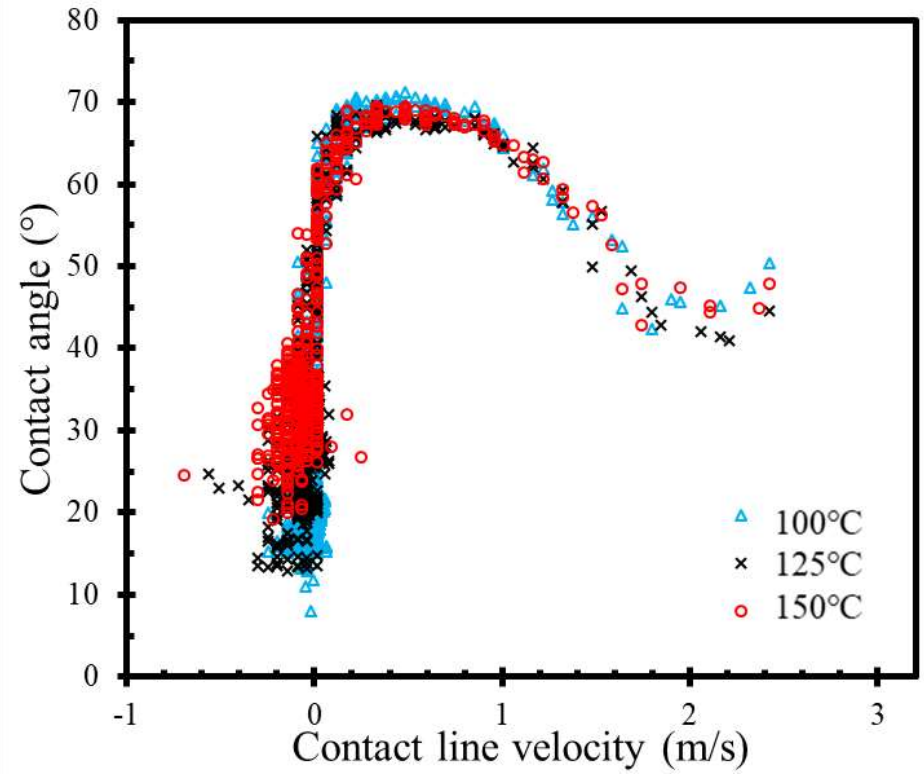

Figure 31. Contact angle vs contact line velocity factor at non-isothermal conditions (heated wall and cold droplet) of temperature in range of 25-150°C

Figure 31 shows the change in contact angle with the contact line velocity. Initially during the spread phase, the contact line velocity rapidly decreases, due to sudden deformation in the initial impingement process. Once after the deformation process, decelerating spread process begins, which is accompanied with increase and then decrease in contact angle. This increase and decrease in contact angle during spread process and a brief period of equilibrium, before which first receding begins, can be attributed to the internal motion of fluid in the confined droplet. The contact angle decreases rapidly for all the three cases rapidly when the receding occurs, and then increases to begin the oscillation phase of advancing and receding.

During these oscillations, the contact line velocity starts to vibrate near 0, and the contact angle also fluctuates around a certain value in that the droplet is supposed to experience

several processes of receding and expansion to acquire a relatively stable state. When the contact line velocity is around zero, the minimum of contact angle increases from 12° to 28°, as the plate temperature rises up from 100℃ to 150℃.

Table 10 lists the maximum spread factor, minimum height ratio and advancing, receding and equilibrium contact angles for the cases in non-isothermal condition of heated wall-cold droplet interactions. The average receding contact angle is calculated like the average advancing contact angle over the receding phase. Only the first receding motion is taken to calculate the average receding phase. Although the contact angle at the last recorded time is shown as equilibrium angle in Table 10, however it is pointed out that 125 and 150℃ cases do not achieve equilibrium at 140 ms. Slight oscillations are still observed in the spread factor vs time at 140 ms for these two conditions as seen in Figure 29. The maximum spread factor, receding Contact angle, and equilibrium Contact angle show positive correlations with the wall temperature increase. The advancing contact angle maintains relative stable value around 64.5°.

Table 10 Maximum spread factor, Minimum height ratio and advancing, receding and equilibrium CAs for all cases in non-isothermal heated wall-cold droplet conditions.

Wall Temperature (°C)	Max Spread factor	Min Height ratio	Advancing Contact Angle (deg.)	Receding Contact Angle (deg.)	Equilibrium Contact Angle (deg.)
100	3.53	0.089	65.16	29.9	22.2
125	3.59	0.079	64	32	34.8
150	3.61	0.082	64.3	36.1	36.2

4.2.2.2.2 HOT WALL-COLD DROPLET

Finally, for the non-isothermal tests, the droplet temperature was heated to 100℃, 125℃ and 150℃, when the initial wall temperature was kept at 25℃. The change of the spread factor and height ratio of the droplet with time under various plate temperature are shown in Figure 32. The spread factor rapidly increases to 4 within ASOI = 4 ms, for all the cases of elevated droplet temperature. Then it continues increasing, but with a quickly decayed increasing rate, to the highest point 4.25 (100℃), 4.4 (125℃) and 4.75 (150℃) at round ASOI = 40 ms and reaches the steady state. This indicates that the higher the droplet temperature, the larger equilibrium spreading diameter the droplets can be obtained partially due to the less energy dissipation during impingement, which is caused by the low viscosity. However, the early (< 4 ms) post impingement dynamics is not affected by the initial droplet temperature. Discrepancy of dynamics is seen after ASOI = 4 ms when the droplet expansion slows down. Therefore, it can be reasoned out that the inertia driven spreading is not affected by droplet temperature, whereas capillary driven spreading is highly impacted by droplet temperature. The higher the spread factor, the

lower the height ratio. Therefore, the overall change of the height ratio over the time shows exactly an opposite tendency to that of the spread factor. The height ratio declines dramatically to approximately 0.06 (100, 125 and 150°C), from 0 to 4ms. Then it gradually decreases and reaches its lowest value at ASOI = 4 ms.

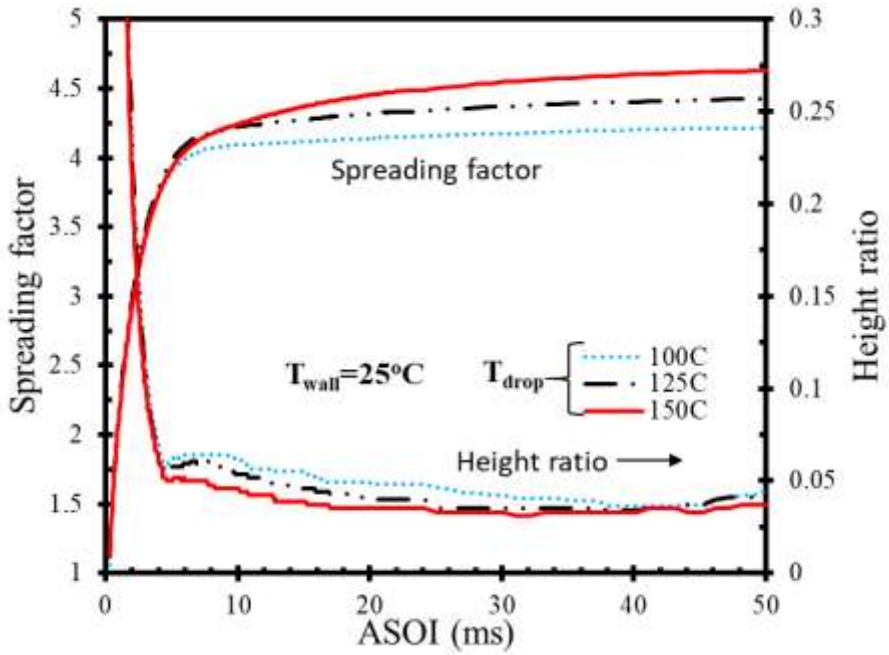

Figure 32. SF and HR of impinging droplet at non-isothermal conditions (cold wall and heated droplet) of temperature in range of 25-150°C.

Figure 33 shows the relationship between Contact angle and spread factor and the change of Spread factor with time. As the spread factor increases, the contact angle dramatically declines from 65° to 35° first (i.e. until spread factor of 1.5), then slowly rise to its peak (54° at 100°C, 51° at 125°C and 49° at 150°C) at spread factor of 3.5 and decreases rapidly between spread factor of 3.6 and 4.4, finally reaches a relative equilibrium value (~15°) after several relative small oscillations in contact angle. Because there is no receding motion in non-isothermal heated droplet conditions, so oscillations here are different with the oscillations discussed in heated plate case. The oscillations here are only reflecting on the contact angle, instead of spread factor and height ratio, when the spreading slows down and transitions to equilibrium state. This type of oscillation is defined as internal oscillation, due to no changes of the droplet location and spreading diameter.

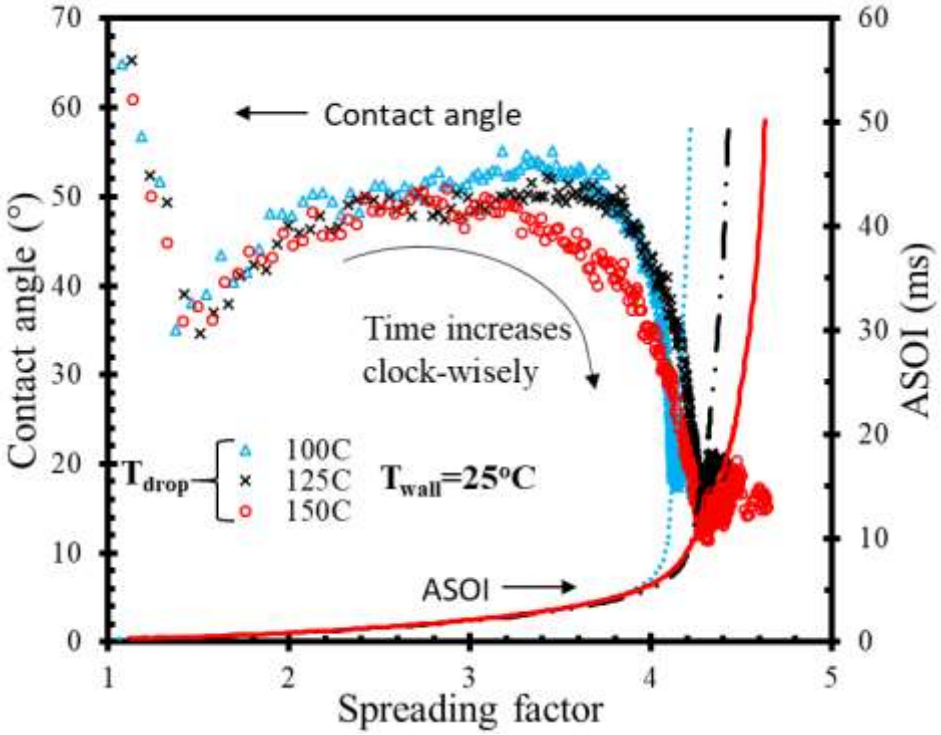

Figure 33. Contact angle vs spreading factor at non-isothermal conditions (cold wall and heated droplet) of temperature in range of 25-150℃

In the non-isothermal heated plate case (Figure 30), three different temperature conditions start showing contact angle variation with temperature in the receding stage, after reaching spread factor of 3.4. However, in the heated droplet case, the contact angle differs when the spread factor becomes 3. Obviously, while the droplet temperature increases from 100 to 150℃, the contact angle keeps decreasing. After the spread factor surpasses 4 (at around ASOI = 5 ms), the contact angles from all three different temperature conditions become similar again and tend to be stable, meanwhile the spread factors continue slowly increasing until the 40 ms.

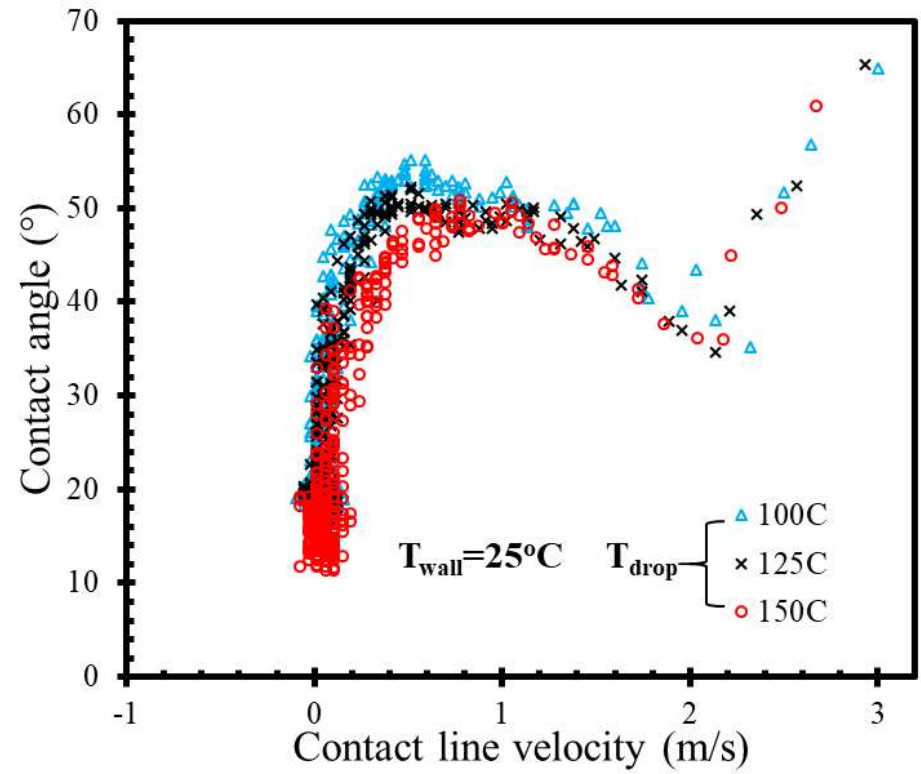

Figure 34. Contact angle vs contact line velocity factor at non-isothermal conditions (cold wall and heated droplet) of temperature in range of 25-150℃

The change of contact line velocity with the impinged droplet contact angle is shown in Figure 34. This is useful information to establish a contact line angle model for CFD simulation. First, no negative contact line velocity data was found in current conditions, which means there is no obvious receding motion. At around contact line velocity = 0.5 m/s, contact angle value reaches a peak (54° at 100℃, 51° at 125℃ and 49° at 150℃) which is smaller than it is in isothermal conditions (73° at 25℃, 60° at 75℃, 62° at 100℃, 64° at 125℃ and 66° at 150℃) and non-isothermal heated plate conditions (~68° at 100, 125 and 150℃). Another finding is that there are large variations in contact angle at zero Contact line velocity. It is may be related to the internal oscillations. When the droplet is approaching the equilibrium state, the spread factor is not changing anymore, however, internal wave bounces between the center and the rim of the droplet causes the internal oscillations and changes mass distraction inside the droplet. The internal oscillations finally lead to the large contact angle variations at zero contact line velocity. The lowest contact angle at zero contact line velocity is also the lowest contact angle overall. In the non-isothermal heated plate conditions (Figure 31), the increased plate temperature leads to higher minimum contact angle (7° at 100℃, 13° at 125℃ and 19° at 150℃). However, the opposite trend is found here in Figure 34, minimum contact angle is 17° at 100℃, 15.5° at 125℃ and 11.6° at 150℃.

Table 11 lists the maximum spread factor, minimum height ration and advancing and equilibrium contact angles for the cases in non-isothermal condition when the heated droplet interacts with the cold wall. Since there is no receding in this case as well, receding dynamic contact angle is not listed out. As plate temperature is increased from 100 to 150℃, the maximum spread factor slightly increases from 4.1 to 4.24, the advancing contact angles and equilibrium contact angles decreases from 45° to 36.6° and from 12° to 9.75°, respectively.

Table 11. Maximum spread factor, Minimum height ratio and advancing and equilibrium contact angles for all cases in non-isothermal heated droplet conditions

Droplet Temperature (°C)	Maximum spread factor	Minimum height ratio	Advancing Contact angle (deg.)	Equilibrium Contact angle (deg.)
100	4.1	0.057	45	12.04
125	4.22	0.053	42.06	10.9
150	4.24	0.046	36.6	9.75

4.2.2.3 ANALYSIS OF EFFECT OF TEMPERATURE

This section discusses a hypothesis that describe a probable reason for different droplet dynamics observed after impingement. Through all the tested conditions including isothermal and non-isothermal conditions, very different droplet dynamics are observed. For example, receding was only found in isothermal 75℃ condition and all the non-isothermal heated plate-cold droplet conditions

To understand this, let's start with isothermal conditions. First, the baseline condition isothermal 25℃ doesn't show any sign of receding. Among all the isothermal conditions, only 75℃ condition has a weak receding. Because no-heat transfer is involved in the isothermal condition, the temperature dependent liquid properties attribute to the changes. As mentioned in Figure 2, both surface tension and liquid viscosity decline while temperature is increased. As temperature is increased, the viscosity initially (below 50°C) declines very rapidly, and then slowly decreases after 100°C. An assumption is made to explain the occurrence of receding that, only when the liquid viscosity is relatively small enough and the surface tension is large enough, the receding could happen. At 25°C, although surface tension forces are high but viscous forces are competing enough to prevent receding. Whereas, at 75°C the viscosity becomes significantly lower thus reducing the interlayer viscous forces and letting the surface tension forces dominate. However, when the temperature is further increased the dominating effect of surface tension is also decreased, thus letting the inertia forces take over both viscous and surface tension forces and lead to increase in spreading. Moving to the non-isothermal conditions, only the heated plate and cold droplet conditions have the receding process, whereas the heated droplet and cold wall shows complete spreading and no receding.

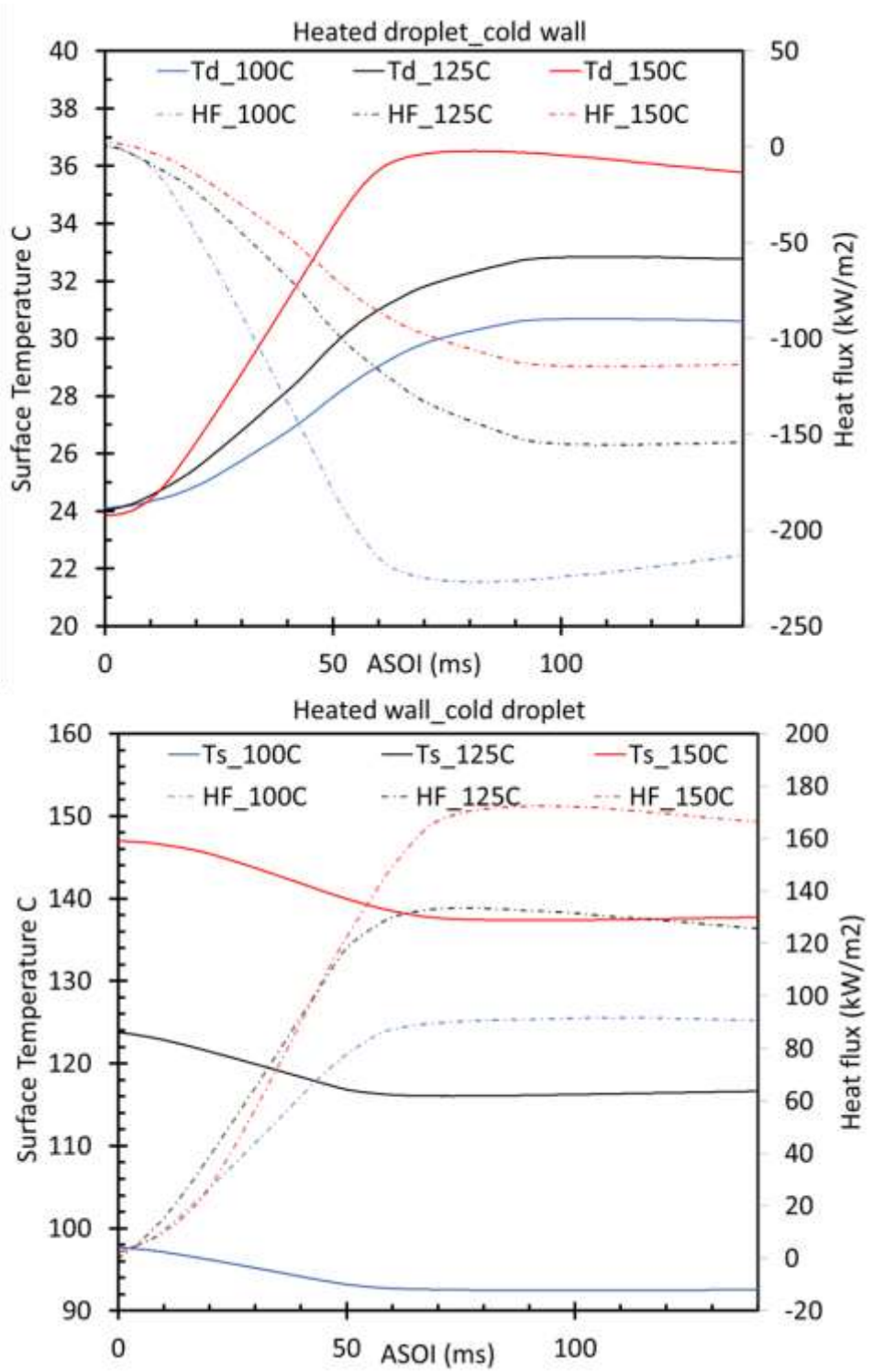

Figure 35. Surface Temperature variation and heat flux between embedded and surface thermocouple for a). heated droplet_cold wall interaction (top) ; and b). heated wall_cold droplet interaction (bottom)

To understand these processes, we look at the surface temperature and heat flux values during the impingement at non-isothermal conditions in Figure 35.Figure 35 shows the surface temperature variation and heat flux between the surface and embedded thermocouple. Figure 35 (top) shows the drop in temperature of a heated plate when the ambient droplet impinges on it, whereas Figure 35 (bottom) shows the increase in ambient temperature plate when an elevated temperature droplet interacts with it. Although the heat flux plot shown in the Figure 35 refers to the heat flux between the embedded and surface thermocouple, but it can be approximated qualitatively to the heat transfer between droplet and wall.

From the results of temperature, it can be concluded that the surface temperature changes in both the conditions. It can be assumed that the boundary near the surface would also change the temperature, because of the heat transfer between the droplet and surface. Although the temperature gradient within the droplet, is not recorded but the heat flux values and surface temperature profile can give the qualitative understanding of the different droplet impingement phenomena.

It can be assumed that during the spreading of the droplet an interfacial layer is formed between liquid and plate. The temperature of this thin layer increases or decreases rapidly due to the heat flux between wall and droplet. However, the temperature of majority of droplet that above the thin layer is slowly increasing due to relative low heat transfer coefficient of liquid compared to metal. This causes viscosity variation in this interfacial boundary layer, which can significantly influence the droplet dynamics and the viscous forces hindering the motion of droplet due to other forces such as surface tension, inertia and capillary. In case of heated droplet and cold wall, it is not difficult to understand that the impinged heated droplet to have no receding, because the initial surface tension and viscosity value of droplet is very low at temperatures such as 100,125 and 150 ^{o}C, that droplet spreads out completely. The inertial forces here dominate both the surface tension and viscous forces. However, a reduction in maximum spreading factor as compared to isothermal condition for same temperature droplet is noted here. (refer Table 9 and Table 11). This is due to decrease in the temperature of boundary layer of heated droplet, near the plate, causing increase in viscosity. This increase in viscosity tries to compete with inertia, thus reducing the maximum spread factor.

Similarly, when the cold droplet interacts with heated wall, the heat flux from the plate to impinged droplet causes the increase in temperature of interfacial boundary layer and hence a decrease in viscosity. However, the overall surface tension remains high enough. This cause extensive receding to take place, as surface tension forces dominate after the inertial forces are damped out after achieving maximum spread factor. It can be said that, higher the heat flux, higher would be temperature increase of boundary layer, and thus higher would be receding and consequent oscillations.

In summary, the heat transfer and thermophysical properties are essential to affect the post impingement droplet dynamics. Thus, further studies are required to understand the

boundary layer temperature and its thickness and relate them quantitatively to the droplet post impingement dynamics.

5 CONCLUSION AND FUTURE WORK

A detailed analysis of the dynamic process of the single droplet impinging on a flat plate with various conditions has been performed. The current experimental work was carried out at the room temperature and pressure. Liquids like water, diesel, dodecane, ethanol and n-heptane were considered as the test fuels and injected at various impact Weber (We) numbers and different temperature conditions. The droplet impingement regimes including deposition-splash criteria is studied and a new correlation in terms of the current experimental data is developed. As well, the study on the evolution of the dynamic process of droplet-wall interaction is one of the unique contributions to expand the database of relevant studies, such as aiding the development of dynamic contact angle model under Direct Numerical Simulation (DNS) or VOF methodology:

(1) In experiment, considering the impingement outcomes, the splashing and non-splashing criterions were summarized based on the earlier research and applied to evaluate the current experimental data. With the droplet impacting on the smooth, roughened, and heated plates, the experimental results generally show good agreement in predicting the splashing and non-splashing phenomena with the published droplet-wall interaction models. Further, a new correlation in terms of Ohnesorge number (*Oh*) and Reynolds number (*Re*) based on our experimental data to indicate the droplet splashing was proposed: $OhRe^{0.826} = 3 \sim 6$.

(2) The effects of the impact *We* and different wall conditions on the time evolution of droplet spreading factor, height ratio, the dynamic contact angle, and the contact line velocity were studied. The dynamic contact angle, contact line velocity, and spread factor vary with the impact *We*. The maximum spreading factor both in diesel and water cases increases with the impact *We*. The averaged advancing contact angle for diesel based on different conditions is around 68°. Furthermore, in diesel case, the receding and equilibrium contact angles at various impact *We* change at a small scale. At water case, the averaged advancing contact angle in terms of all various conditions is about 75°. The receding contact angle is quite smaller compared with the equilibrium contact angle at each condition. As well, the receding and equilibrium contact angles at each condition show clear differences, they decrease with the impact *We*.

(3) Effect of thermophysical properties on droplet impingement dynamics is prominent in isothermal case. The spreading factor increases with increase in temperature, thus explaining the decrease in viscous forces and surface tension forces with increase in temperature. This experiment also helps in understanding the competing effect of surface tension and viscous forces. The baseline isothermal condition of 25°C, and the elevated isothermal condition of 100, 125 and 150 C doesn't show any sign of receding. However, 75°C condition has a weak receding. In addition, the 75°C cases also have the lowest advancing and equilibrium contact angles. This variation is clearly explained based on the different rate of thermophysical property changes.

(4) For the non-isothermal heated plate cold droplet conditions significant receding behavior is shown. The spread factor and height ratio in non-isothermal heated plate

condition experienced oscillation before reaching equilibrium. Thus, a cold droplet interacting with a hot plate is more probable to recoil or rebound.

(5) In non-isothermal heated droplet and cold wall conditions, a similar behavior to isothermal condition is seen. However, if carefully observed the spreading factor for the same temperature droplet is different when the droplet temperature changed from ambient to hot. A heated droplet interacting with heated surface has higher spread factor, as compared to heated droplet-cold wall.

(6) These different behaviors of droplet wall interaction in non-isothermal and isothermal conditions are explained through a hypothesis involving interfacial boundary layer. The heat transfer can quickly change the temperature in the thin liquid solid interfacial layer, and further vary the thermophysical properties which is are essential to affect the post impingement droplet dynamics. Thus, the understanding of role of boundary layer in droplet wall interaction is essential.

FUTURE RECOMMENDATIONS:

For future works, various test conditions with single or multi-train droplets, such as a sensitivity analysis of ambient condition, plate temperature, and droplet size, will be considered to study droplet-wall impingement and further improve the correlation of deposition-splash criteria. The various liquid fuel at non-splashing and splashing conditions will be studied numerically with a physics-based CFD modeling approach for predicting droplet-wall interactions.

Moreover, multiple points temperature measurement inside the droplet will be considered in the future to obtain the temperature map of the droplet contacting region and help understand the underlying mechanism of spray-wall interaction. A modeling approach for predicting droplet-wall interactions characteristics at isothermal condition and a conjugated heat transfer model for computing the temperature gradient inside the droplets at non-isothermal conditions will be numerically studied.

6 REFERENCE LIST

1. A. Yarin, Drop impact dynamics: splashing, spreading, receding, bouncing…, Annu. Rev. Fluid Mech. 38 (2006) 159-192
2. Stanton, D.W. and Rutland, C.J., "Modeling Fuel Film Formation and Wall Interaction in Diesel Engines," SAE Technical Paper 960628, 1996, doi:10.4271/960628.
3. Drake, M.C., Fansler, T.D., Solomon, A.S., and Szekely, G.A., "Piston Fuel Films as a Source of Smoke and Hydrocarbon Emissions from a Wall-Controlled Spark-Ignited Direct-Injection Engine," SAE Technical Paper 2003-01-0547, 2003, doi:10.4271/2003-01-0547.
4. Lindagren, R. and Denbratt, I., "Influence of Wall Properties on the Characteristics of a Gasoline Spray after Wall Impingement," SAE Technical Paper 2004-01-1951, 2004, doi:10.4271/2004-01-1951.
5. J. Yang, L. Chow, M. Pais, Nucleate boiling heat transfer in spray cooling, Journal of Heat Transfer 118(3) (1996) 668-671
6. C. Bai, A. Gosman, Development of methodology for spray impingement simulation, SAE Technical Paper, 1995
7. Jadidbonab H, Malgarinos I, Karathanassis I, Mitroglou N, Gavaises M. 2018 We-T classification of diesel fuel droplet impact regimes. Proc. R. Soc. A 474: 20170759. http://dx.doi.org/10.1098/rspa.2017.0759
8. Riboux, Guillaume, and José Manuel Gordillo. "Experiments of drops impacting a smooth solid surface: a model of the critical impact speed for drop splashing." Physical review letters 113, no. 2 (2014): 024507.
9. Chen, Longquan, and Elmar Bonaccurso. "Effects of surface wettability and liquid viscosity on the dynamic wetting of individual drops." Physical Review E 90, no. 2 (2014): 022401.
10. Markt D. P , Z.L., Zhu X., Pathak A., Torelli R., Lee S-Y., Raessi M. , "An Experimental and Computational Study of a Single Diesel Droplet Impinging on a Dry Surface." ICLASS 2018, 14th Triennial International Conference on Liquid Atomization and Spray Systems
11. Tang, Chenglong, Mengxiao Qin, Xinyan Weng, Xuhui Zhang, Peng Zhang, Jianling Li, and Zuohua Huang. "Dynamics of droplet impact on solid surface with different roughness." International Journal of Multiphase Flow 96 (2017): 56-69.
12. Stow C.D. , H.M.G., "An Experimental Investigation of Fluid Flow Resulting from the Impact of a Water Drop with an Unyielding Dry Surface," Proceedings of the Royal Society of London. A. Mathematical and Physical Sciences 373(1755):419, 1981
13. Lindagren, R. and Denbratt, I., "Influence of Wall Properties on the Characteristics of a Gasoline Spray after Wall Impingement," SAE Technical Paper 2004-01-1951, 2004, doi:10.4271/2004-01-1951

14. Yarin, A.L. and Weiss, D.A., "Impact of Drops on Solid Surfaces: Self-Similar Capillary Waves, and Splashing as a New Type of Kinematic Discontinuity," Journal of Fluid Mechanics 283(141-173,1995, doi:10.1017/S0022112095002266
15. Mundo, C., Sommerfeld, M., and Tropea, C., "Droplet-Wall Collisions: Experimental Studies of the Deformation and Breakup Process," *International journal of multiphase flow* 21(2):151-173, 1995, doi:10.1016/0301-9322(94)00069-V.
16. Rioboo, R., Tropea, C., and Marengo, M., "Outcomes from a Drop Impact on Solid Surfaces," 11(2):12, 2001, doi:10.1615/AtomizSpr.v11.i2.40.
17. O'Rourke, P.J. and Amsden, A.A., "A Particle Numerical Model for Wall Film Dynamics in Port-Injected Engines," SAE Technical Paper 961961, 1996, doi:10.4271/961961
18. Naber, J.D. and Reitz, R.D., "Modeling Engine Spray/Wall Impingement," SAE Technical Paper 880107, 1988, doi:10.4271/880107
19. Han, Z., Xu, Z., and Trigui, N., "Spray/Wall Interaction Models for Multidimensional Engine Simulation," International Journal of Engine Research 1(1):127-146, 2000,
20. Bai, C.X., Rusche, H., and Gosman, A.D., "Modeling of Gasoline Spray Impingement," Atomization and Sprays 12(1-3):1-27, 2002, doi:10.1615/AtomizSpr.v12.i123.10.
21. O'Rourke, P.J. and Amsden, A.A., "A Spray/Wall Interaction Submodel for the Kiva-3 Wall Film Model," SAE Technical Paper 2000-01-0271, 2000, doi:10.4271/2000-01-0271
22. Han, Z. and Xu, Z., "Wall Film Dynamics Modeling for Impinging Sprays in Engines". 2004, SAE Technical Paper
23. Ma, T., Feng, L., Wang, H., Liu, H., et al., "A Numerical Study of Spray/Wall Impingement Based on Droplet Impact Phenomenon," International Journal of Heat and Mass Transfer 112(401-412, 2017, doi:https://doi.org/10.1016/j.ijheatmasstransfer.2017.04.110.
24. Palacios, J., Hernández, J., Gómez, P., Zanzi, C., et al., "Experimental Study of Splashing Patterns and the Splashing/Deposition Threshold in Drop Impacts onto Dry Smooth Solid Surfaces," Experimental Thermal and Fluid Science 44(571-582, 2013, doi:https://doi.org/10.1016/j.expthermflusci.2012.08.020.
25. Wal, R.L.V., Berger, G.M., and Mozes, S.D., "The Splash/Non-Splash Boundary Upon a Dry Surface and Thin Fluid Film," Experiments in Fluids 40(1):53-59, 2006, doi:10.1007/s00348-005-0045-1.
26. James, C.B., Scott, S.H.T., and Howard, A.S., "Inclined to Splash: Triggering and Inhibiting a Splash with Tangential Velocity," New Journal of Physics 11(6):063017, 2009,
27. Pan, K.-L., Tseng, K.-C., and Wang, C.-H., "Breakup of a Droplet at High Velocity Impacting a Solid Surface," Experiments in Fluids 48(1):143-156, 2010, doi:10.1007/s00348-009-0697-3
28. Xu, Lei, Wendy W. Zhang, and Sidney R. Nagel. "Drop splashing on a dry smooth surface." Physical review letters 94, no. 18 (2005): 184505.

29. Hu, J., Xiong, X., Xiao, H., and Wan, K.-t., "Effects of Contact Angle on the Dynamics of Water Droplet Impingement," presented at COMSOL, Boston, 2015.
30. Vadillo, D.C., Soucemarianadin, A., Delattre, C., and Roux, D.C.D., "Dynamic Contact Angle Effects onto the Maximum Drop Impact Spreading on Solid Surfaces," Physics of Fluids 21(12):122002, 2009, doi:10.1063/1.3276259.
31. Šikalo, Š., Wilhelm, H.-D., Roisman, I.V., Jakirlić, S., et al., "Dynamic Contact Angle of Spreading Droplets: Experiments and Simulations," Physics of Fluids 17(6):062103, 2005, doi:10.1063/1.1928828.
32. Schrader, M.E., "Young-Dupre Revisited," Langmuir 11(9):3585-3589, 1995, doi:10.1021/la00009a049.
33. Malgarinos, I., Nikolopoulos, N., Marengo, M., Antonini, C., et al., "Vof Simulations of the Contact Angle Dynamics During the Drop Spreading: Standard Models and a New Wetting Force Model," Advances in Colloid and Interface Science 212(1-20, 2014, doi:https://doi.org/10.1016/j.cis.2014.07.004.
34. Roisman, I.V., Opfer, L., Tropea, C., Raessi, M., et al., "Drop Impact onto a Dry Surface: Role of the Dynamic Contact Angle," Colloids and Surfaces A: Physicochemical and Engineering Aspects 322(1–3):183-191, 2008, doi:https://doi.org/10.1016/j.colsurfa.2008.03.005.
35. Schiaffino, S. and Sonin, A.A., "Molten Droplet Deposition and Solidification at Low Weber Numbers," *Physics of Fluids* 9(11):3172-3187, 1997, doi:10.1063/1.869434
36. Jadidbonab H, Malgarino I, Karathanassis I, Mitroglou N, Gavaises M. 2018 We-T classification of diesel fuel droplet impact regimes. Proc. R. Soc. A474: 20170759. http://dx.doi.org/10.1098/rspa.2017.0759
37. H.S. Ahn, J. Kim, M.H. Kim, Investigation of pool boiling critical heat flux enhancement on a modified surface through the dynamic wetting of water droplets, J. Heat Transf.-Trans. ASME 134 (7) (2012) 071504
38. Tamura, Z. and Tanasawa, Y., "Evaporation and Combustion of a Drop Contacting with a Hot Surface." Symposium (International) on Combustion 7(1):509-522, 1958, doi:https://doi.org/10.1016/S0082-0784(58)80086-7.
39. Kang, B.S. and Lee, D.H., "On the Dynamic Behavior of a Liquid Droplet Impacting Upon an Inclined Heated Surface." Experiments in Fluids 29(4):380-387, 2000, doi:10.1007/s003489900104.
40. Manzello, S. and C Yang, J., An Experimental Study of High Weber Number Impact of Methoxy-Nonafluorobutane C4f9och3 (Hfe-7100) and N-Heptane Droplets on a Heated Solid Surface* 1. Vol. 45. 2002.10.1016/S0017-9310(02)00103-5
41. Nukiyama, S., "The Maximum and Minimum Values of the Heat Q Transmitted from Metal to Boiling Water under Atmospheric Pressure." International Journal of Heat and Mass Transfer 9(12):1419-1433, 1966, doi:https://doi.org/10.1016/0017-9310(66)90138-4.
42. Leidenfrost, J.G., "On the Fixation of Water in Diverse Fire." International Journal of Heat and Mass Transfer 9(11):1153-1166, 1966, doi:https://doi.org/10.1016/0017-9310(66)90111-6.

43. Healy WM, Hartley JG, Abdel-Khalik SI. 2001 On the validity of the adiabatic spreading assumption in droplet impact cooling. Int. J. Heat Mass Transf. 44, 3869–3881. (doi:10.1016/S0017-9310(01)00041-2)
44. Kandlikar S, Steinke M. 2002 Contact angles and interface behavior during rapid evaporation of liquid on a heated surface. Int. J. Heat Mass Transf. 45, 3771–3780. (doi:10.1016/S0017-9310(02)00090-X)
45. Eotvos Ramsay-Shield relation of Surface Tension and Temperature Calculator | Calistry(2018). [online] Available at http://calistry.org/calculate/eotvosRule
46. API Manual of Petroleum Measurement Standards, Chapter 11- physical properties Data, Section 1: Temperature and pressure volume correction factors for generalised crude oils, refined products and lubricating oils
47. Otsu, N., "A Threshold Selection Method from Gray-Level Histograms," *IEEE transactions on systems, man, and cybernetics* 9(1):62-66, 1979
48. Stanton, D.W. and Rutland, C.J., "Multi-Dimensional Modeling of Thin Liquid Films and Spray-Wall Interactions Resulting from Impinging Sprays," International Journal of Heat and Mass Transfer 41(20):3037-3054, 1998, doi:https://doi.org/10.1016/S0017-9310(98)00054-4.
49. Geppert, A., Chatzianagnostou, D., Meister, C., Gomaa, H., et al., "Classification of Impact Morphology and Splashing/Deposition Limit for N-Hexadecane," 26(10):983-1007, 2016, doi:10.1615/AtomizSpr.2015013352.
50. Cossali, G.E., Coghe, A., and Marengo, M., "The Impact of a Single Drop on a Wetted Solid Surface," Experiments in Fluids 22(6):463-472, 1997, doi:10.1007/s003480050073.
51. Wal, R.L.V., Berger, G.M., and Mozes, S.D., "The Splash/Non-Splash Boundary Upon a Dry Surface and Thin Fluid Film," *Experiments in Fluids* 40(1):53-59, 2006, doi:10.1007/s00348-005-0045-1
52. Bernard, R., Foltyn, P., Geppert, A., Lamanna, G., et al., Generalized Analysis of the Deposition/Splashing Limit for One- and Two-Component Droplet Impacts Upon Thin Films. 2017.10.4995/ILASS2017.2017.4810
53. Lee, B.-B., Ravindra, P., and Chan, E.-S., "New Drop Weight Analysis for Surface Tension Determination of Liquids." *Colloids and Surfaces A: Physicochemical and Engineering Aspects* 332(2):112-120, 2009, doi:https://doi.org/10.1016/j.colsurfa.2008.09.003

A MATLAB codes

A.1 Image Processing

A.1.1 Program with Contact angle measurement using linear fitting.

```
clear all;
close all;
% clear previous data in the memory

% defining the path
dir_raw = 'E:\CSELLAB Isothermal droplet test\';
YYYYMMDD = '20180820';
HHMM = '0959fist500_C001H001S0001';
HHMM1 = '0959skip20_C001H001S0001';

%% compiling first 500 and skip 20 images into one processing
[starttime,lengthskip20,initial500,matchid]=startno(dir_raw,YYYYMMDD,HH
MM,HHMM1);

%% moving to first 500 folder
cd([dir_raw '/' YYYYMMDD '/' HHMM]) % Change the working directory to
the desired folder

%% Create movie.
writerObj = VideoWriter('Dropletanalysis.avi');
writerObj.FrameRate = 20;
open(writerObj);

%% Predetermined parameters
Impinging_time =20; % frame number
Center_Location =487;% frame number
Appearing_time =8; % frame number
Ending_time = matchid; %+430+(350-142);
fontSize = 6;
frame_speed = 20000; % frame/sec
scale = 0.0158; % mm/pixel
rho=848; % kg/m^3 Density for the fluid being impinged
mu=2.6e-6; % m^2/s Kinematic viscosity for the fluid being impinged
sigma=24e-3;% N/m surface tension of fluid being impinged
Height=104.05;% mm between nozzle to plate
Fluid = 'Diesel'; % fluid being impinged
Vg=(2*9.8*Height/1000)^0.5; %based on the gravity

figure('units','normalized','outerposition',[0 0 1 1])
for i=Appearing_time: Ending_time+lengthskip20-starttime% Read files
after start of drop
    %% Read Image
    if i<=Ending_time
        if i < 10
            fullFileName = [dir_raw '/' YYYYMMDD '/' HHMM '/' HHMM
'00000' num2str(i) '.bmp'];
        elseif i < 100
            fullFileName = [dir_raw '/' YYYYMMDD '/' HHMM '/' HHMM
'0000' num2str(i) '.bmp'];
```

```
        elseif i < 1000
            fullFileName = [dir_raw '/' YYYYMMDD '/' HHMM '/' HHMM
'000' num2str(i) '.bmp'];
        elseif i < 10000
            fullFileName = [dir_raw '/' YYYYMMDD '/' HHMM '/' HHMM '00'
num2str(i) '.bmp'];
        end
        time(i)=(1/frame_speed)*1000*(i -(Appearing_time)); % ms
        Impingingtime(i)=(1/frame_speed)*1000*(i -(Impinging_time)); %
ms
        lasttime=time(i);
        Impingingtimelast=Impingingtime(i);
    else
        k=i-Ending_time+starttime;
        if k < 10
            fullFileName = [dir_raw '/' YYYYMMDD '/' HHMM1 '/' HHMM1
'00000' num2str(k) '.bmp'];
        elseif k < 100
            fullFileName = [dir_raw '/' YYYYMMDD '/' HHMM1 '/' HHMM1
'0000' num2str(k) '.bmp'];
        elseif k < 1000
            fullFileName = [dir_raw '/' YYYYMMDD '/' HHMM1 '/' HHMM1
'000' num2str(k) '.bmp'];
        elseif k < 10000
            fullFileName = [dir_raw '/' YYYYMMDD '/' HHMM1 '/' HHMM1
'00' num2str(k) '.bmp'];
        end
        frame_speed=1000;
        time(i)=lasttime+(k-starttime)*(1/frame_speed)*1000;
        Impingingtime(i)=Impingingtimelast+(k-
starttime)*(1/frame_speed)*1000;
    end
Original_Image = (imread(fullFileName));
TI=imcrop(Original_Image,[0,0,896,28]);
OI=imcrop(Original_Image,[0,29,896,144]);
subplot(3,1,1)
imshow(TI);
subplot(3,1,2)
imshow(OI);

%% binaryImage conversion
if i < Impinging_time %% before impingement calculations
    level=graythresh(OI);
    BI=imcomplement(imbinarize(OI,level-0.1));
    se = strel('disk', 2, 0);
    BI=imfill(BI,'holes');
    numberToExtract =1;
    binaryImage = ExtractNLargestBlobs(BI, numberToExtract);
    subplot(3,1,3);
    imshow(binaryImage)
    for j=1:144
        if ismember(1,binaryImage(j,:))
            Horizontal_Location_right(j) = find(binaryImage(j,:) == 1,
1, 'last' );
```

```
            Horizontal_Location_left(j) = find(binaryImage(j,:) == 1,
1, 'first' );
            Secant(j)=Horizontal_Location_right(j)-
Horizontal_Location_left(j);
        end
    end
    Dia(i)= max(Secant)*scale;
else % after impingemnet
    level=graythresh(OI);
    BI=imcomplement(imbinarize(OI,level-0.1));
    se = strel('disk', 2, 0);
    BI=imfill(BI,'holes');
    numberToExtract =1;
    binaryImage = ExtractNLargestBlobs(BI, numberToExtract);
    subplot(3,1,3);
    imshow(binaryImage)
    hold on;
    % boundary extraction
boundaries = bwboundaries(binaryImage);
A = cell2mat(boundaries) ;
x_corners = A(:,2);
y_corners = A(:,1);
%% corners extracted for calculations
[rows,columns]=size(binaryImage);
heights = zeros(1, columns);
topEdge = zeros(1, columns);
bottomEdge = zeros(1, columns);

 %% calculation of heights
for col = 1:columns
    thisCol = binaryImage(:,col);
    TOPIndex = find(thisCol, 1, 'first');
    if ~isempty(TOPIndex)
        topEdge(col) = TOPIndex; % use for height calculation
        bottomEdge(col) = find(thisCol, 1, 'last');
    end
end
%% calculation of bottomedge dia
BE=max(bottomEdge);
    thisRow = binaryImage(BE,:);
    TOPIndex = find(thisRow, 1, 'first');
    if ~isempty(TOPIndex)
        lE = TOPIndex;
        rE = find(thisRow, 1, 'last');
        beDIA(i)= rE - lE; % bottomedge dia
    end

%% removing the bottom edge from the boundary
removeBE=find(y_corners~=BE);
Topboundary=cat(2,x_corners(removeBE),y_corners(removeBE));
Leftbottompoint=[lE,BE];
Rightbottompoint=[rE,BE];
Total_topBoundary=cat(1,Topboundary,Leftbottompoint,Rightbottompoint);
x_corners=Total_topBoundary(:,1);
y_corners=Total_topBoundary(:,2);
```

```
plot(x_corners, y_corners, '.r')
hold on

%% calculation of contact angle
ldiffx=abs(Total_topBoundary(:,1)-lE);
ldiffy=abs(Total_topBoundary(:,2)-BE);
ldistance=((ldiffx).^2+(ldiffy).^2).^(0.5);
Left_topBoundary=cat(2,Total_topBoundary,ldistance);
Left_topBoundary=sortrows(Left_topBoundary,3);
Right_topBoundary=cat(2,x_corners,y_corners);
rdiffx=abs(Right_topBoundary(:,1)-rE);
rdiffy=abs(Right_topBoundary(:,2)-BE);
rdistance=((rdiffx).^2+(rdiffy).^2).^(0.5);
Right_topBoundary=cat(2,Right_topBoundary,rdistance);
Right_topBoundary=sortrows(Right_topBoundary,3);

% deciding nop = no of points to be taken for calculating contact angle

if beDIA(i)>beDIA(i-1)&& beDIA(i)>=max(beDIA)
    nop=4;
elseif beDIA(i)>720 && beDIA(i)<800
        nop=15;
elseif beDIA(i)<max(beDIA)&& beDIA(i)>=0.94*max(beDIA)
    nop=10;
elseif beDIA(i)<0.94*max(beDIA)
    nop=15;
end

lx=Left_topBoundary(1:nop,1);
ly=Left_topBoundary(1:nop,2);
plot(lx, ly, '.b')
hold on
rx=Right_topBoundary(1:nop,1);
ry=Right_topBoundary(1:nop,2);
plot(rx, ry, '.b')
hold on
leftCoefficients = polyfit(ly,lx,1);
rightCoefficients = polyfit(ry,rx,1);
yleftFit = polyval(leftCoefficients, ly);
plot(yleftFit, ly,'y-', 'LineWidth', 1);hold on
yrightFit = polyval(rightCoefficients, ry);
plot(yrightFit, ry, 'y-', 'LineWidth', 1); hold on;
leftAngle(i) = 90+atand(leftCoefficients(1)); %% left contact angle
rightAngle(i) = 90-atand(rightCoefficients(1)); %% right contact angle


%% other impingement characteristics calculations
stats2 = regionprops(binaryImage,'Extrema');
Extrema1 = [stats2.Extrema];
bottomleft=Extrema1(6,1);
bottomright=Extrema1(5,1);
SpreadingDiameter(i)=(bottomright-bottomleft)*scale;
top=topEdge(topEdge>0);
h1(i)=BE-min(top);
ht=h1(i)*scale;
```

```
HeightRatio(i)=(h1(i)*scale)/Dia(1,end);
SpreadRatio(i)=SpreadingDiameter(i)/(Dia(1,end));
Spreadingvelocity(i)=(SpreadingDiameter(i)-SpreadingDiameter(i-
1))/((time(i)-time(i-1)));

% displaying values
str=strcat('\bf spreading
velocity=',num2str(Spreadingvelocity(i),'%.2f'),'m/s');
text(600,-320,str,'HorizontalAlignment','center','VerticalAlignment',
'top','FontSize', fontSize+10,'Color','k');
str=strcat('\bf spreading
diameter=',num2str(SpreadingDiameter(i),'%.2f'),'mm');
text(100,-280,str,'HorizontalAlignment','center','VerticalAlignment',
'top','FontSize', fontSize+10,'Color','k');
str=strcat('\bf height=',num2str(ht,'%.2f'),'mm');
text(100,-260,str,'HorizontalAlignment','center','VerticalAlignment',
'top','FontSize', fontSize+10,'Color','k');
str=strcat('\bf spreading ratio(d/D)=',num2str(SpreadRatio(i),'%.2f'));
text(100,-240,str,'HorizontalAlignment','center','VerticalAlignment',
'top','FontSize', fontSize+10,'Color','k');
str=strcat('\bf height ratio(h/D)=',num2str(HeightRatio(i),'%.2f'));
text(600,-300,str,'HorizontalAlignment','center','VerticalAlignment',
'top','FontSize', fontSize+10,'Color','k');
str=strcat('\bf Left \theta=',num2str(leftAngle(i),'%.2f'),'\circ');
text(600,-280,str,'HorizontalAlignment','center','VerticalAlignment',
'top','FontSize', fontSize+10,'Color','k');
str=strcat('\bf Right \theta =',num2str(rightAngle(i),'%.2f'),'\circ');
text(600,-260,str,'HorizontalAlignment','center','VerticalAlignment',
'top','FontSize', fontSize+10,'Color','k');
str=strcat('\bf Average \theta
=',num2str((leftAngle(i)+rightAngle(i))/2,'%.2f'),'\circ');
text(600,-240,str,'HorizontalAlignment','center','VerticalAlignment',
'top','FontSize', fontSize+10,'Color','k');

end
str=strcat('\bf HOI=',num2str(Height,'%.2f'),'mm');
text(100,-320,str,'HorizontalAlignment','center','VerticalAlignment',
'top','FontSize', fontSize+10,'Color','k');
str=strcat('\bf D=',num2str(Dia(1,end),'%.2f'),'mm');
text(100,-300,str,'HorizontalAlignment','center','VerticalAlignment',
'top','FontSize', fontSize+10,'Color','k');

pause(0.1)
hold off;
drawnow;
frame = getframe(figure(1));
writeVideo(writerObj,frame);
end
close(writerObj);
Impingingtime=Impingingtime';
time=time';
leftAngle=leftAngle';
rightAngle=rightAngle';
Spreadfactor=SpreadRatio';
SpreadingDiameter=SpreadingDiameter';
```

```
HeightRatio=HeightRatio';
Dia=Dia';

% writing in excel file
col_header={'Time (ms)', 'Impingingtime','Left Collision angle
(deg)','Right Collision Angle(deg)','Spread factor', 'Spread diameter',
'Height Ratio','Diametr before Impinegement'};
xlswrite(strcat(HHMM,'.xlsx'),time,1,'A2');
xlswrite(strcat(HHMM,'.xlsx'),Impingingtime,1,'B2');
xlswrite(strcat(HHMM,'.xlsx'),leftAngle,1,'C2');
xlswrite(strcat(HHMM,'.xlsx'),rightAngle,1,'D2');
xlswrite(strcat(HHMM,'.xlsx'),Spreadfactor,1,'E2');
xlswrite(strcat(HHMM,'.xlsx'),SpreadingDiameter,1,'F2');
xlswrite(strcat(HHMM,'.xlsx'),HeightRatio,1,'G2');
xlswrite(strcat(HHMM,'.xlsx'),Dia,1,'H2');

function binaryImage = ExtractNLargestBlobs(binaryImage,
numberToExtract)
try
    % Get all the blob properties.  Can only pass in originalImage in
version R2008a and later.
    [labeledImage, numberOfBlobs] = bwlabel(binaryImage);
    blobMeasurements = regionprops(labeledImage, 'area');
    % Get all the areas
    allAreas = [blobMeasurements.Area];
    if numberToExtract > length(allAreas);
        % Limit the number they can get to the number that are
there/available.
        numberToExtract = length(allAreas);
    end
    if numberToExtract > 0
        % For positive numbers, sort in order of largest to smallest.
        % Sort them.
        [sortedAreas, sortIndexes] = sort(allAreas, 'descend');
    elseif numberToExtract < 0
        % For negative numbers, sort in order of smallest to largest.
        % Sort them.
        [sortedAreas, sortIndexes] = sort(allAreas, 'ascend');
        % Need to negate numberToExtract so we can use it in
sortIndexes later.
        numberToExtract = -numberToExtract;
    else
        % numberToExtract = 0.  Shouldn't happen.  Return no blobs.
        binaryImage = false(size(binaryImage));
        return;
    end
    % Extract the "numberToExtract" largest blob(a)s using ismember().
    biggestBlob = ismember(labeledImage,
sortIndexes(1:numberToExtract));
    % Convert from integer labeled image into binary (logical) image.
    binaryImage = biggestBlob > 0;
catch ME
    errorMessage = sprintf('Error in function
ExtractNLargestBlobs().\n\nError Message:\n%s', ME.message);
    fprintf(1, '%s\n', errorMessage);
```

```
    uiwait(warndlg(errorMessage));

end
end

function
[fileno,lengthskip,initiallength,matchid]=startno(dir_raw,YYYYMMDD,HHMM
,HHMM1)
filePattern = fullfile([dir_raw '/' YYYYMMDD '/' HHMM], '*.bmp');
files = dir(filePattern);
j1(:,1) = length(files)-[1:20];
j1=sort(j1);
initiallength=length(files);
k=1;
for  i=j1(1) : j1(end)
if i < 10
     fullFileName = [dir_raw '/' YYYYMMDD '/' HHMM '/' HHMM '00000'
num2str(i) '.bmp'];
    elseif i < 100
     fullFileName = [dir_raw '/' YYYYMMDD '/' HHMM '/' HHMM '0000'
num2str(i) '.bmp'];
    elseif i < 1000
    fullFileName = [dir_raw '/' YYYYMMDD '/' HHMM '/' HHMM '000'
num2str(i) '.bmp'];
    elseif i < 10000
    fullFileName = [dir_raw '/' YYYYMMDD '/' HHMM '/' HHMM '00'
num2str(i) '.bmp'];
end
Original_Image = (imread(fullFileName));
TI(:,:,k)=imcrop(Original_Image,[0,0,896,29]);
k=k+1;
end
cd([dir_raw '/' YYYYMMDD '/' HHMM1]) % Change the working directory to
the desired folder
filePattern = fullfile([dir_raw '/' YYYYMMDD '/' HHMM1], '*.bmp');
files = dir(filePattern);
lengthskip=length(files);
for i = 1:length(files)
if i < 10
     fullFileName = [dir_raw '/' YYYYMMDD '/' HHMM1 '/' HHMM1 '00000'
num2str(i) '.bmp'];
    elseif i < 100
     fullFileName = [dir_raw '/' YYYYMMDD '/' HHMM1 '/' HHMM1 '0000'
num2str(i) '.bmp'];
    elseif i < 1000
    fullFileName = [dir_raw '/' YYYYMMDD '/' HHMM1 '/' HHMM1 '000'
num2str(i) '.bmp'];
    elseif i < 10000
    fullFileName = [dir_raw '/' YYYYMMDD '/' HHMM1 '/' HHMM1 '00'
num2str(i) '.bmp'];
end
Original_Image = (imread(fullFileName));
TI1=imcrop(Original_Image,[0,0,896,29]);
fileno=0;
for j=1:20
```

```
if TI1==TI(:,:,j)
    fileno=i;
    matchid=j1(j);
    break;
end
end
if fileno~=0
    break
end
end
end
```

A.1.2 Program with Contact angle measurement with polynomial fitting.

```
tic
clear all;
close all;
dir_raw = 'G:\CSELLAB Isothermal droplet test\';
YYYYMMDD = '20180917';
HHMM = '1234first500';
HHMM1 = '1234skip20';
cd([dir_raw '/' YYYYMMDD '/' HHMM]) % Change the working directory to
the desired folder

% Create movie.
writerObj = VideoWriter('Dropletanalysis1.avi');
writerObj.FrameRate = 20;
open(writerObj);

%% Predetermined parameters
Impinging_time =51; % frame number
Center_Location =537;% frame number
Appearing_time =18; % frame number
Ending_time = 501; %+430+(350-142);
fontSize = 6;
frame_speed = 20000; % pixel/sec
scale = 0.019; % mm/pixel
rho=848; % kg/m^3 Density for the fluid being impinged
mu=2.6e-6; % m^2/s Kinematic viscosity for the fluid being impinged
sigma=24e-3;% N/m surface tension of fluid being impinged
Height=104.05;% mm between nozzle to plate
Fluid = 'Diesel'; % fluid being impinged
Vg=(2*9.8*Height/1000)^0.5; %based on the gravity
starttime=26;

% Creation of backgrounfd image
fullFileName = [dir_raw '/' YYYYMMDD '/' HHMM '/' HHMM '00000'
num2str(1) '.bmp'];
BG=imread(fullFileName);
sizeimg=size(BG);
rows1=round(sizeimg(1)/2);
BG(29:98,:)=255;
lengthskip20=151;
```

```
% starting the loop over all the images
figure('units','normalized','outerposition',[0 0 1 1])
for i=Appearing_time:Impinging_time+10% Ending_time+lengthskip20-
starttime% Read files after start of drop
%% Read Image
if i<=Ending_time
    if i < 10
        fullFileName = [dir_raw '/' YYYYMMDD '/' HHMM '/' HHMM '00000'
num2str(i) '.bmp'];
    elseif i < 100
        fullFileName = [dir_raw '/' YYYYMMDD '/' HHMM '/' HHMM '0000'
num2str(i) '.bmp'];
    elseif i < 1000
        fullFileName = [dir_raw '/' YYYYMMDD '/' HHMM '/' HHMM '000'
num2str(i) '.bmp'];
    elseif i < 10000
        fullFileName = [dir_raw '/' YYYYMMDD '/' HHMM '/' HHMM '00'
num2str(i) '.bmp'];
    end
    time(i)=(1/frame_speed)*1000*(i -(Appearing_time)); % ms
    Impingingtime(i)=(1/frame_speed)*1000*(i -(Impinging_time)); % ms
    lasttime=time(i);
    Impingingtimelast=Impingingtime(i);
else
    k=i-Ending_time+starttime;
    if k < 10
        fullFileName = [dir_raw '/' YYYYMMDD '/' HHMM1 '/' HHMM1
'00000' num2str(k) '.bmp'];
    elseif k < 100
        fullFileName = [dir_raw '/' YYYYMMDD '/' HHMM1 '/' HHMM1 '0000'
num2str(k) '.bmp'];
    elseif k < 1000
        fullFileName = [dir_raw '/' YYYYMMDD '/' HHMM1 '/' HHMM1 '000'
num2str(k) '.bmp'];
    elseif k < 10000
        fullFileName = [dir_raw '/' YYYYMMDD '/' HHMM1 '/' HHMM1 '00'
num2str(k) '.bmp'];
    end
    frame_speed=1000;
    time(i)=lasttime+(k-starttime)*(1/frame_speed)*1000;
    Impingingtime(i)=Impingingtimelast+(k-
starttime)*(1/frame_speed)*1000;
end
Original_Image =imadjust(BG-imread(fullFileName));
TI=imcrop(Original_Image,[0,0,sizeimg(2),28]);
OI2=imcrop(Original_Image,[0,29,Center_Location,sizeimg(1)-28]);
OI1=imcrop(Original_Image,[Center_Location+1,29,sizeimg(2)-
Center_Location,sizeimg(1)-28]);

    if i <Impinging_time
    BI=imbinarize(Original_Image);
    se = strel('disk', 2, 0);
    BI=imfill(BI,'holes');
    numberToExtract =1;
    binaryImage = ExtractNLargestBlobs(BI, numberToExtract);
```

```
    subplot(2,3,1)
    imshow(binaryImage)
    hold on;
    Circlefit=bwboundaries(binaryImage);
    XY=cell2mat(Circlefit);
    plot(XY(:,2),XY(:,1),'.r');
    indexfit=find(XY(:,1)~=29);
    hold on;
     plot(XY(indexfit,2),XY(indexfit,1),'.b');
    sizebi=size(binaryImage);
    for j=1:sizebi(1)
        if ismember(1,binaryImage(j,:))
            Horizontal_Location_right(j) = find(binaryImage(j,:) == 1,
1, 'last' );
            Horizontal_Location_left(j) = find(binaryImage(j,:) == 1,
1, 'first' );
            Secant(j)=Horizontal_Location_right(j)-
Horizontal_Location_left(j);
        end
    end
    maxdia= max(Secant);
    array1=find(Secant==maxdia);
    midpoint(i)=(array1(1)+array1(end))/2;
    right_h= find(binaryImage(round(midpoint(i)),:) == 1, 1, 'last' );
    left_h=find(binaryImage(round(midpoint(i)),:)==1,1,'first');
    center(i,:)=[midpoint(i),((right_h+left_h)/2)];
    hold on;
    plot(center(i,2),center(i,1),'*y');
    dia=2.*((XY(indexfit,2)-center(i,2)).^2+(XY(indexfit,1)-
center(i,1)).^2).^(0.5);
    diameter(i)=mean(dia)*scale;
    velocity(i)=scale*(midpoint(i)-midpoint(i-2))/(time(i)-time(i-2));
      str=strcat('\bf diameter=',num2str(diameter(i),'%.2f'),'mm');
    text(00,-
150,str,'HorizontalAlignment','center','VerticalAlignment',
'top','FontSize', fontSize+10,'Color','k');
    str=strcat('\bf velocity=',num2str(velocity(i),'%.2f'),'m/s');
    text(-600,-
150,str,'HorizontalAlignment','center','VerticalAlignment',
'top','FontSize', fontSize+10,'Color','k');
    hold off;
    elseif i>=Impinging_time && i<Impinging_time+7
        BI=imbinarize(Original_Image);
    se = strel('disk', 2, 0);
    BI=imfill(BI,'holes');
    numberToExtract =1;
    binaryImage = ExtractNLargestBlobs(BI, numberToExtract);
    subplot(2,3,1)
    imshow(binaryImage)
    hold on;
    stats2 = regionprops(binaryImage,'Extrema');
    Extrema1 = [stats2.Extrema];
    bottomleft=Extrema1(6,1);
    bottomright=Extrema1(5,1);
```

```
    SD(i)=(bottomright-bottomleft)*scale;
    SF(i)=SD(i)/diameter(end);
    [rows,columns]=size(binaryImage);
    heights = zeros(1, columns);
    topEdge = zeros(1, columns);
    bottomEdge = zeros(1, columns);
    for col = 1:columns
    thisCol = binaryImage(:,col);
    topIndex = find(thisCol, 1, 'first');
    if ~isempty(topIndex)
        topEdge(col) = topIndex; % it is not necessary since yInj is
fixed
        bottomEdge(col) = find(thisCol, 1, 'last');
        heights(col) = bottomEdge(col) - topIndex;
    end
    end
    Htratio(i)=scale*max(heights)/diameter(end);
    str=strcat('\bf Spreadfactor=',num2str(SF(i),'%.2f'));
    text(-600,-
100,str,'HorizontalAlignment','center','VerticalAlignment',
'top','FontSize', fontSize+10,'Color','k');
    str=strcat('\bf Heightratio=',num2str(Htratio(i),'%.2f'));
    text(-00,-
100,str,'HorizontalAlignment','center','VerticalAlignment',
'top','FontSize', fontSize+10,'Color','k');
    hold off;
elseif i>=Impinging_time+7
    %%binarization of right image
    subplot(2,3,1)
    imshow(OI1);
    subplot(2,3,4)
    imshow(OI2);
    level=graythresh(OI1);
    BI1=imbinarize(OI1);
    numberToExtract =1;
    binaryImage1 = ExtractNLargestBlobs(BI1, numberToExtract);
    subplot(2,3,2);
    imshow(binaryImage1)
    hold on;
    %%boundary extraction
    boundaries = bwboundaries(binaryImage1);
    A = cell2mat(boundaries) ;
    hold on;
    plot(A(:,2), A(:,1),'.r');

    %% corners extracted for calculations
    [rows,columns]=size(binaryImage1);
    stats2 = regionprops(binaryImage1,'Extrema');
    Extrema1 = [stats2.Extrema];
    hold on;
    righttop=Extrema1(3,:);
    rightbottom=Extrema1(4,:);
    diff_righttopx=(A(:,2)-righttop(1,1));
    diff_righttopy=(A(:,1)-righttop(1,2));
    dist_righttop=((diff_righttopx).^2+(diff_righttopy).^2).^(1/2);
```

```
    [value1,index1]=min(dist_righttop);
    diff_rightbottomx=(A(:,2)-rightbottom(1,1));
    diff_rightbottomy=(A(:,1)-rightbottom(1,2));

dist_rightbottom=((diff_rightbottomx).^2+(diff_rightbottomy).^2).^(1/2)
;
    [value2,index2]=min(dist_rightbottom);
    plot((A(index1,2)),(A(index1,1)),'*y');
    hold on;
    plot((A(index2,2)),(A(index2,1)),'*y');

    BE(i)=round((A(index1,1)+A(index2,1))/2);
    binaryImage1((BE(i)+1:end),:)=0;
    x= find(binaryImage1(BE(i),:), 1, 'last');
    lx(i)=x;
    y=BE(i);
    binaryImage1(BE(i),1:x)=1;
    se = strel('disk',1, 0);
    binaryImage1=imfill(binaryImage1,'holes');
    %% contact angle calculation
    subplot(2,3,3);
    imshow(binaryImage1);
    hold on;
    boundaries1 = bwboundaries(binaryImage1);
    A1 = cell2mat(boundaries1) ;
    plot(A1(:,2), A1(:,1),'.r');
    index=find(A1(:,1)~=BE(i)& A1(:,2)~=Center_Location);
    x_corners=A1(index,2);
    y_corners=A1(index,1);
    x_corners = [x_corners;x];
    y_corners = [y_corners;y];
    hold on;
    plot(x_corners,y_corners,'.b');
    distarray=((x_corners-x).^2+(y_corners-y).^2).^(1/2);
    B2=cat(2,x_corners,y_corners,distarray);
    B2=sortrows(B2,3);
    j=1;
for n=2:4
for nop=30
    Coefficients = polyfitn(B2(1:nop,1),B2(1:nop,2),n);
    Rsqr(j)=Coefficients.AdjustedR2;
        Rmse(j)=Coefficients.RMSE;
    der1=polyder(Coefficients.Coefficients);
    der2=polyder(der1);
    p=Coefficients.Coefficients(n+1)-BE(i);
    Coefficients.Coefficients(n+1)=p;
    Tpp=real(roots(Coefficients.Coefficients));
    diff=abs(Tpp-x);
    [~,indextpp]=min(diff);
    Tppx=Tpp(indextpp);
    Tppy=BE(i);
    direc=polyval(der2,Tppx);
    MatrixRqrco(j,:)=[Rsqr(j),nop,n,direc];
    j=j+1;
end
```

```
end
    index0=find(MatrixRqrco(:,4)>=0);
    mat0=MatrixRqrco(index0,:);
    Mat1=sortrows(mat0,1);
    if ~isempty(Mat1)
    RR=Mat1(end,1);
        n=Mat1(end,3);
    else
        n=1;
    end
    hold on;
    nop=30;
    plot(B2(1:nop,1),B2(1:nop,2),'.y');
    Fitting = polyfitn(B2(1:nop,1),B2(1:nop,2),n);
    Coefficients=Fitting.Coefficients;
    Rsqr_1(i)=Fitting.R2;
    der=polyder(Coefficients);
    finex=[max(x_corners)-nop:0.5: max(x_corners)+5];
    leftFit = polyval(Coefficients,finex);
    plot(finex,leftFit, 'g-', 'LineWidth', 1);hold on
    p=Coefficients(n+1)-BE(i);
    Coefficients(n+1)=p;
    Tpp=real(roots(Coefficients));
    diff=abs(Tpp-x);
    [valuetpp,indextpp]=min(diff);
    Tppx=Tpp(indextpp);
    Tppy=BE(i);
    slope(i)=polyval(der,Tppx);
    xtangline=[x-nop:0.05:x];
    ytangline=slope(i).*xtangline-slope(i)*Tppx+Tppy;
    contactangle(i)=(atand(slope(i)));
    if contactangle(i)<0
        contactangle(i)=90-contactangle(i);
    end

    plot(xtangline,ytangline,'m-');hold on;
    [rows,columns]=size(binaryImage1);
    heights = zeros(1, columns);
    topEdge = zeros(1, columns);
    bottomEdge = zeros(1, columns);
    for col = 1:columns
    thisCol = binaryImage1(:,col);
    topIndex = find(thisCol, 1, 'first');
    if ~isempty(topIndex)
        topEdge(col) = topIndex; % it is not necessary since yInj is
fixed
        bottomEdge(col) = find(thisCol, 1, 'last');
        heights(col) = bottomEdge(col) - topIndex;
    end
    end
    Htratio1(i)=scale*max(heights)/diameter(end);

    %% left imaging
    level=graythresh(OI2);
    BI2=imbinarize(OI2);
```

```
    numberToExtract =1;
    binaryImage2 = ExtractNLargestBlobs(BI2, numberToExtract);
    subplot(2,3,5);
    imshow(binaryImage2)
    hold on;

    %%boundary
    boundaries2 = bwboundaries(binaryImage2);
    A2 = cell2mat(boundaries2) ;
    hold on;
    plot(A2(:,2), A2(:,1),'.r');

%% corners extracted for calculations
    [rows2,columns2]=size(binaryImage2);
    stats22 = regionprops(binaryImage2,'Extrema');
    Extrema2 = [stats22.Extrema];
    hold on;
    lefttop=Extrema2(8,:);
    leftbottom=Extrema2(7,:);
    diff_lefttopx=(A2(:,2)-lefttop(1,1));
    diff_lefttopy=(A2(:,1)-lefttop(1,2));
    dist_lefttop=((diff_lefttopx).^2+(diff_lefttopy).^2).^(1/2);
    [value21,index21]=min(dist_lefttop);
    diff_leftbottomx=(A2(:,2)-leftbottom(1,1));
    diff_leftbottomy=(A2(:,1)-leftbottom(1,2));

dist_leftbottom=((diff_leftbottomx).^2+(diff_leftbottomy).^2).^(1/2);
    [value22,index22]=min(dist_leftbottom);
    plot((A2(index21,2)),(A2(index21,1)),'*y');
    hold on;
    plot((A2(index22,2)),(A2(index22,1)),'*y');
    BE2(i)=round((A2(index21,1)+A2(index22,1))/2);

    %% contact angle calculation
    binaryImage2(BE2(i)+1:end,:)=0;
    sizeleft=size(binaryImage2);
    x2= find(binaryImage2(BE2(i),:), 1, 'first');
    lx2(i)=sizeleft(2)-x2;

    y2=BE2(i);
    binaryImage2(BE2(i),x2:end)=1;
    se = strel('disk', 1, 0);
    binaryImage2=imfill(binaryImage2,'holes');
    subplot(2,3,6);
    imshow(binaryImage2);
    hold on;
    boundaries21 = bwboundaries(binaryImage2);
    A21 = cell2mat(boundaries21) ;
    plot(A21(:,2), A21(:,1),'.r');
    index201=find(A21(:,1)~=BE2(i)& A21(:,2)~=Center_Location);
    x_corners21=A21(index201,2);
    y_corners21=A21(index201,1);


    x_corners21 = [x_corners21;x2];
```

```
    y_corners21 = [y_corners21;y2];
    hold on;
    plot(x_corners21,y_corners21,'.b');

    distarray2=((x_corners21-x2).^2+(y_corners21-y2).^2).^(1/2);
    B22=cat(2,x_corners21,y_corners21,distarray2);
    B22=sortrows(B22,3);
    j2=1;

    for n2=2:4
    for nop2=30
        Coefficients2 = polyfitn(B22(1:nop2,1),B22(1:nop2,2),n2);
        Rsqr2(j2)=Coefficients2.AdjustedR2
        der21=polyder(Coefficients2.Coefficients);
        der22=polyder(der21);
        p2=Coefficients2.Coefficients(n2+1)-BE2(i);
        Coefficients2.Coefficients(n2+1)=p2;
        Tpp2=real(roots(Coefficients2.Coefficients));
        diff2=abs(Tpp2-x2);
        [~,indextpp2]=min(diff2);
        Tppx2=Tpp2(indextpp2);
        Tppy2=BE2(i);
        direc2=polyval(der22,Tppx2);
        MatrixRqrco2(j2,:)=[Rsqr2(j2),nop2,n2,direc2];
        j2=j2+1;
    end
    end
    index02=find(MatrixRqrco2(:,4)>=0);
    mat02=MatrixRqrco2(index02,:);
    Mat21=sortrows(mat02,1);
    if ~isempty(Mat21)
    RR2=Mat21(end,1);
%     nop2=Mat21(end,2);
    n2=Mat21(end,3);
    else
        n2=1;
    end
    nop2=30;

%     direc21(i)=Mat21(end,4);
    hold on;
    plot(B22(1:nop2,1),B22(1:nop2,2),'.y');
    Fitting2 = polyfitn(B22(1:nop2,1),B22(1:nop2,2),n2);
    Coefficients2=Fitting2.Coefficients;
    der=polyder(Coefficients2);
    Rsqr_2(i)=Fitting2.R2;
    finex=[min(x_corners21):0.5: min(x_corners21)+nop2];
    leftFit = polyval(Coefficients2,finex);

    p2=Coefficients2(n2+1)-BE2(i);
    Coefficients2(n2+1)=p2;
    Tpp2=real(roots(Coefficients2));
    diff2=abs(Tpp2-x2);
    [valuetpp2,indextpp2]=min(diff2);
    Tppx2=Tpp2(indextpp2);
```

```
    Tppy2=BE2(i);
    slope2(i)=polyval(der,Tppx2);
    xtangline2=[Tppx2:0.05:Tppx2+nop2];
    ytangline2=slope2(i).*xtangline2-slope2(i)*Tppx2+Tppy2;
    contactangle2(i)=abs(atand(slope2(i)));
    hold on;
    plot(finex,leftFit, 'g-', 'LineWidth', 1);hold on
    plot(xtangline2,ytangline2,'m-');hold on;
    SD(i)=scale*(lx(i)+lx2(i))
    Contactlinevelocityright(i)=scale*(lx(i)-lx(i-1))/(time(i)-time(i-
1));
    Contactlinevelocityleft(i)=scale*(lx2(i)-lx2(i-1))/(time(i)-time(i-
1));
    SF(i)=SD(i)/diameter(end);
    [rows2,columns2]=size(binaryImage2);
    heights2 = zeros(1, columns2);
    topEdge2 = zeros(1, columns2);
    bottomEdge2 = zeros(1, columns2);
    for col2 = 1:columns2
    thisCol2 = binaryImage2(:,col2);
    topIndex2 = find(thisCol2, 1, 'first');
    if ~isempty(topIndex2)
        topEdge2(col2) = topIndex2; % it is not necessary since yInj is
fixed
        bottomEdge2(col2) = find(thisCol2, 1, 'last');
        heights2(col) = bottomEdge2(col2) - topIndex2;
    end
    end
    Htratio2(i)=scale*max(heights2)/diameter(end);
    Htratio(i)=max(Htratio1(i),Htratio2(i));

    str=strcat('\bf Left
\theta=',num2str(contactangle2(i),'%.2f'),'\circ');
    text(00,-
150,str,'HorizontalAlignment','center','VerticalAlignment',
'top','FontSize', fontSize+10,'Color','k');
    str=strcat('\bf ASOI=',num2str(Impingingtime(i),'%.2f'),'ms');
    text(-600,-
150,str,'HorizontalAlignment','center','VerticalAlignment',
'top','FontSize', fontSize+10,'Color','k');
    str=strcat('\bf Right
\theta=',num2str(contactangle(i),'%.2f'),'\circ');
    text(-300,-
150,str,'HorizontalAlignment','center','VerticalAlignment',
'top','FontSize', fontSize+10,'Color','k');
    str=strcat('\bf LeftRsqr=',num2str(Rsqr_1(i),'%.2f'));
    text(00,-
100,str,'HorizontalAlignment','center','VerticalAlignment',
'top','FontSize', fontSize+10,'Color','k');
    str=strcat('\bf RightRsqr=',num2str(Rsqr_2(i),'%.2f'));
    text(-300,-
100,str,'HorizontalAlignment','center','VerticalAlignment',
'top','FontSize', fontSize+10,'Color','k');
   str=strcat('\bf Spreadfactor=',num2str(SF(i),'%.2f'));
```

```
    text(-600,-
100,str,'HorizontalAlignment','center','VerticalAlignment',
'top','FontSize', fontSize+10,'Color','k');
    str=strcat('\bf Heightratio=',num2str(Htratio(i),'%.2f'));
    text(-1000,-
100,str,'HorizontalAlignment','center','VerticalAlignment',
'top','FontSize', fontSize+10,'Color','k');
    str=strcat('\bf Spreaddiameter=',num2str(SD(i),'%.2f'));
    text(-1000,-
150,str,'HorizontalAlignment','center','VerticalAlignment',
'top','FontSize', fontSize+10,'Color','k');

    hold off;
    end
 drawnow;
    frame = getframe(figure(1));
    writeVideo(writerObj,frame);
    pause(0.1);
end
cd([dir_raw '/' YYYYMMDD '/' HHMM1]) % Change the working directory to
the desired folder

% writing in excel file
col_header={'Time (ms)', 'Impingingtime','Left Collision angle
(deg)','Right Collision Angle(deg)','Spread factor', 'Spread diameter',
'Height Ratio','Diametr before Impinegement'};
xlswrite(strcat(HHMM,'.xlsx'),time',2,'A2');
xlswrite(strcat(HHMM,'.xlsx'),Impingingtime',2,'B2');
xlswrite(strcat(HHMM,'.xlsx'),contactangle2',2,'C2');
xlswrite(strcat(HHMM,'.xlsx'),contactangle',2,'D2');
xlswrite(strcat(HHMM,'.xlsx'),SD',2,'E2');
xlswrite(strcat(HHMM,'.xlsx'),SF',2,'F2');
xlswrite(strcat(HHMM,'.xlsx'),Htratio',2,'G2');
xlswrite(strcat(HHMM,'.xlsx'),Contactlinevelocityright',2,'H2');
xlswrite(strcat(HHMM,'.xlsx'),Contactlinevelocityleft',2,'I2');
toc
function binaryImage = ExtractNLargestBlobs(binaryImage,
numberToExtract)
try
% Get all the blob properties.  Can only pass in originalImage in
version R2008a and later.
[labeledImage, numberOfBlobs] = bwlabel(binaryImage);
blobMeasurements = regionprops(labeledImage, 'area');
% Get all the areas
allAreas = [blobMeasurements.Area];
if numberToExtract > length(allAreas);
    % Limit the number they can get to the number that are
there/available.
    numberToExtract = length(allAreas);
end
if numberToExtract > 0
    % For positive numbers, sort in order of largest to smallest.
    % Sort them.
    [sortedAreas, sortIndexes] = sort(allAreas, 'descend');
elseif numberToExtract < 0
```

```
    % For negative numbers, sort in order of smallest to largest.
    % Sort them.
    [sortedAreas, sortIndexes] = sort(allAreas, 'ascend');
    % Need to negate numberToExtract so we can use it in sortIndexes
later.
    numberToExtract = -numberToExtract;
else
    % numberToExtract = 0.  Shouldn't happen.  Return no blobs.
    binaryImage = false(size(binaryImage));
    return;
end
% Extract the "numberToExtract" largest blob(a)s using ismember().
biggestBlob = ismember(labeledImage, sortIndexes(1:numberToExtract));
% Convert from integer labeled image into binary (logical) image.
binaryImage = biggestBlob > 0;
catch ME
errorMessage = sprintf('Error in function
ExtractNLargestBlobs().\n\nError Message:\n%s', ME.message);
fprintf(1, '%s\n', errorMessage);
uiwait(warndlg(errorMessage));

end
end
```

A.2 Heat Flux

Main Program

```
dir_raw = 'D:\dropletheatflux\version2';
cd(dir_raw); %%calling subprograms for data
[t_150,T_AVE_A_E_150,T_AVE_A_S_150,T_STD_A_E_150
,T_STD_A_S_150,HF_AVE_A_150 , HF_STD_A_150]=heat_flux_data_150();
cd(dir_raw);
[t_185,T_AVE_A_E_185,T_AVE_A_S_185,T_STD_A_E_185
,T_STD_A_S_185,HF_AVE_A_185 , HF_STD_A_185]=heat_flux_data_185();
cd(dir_raw);
[t_220,T_AVE_A_E_220,T_AVE_A_S_220,T_STD_A_E_220
,T_STD_A_S_220,HF_AVE_A_220 , HF_STD_A_220]=heat_flux_data_220();
close all;

%% plotting surface temp
figure;

plot(1000.*t_150(1:50:end),T_AVE_A_S_150(1:50:end),'r','lineWidth',2);
hold on;
plot(1000.*t_185(1:20:end),T_AVE_A_S_185(1:20:end),'b','lineWidth',2);
hold on;
plot(1000.*t_220(1:20:end),T_AVE_A_S_220(1:20:end),'k','lineWidth',2);
hold on;
shadedErrorBar(1000.*t_150(1:50:end),T_AVE_A_S_150(1:50:end),T_STD_A_S_
150(1:50:end),'lineProps','r','transparent',1,'patchSaturation',0.2);
hold on;
```

```
shadedErrorBar(1000.*t_185(1:20:end),T_AVE_A_S_185(1:20:end),T_STD_A_S_
185(1:20:end),'lineProps','b','transparent',1,'patchSaturation',0.2);
hold on;
shadedErrorBar(1000.*t_220(1:20:end),T_AVE_A_S_220(1:20:end),T_STD_A_S_
220(1:20:end),'lineProps','k','transparent',1,'patchSaturation',0.2);
xlabel('ASOI [ms]','FontSize',15);
ylabel('Surface temperature [^oC]','FontSize',15);
axes = gca(figure(1));
axes.FontSize = 20;
legend('150^oC', '260^oC','295^oC');

%% Average temperature plot
figure;
plot(1000.*t_150(1:50:end),T_AVE_A_E_150(1:50:end),'r','lineWidth',2);
hold on;
plot(1000.*t_185(1:20:end),T_AVE_A_E_185(1:20:end),'b','lineWidth',2);
hold on;
plot(1000.*t_220(1:20:end),T_AVE_A_E_220(1:20:end),'k','lineWidth',2);
hold on;
shadedErrorBar(1000.*t_150(1:50:end),T_AVE_A_E_150(1:50:end),T_STD_A_E_
150(1:50:end),'lineProps','r','transparent',1,'patchSaturation',0.2);
hold on;
shadedErrorBar(1000.*t_185(1:50:end),T_AVE_A_E_185(1:50:end),T_STD_A_E_
185(1:50:end),'lineProps','b','transparent',1,'patchSaturation',0.2);
hold on;
shadedErrorBar(1000.*t_220(1:50:end),T_AVE_A_E_220(1:50:end),T_STD_A_E_
220(1:50:end),'lineProps','k','transparent',1,'patchSaturation',0.2);
xlabel('ASOI [ms]','FontSize',15);
ylabel('Embedded temperature [^oC]','FontSize',15);
legend('150^oC', '260^oC','295^oC');
axes = gca(figure(1));
axes.FontSize = 20;

%% Average heat flux plot
figure;
plot(1000.*t_150(1:50:end),HF_AVE_A_150(1:50:end),'r','lineWidth',2);
hold on;
plot(1000.*t_185(1:20:end),HF_AVE_A_185(1:20:end),'b','lineWidth',2);
hold on;
plot(1000.*t_220(1:20:end),HF_AVE_A_220(1:20:end),'k','lineWidth',2);
hold on;
shadedErrorBar(1000.*t_150(1:50:end),HF_AVE_A_150(1:50:end),HF_STD_A_15
0(1:50:end),'lineProps','r','transparent',1,'patchSaturation',0.2);
hold on;
shadedErrorBar(1000.*t_185(1:5:end),HF_AVE_A_185(1:5:end),HF_STD_A_185(
1:5:end),'lineProps','b','transparent',1,'patchSaturation',0.2);
hold on;
shadedErrorBar(1000.*t_220(1:5:end),HF_AVE_A_220(1:5:end),HF_STD_A_220(
1:5:end),'lineProps','k','transparent',1,'patchSaturation',0.2);
xlabel('ASOI [ms]','FontSize',15);
ylabel('Heat flux [kW/m^2]','FontSize',15);
legend('150^oC', '260^oC','295^oC');
axes = gca(figure(1));
axes.FontSize = 20;
```

```
%% Integrated heat flux calculation
for i =2: length(t_150)
    if(t_150(i)>0)
    time=1000.*(t_150(1:i)+0.26);
    HF_150(i)=trapz(time,HF_AVE_A_150(1:i));
    else
    HF_150(i)=0;
    end
end
for i=2: length(t_185)
    if(t_185(i)>0)
    time=1000.*(t_185(1:i)+1.4665);
    HF_185(i)=trapz(time,HF_AVE_A_185(1:i))-1.924E+4;
    else
        HF_185(i)=0;
    end
end
for i=2:length(t_220)
    if(t_220(i)>0)
time=1000.*(t_220(1:i)+1.4658);
    HF_220(i)=trapz(time,HF_AVE_A_220(1:i))-1.924E+4;
    else
        HF_220(i)=0;
    end
end

%% Integrated heat flux plot
figure;
 plot(1000.*t_150,HF_150,'r','lineWidth',2);
    hold on;
     plot(1000.*t_185,HF_185,'b','lineWidth',2);
    hold on;
     plot(1000.*t_220,HF_220,'k','lineWidth',2);
     xlabel('ASOI [ms]','FontSize',15);
ylabel('Integrated Heat flux [kJ/m^2]','FontSize',15);
legend('150^oC', '260^oC','295^oC');
```

Sample sub program

```
function[t,T_AVE_A_E,T_AVE_A_S,T_STD_A_E ,T_STD_A_S,HF_AVE_A ,
HF_STD_A]= heat_flux_data_150()
%% Reading data from excel file
clear all
dir_raw = 'G:\Droplet research\droplet_heatflux';
cd(dir_raw);
%% Extract the raw data
start = 10000;
%% Plot raw data
L = 60000;
K = 44.5; % W/mK
dx = 2; % mm
Fs = 10000;
```

```
T = 1/Fs;
t = (0:L-1)*T;
t=t';
% Injection_start = 10000;
Repeat_1 = 1744;
Repeat_2 = 1745;
Repeat_3 = 1746;
Repeat_4 = 1747;
Repeat_5 = 1748;
% Repeat 1
LA_e_1 = xlsread([num2str(Repeat_1) '.xlsx'],2,'A1:A60001');
LA_s_1 = xlsread([num2str(Repeat_1) '.xlsx'],2,'B1:B60001');
index=find(LA_s_1<160 & LA_s_1>90 & LA_e_1<160 & LA_e_1>140);
LA_e_1 = LA_e_1(index);
LA_s_1 = LA_s_1(index);
% te_1=t(index);
ts_1=t(index);

% Repeat 2
LA_e_2 = xlsread([num2str(Repeat_2) '.xlsx'],2,'A1:A60001');
LA_s_2 = xlsread([num2str(Repeat_2) '.xlsx'],2,'B1:B60001');

index=find(LA_s_2<160 & LA_s_2>90 & LA_e_2<160 & LA_e_2>140);
LA_e_2 = LA_e_2(index);
LA_s_2 = LA_s_2(index);
% te_2=t(index);
ts_2=t(index);

% Repeat 3
LA_e_3 = xlsread([num2str(Repeat_3) '.xlsx'],2,'A1:A60001');
LA_s_3 = xlsread([num2str(Repeat_3) '.xlsx'],2,'B1:B60001');

index=find(LA_s_3<160 & LA_s_3>90 & LA_e_3<160 & LA_e_3>140);
LA_e_3 = LA_e_3(index);
LA_s_3 = LA_s_3(index);
% te_3=t(index);
ts_3=t(index);

% Repeat 4
LA_e_4 = xlsread([num2str(Repeat_4) '.xlsx'],2,'A1:A60001');
LA_s_4 = xlsread([num2str(Repeat_4) '.xlsx'],2,'B1:B60001');
index=find(LA_s_4<160 & LA_s_4>90 & LA_e_4<160 & LA_e_4>140);
LA_e_4 = LA_e_4(index);
LA_s_4 = LA_s_4(index);
% te_4=t(index);
ts_4=t(index);

% Repeat 5
LA_e_5 = xlsread([num2str(Repeat_5) '.xlsx'],2,'A1:A60001');
LA_s_5 = xlsread([num2str(Repeat_5) '.xlsx'],2,'B1:B60001');
index=find(LA_s_5<160 & LA_s_5>90 & LA_e_5<160 & LA_e_5>140);
LA_e_5 = LA_e_5(index);
LA_s_5 = LA_s_5(index);
% te_5=t(index);
ts_5=t(index);
```

```
%% Median Filter
%% Median Filter
order = 50;
ordere =50;
% Repeat 1
LA_median_e_1 = medfilt1(LA_e_1,ordere);
LA_median_s_1 = medfilt1(LA_s_1,order);
ch1=findchangepts(LA_median_s_1);
chts_1=ts_1-ts_1(ch1);
figure;
l1=ch1-2500;
u1=ch1+15000;
plot(chts_1(l1:u1),LA_median_s_1(l1:u1),'r');
hold on;
plot(chts_1(l1:u1),LA_median_e_1(l1:u1),'b');

% Repeat 2
LA_median_e_2 = medfilt1(LA_e_2,ordere);
LA_median_s_2 = medfilt1(LA_s_2,order);
ch2=findchangepts(LA_median_s_2);
chts_2=ts_2-ts_2(ch2);
hold on;
l2=ch2-2500;
u2=ch2+15000;
plot(chts_2(l2:u2),LA_median_s_2(l2:u2),'r');
hold on;
plot(chts_2(l2:u2),LA_median_e_2(l2:u2),'b');
% % Repeat 3
LA_median_e_3 = medfilt1(LA_e_3,ordere);
LA_median_s_3 = medfilt1(LA_s_3,order);
ch3=findchangepts(LA_median_s_3);
chts_3=ts_3-ts_3(ch3);
hold on;
l3=ch3-2500;
u3=ch3+15000;
plot(chts_3(l3:u3),LA_median_s_3(l3:u3),'r');
hold on;
plot(chts_3(l3:u3),LA_median_e_3(l3:u3),'b');
% Repeat 4
LA_median_e_4 = medfilt1(LA_e_4,ordere);
LA_median_s_4 = medfilt1(LA_s_4,order);
ch4=findchangepts(LA_median_s_4);
chts_4=ts_4-ts_4(ch4);
hold on;
l4=ch4-2500;
u4=ch4+15000;
plot(chts_4(l4:u4),LA_median_s_4(l4:u4),'r');
hold on;
plot(chts_4(l4:u4),LA_median_e_4(l4:u4),'b');
% Repeat 5
LA_median_e_5 = medfilt1(LA_e_5,ordere);
LA_median_s_5 = medfilt1(LA_s_5,order);
ch5=findchangepts(LA_median_s_5);
chts_5=ts_5-ts_5(ch5);
```

```
hold on;
l5=ch5-2500;
u5=ch5+15000;
plot(chts_5(l5:u5),LA_median_s_5(l5:u5),'r');
hold on;
plot(chts_5(l5:u5),LA_median_e_5(l5:u5),'b');

T_A_E1 = LA_median_e_1(l1:u1);
T_A_E2 = LA_median_e_2(l2:u2);
T_A_E3 = LA_median_e_3(l3:u3);
T_A_E4 = LA_median_e_4(l4:u4);
T_A_E5 = LA_median_e_5(l5:u5);
T_A_E=cat(2,T_A_E1,T_A_E2,T_A_E3,T_A_E4,T_A_E5);

T_A_S1 = LA_median_s_1(l1:u1);
T_A_S2 = LA_median_s_2(l2:u2);
T_A_S3 = LA_median_s_3(l3:u3);
T_A_S4 = LA_median_s_4(l4:u4);
T_A_S5 = LA_median_s_5(l5:u5);
T_A_S=cat(2,T_A_S1,T_A_S2,T_A_S3,T_A_S4,T_A_S5);

t=chts_2(l2:u2);
%% Surface temperature profile plot
T_AVE_A_E = (T_A_E1+T_A_E2 + T_A_E3+  T_A_E4 + T_A_E5)./5;
T_AVE_A_S = (T_A_S1+T_A_S2 + T_A_S3+  T_A_S4 + T_A_S5)./5;
T_STD_A_E = std(T_A_E,0,2);
T_STD_A_S = std(T_A_S,0,2);

figure;
errorbar(t(1:50:end),T_AVE_A_S(1:50:end),T_STD_A_S(1:50:end),'r');
hold on;
errorbar(t(1:50:end),T_AVE_A_E(1:50:end),T_STD_A_E(1:50:end) ,'b');
xlabel('ASOI (s)','FontSize',15);
ylabel('Temperature (^oC)','FontSize',15);
axes = gca(figure(1));
axes.FontSize = 20;
legend('Surface temp','Embedded temp');
title('150')
%% Heat Flux calculation
% Repeat 1
HF_A_1 = K * (T_A_E1 - T_A_S1) / dx;
HF_A_2 = K * (T_A_E2 - T_A_S2) / dx;
HF_A_3 = K * (T_A_E3 - T_A_S3) / dx;
HF_A_4 = K * (T_A_E4 - T_A_S4) / dx;
HF_A_5 = K * (T_A_E5 - T_A_S5) / dx;

% Average heat flux and standard deviation;
% Location A
HF_AVE_A = (HF_A_2 +  HF_A_3 + HF_A_4 + HF_A_5)/5;
HF_A(:,1) = HF_A_1;
HF_A(:,2) = HF_A_2;
HF_A(:,3) = HF_A_3;
HF_A(:,4) = HF_A_4;
HF_A(:,5) = HF_A_5;
HF_STD_A = std(HF_A,0,2);
```

B Copyright documentation

The Copyrighted material used in this report are all second authored by me. One of them is published and the permission to use it specified below. The other two are yet to be published, therefore I need to hold the publication of my report.

1. Zhao, Le, Nitisha Ahuja, Xiucheng Zhu, Zhihao Zhao, and Seong-Young Lee. *Splashing criterion and topological features of a single droplet impinging on the flat plate*. No. 2018-01-0289. SAE Technical Paper, 2018.

Yet to be published:

2. Zhao, Le, Nitisha Ahuja, Xiucheng Zhu, Zhihao Zhao, and Seong-Young Lee. *Characterization of Impingement Dynamics of Single Droplet Impacting on a Flat Surface*. No. 2019-01-0064. SAE Technical Paper, 2019.
3. Investigation of the Effects of Heat Transfer and Thermophysical Properties on Dynamics of Droplet-wall Interaction

Michigan Tech

Nitisha Ahuja <nahuja@mtu.edu>

A kind request for permission to re-publish my papers in my master's dissertation

---

copyright <copyright@sae.org> Mon, Nov 5, 2018 at 3:26 PM

To: Nitisha Ahuja <nahuja@mtu.edu>

Dear Nitisha,

I apologize for the inconvenience. I have a work order being processed for CCC in regards to the 2018-01-0289 paper. Per our conversation your paper SAE 2018-01-0289 the embargo period has expired and you are free to use the author copy format of your paper in your dissertation. Best of luck to you on the completion of your paper. Under your terms of your WCX contract, you may store your manuscript in your university's electronic database for five years after publication. Please note that you may store the manuscript only, not the paged, SAE formatted paper. In addition, the SAE copyright statement must be clearly indicated.

Thank you very much for contributing to SAE.

Best regards,

Heather Kindsvatter

Intellectual Property Specialist

Content Management

SAE INTERNATIONAL

400 Commonwealth Drive

Warrendale, PA 15096

o: 1.724.772.8515

e: heather.kindsvatter@sae.org

www.sae.org

From: Nitisha Ahuja <nahuja@mtu.edu>
Sent: Monday, November 5, 2018 2:53 PM
To: Heather Kindsvatter <heather.kindsvatter@sae.org>; copyright <copyright@sae.org>
Subject: Re: A kind request for permission to re-publish my papers in my master's dissertation

[Quoted text hidden]

[Quoted text hidden]